



**U.S. Army Corps of Engineers
Walla Walla District**

Two-Dimensional Hydrodynamic, Water Quality, and Fish Exposure Modeling of the Columbia and Snake Rivers.

Part 1: Summary and Model Formulation.

FINAL REPORT

February 1999

**M.C. Richmond
W.A. Perkins
T.D. Scheibe**

**Battelle Pacific Northwest Division
P.O. Box 999
Richland, Washington 99352
Contract DACW68-96-D-0002**

LEGAL NOTICE

This report was prepared by Battelle Memorial Institute (Battelle) as an account of sponsored research activities. Neither Client nor Battelle nor any person acting on behalf of either:

MAKES ANY WARRANTY OR REPRESENTATION, EXPRESS OR IMPLIED with respect to the accuracy, completeness, or usefulness of the information contained in this report, or that the use of any information, apparatus, process, or composition disclosed in this report may not infringe privately owned rights; or

Assumes any liabilities with respect to the use of, or for damages resulting from the use of, any information, apparatus, process, or composition disclosed in this report.

Reference herein to any specific commercial product, process, or service by trade name, trademark, manufacturer, or otherwise, does not necessarily constitute or imply its endorsement, recommendation, or favoring by Battelle. The views and opinions of authors expressed herein do not necessarily state or reflect those of Battelle.



This document was printed on recycled paper.

Abstract

One of the major goals for the U.S. Army Corps of Engineers Dissolved Gas Abatement Study is to identify measures that could reduce levels of dissolved gas supersaturation in the Columbia and Snake Rivers caused by spillway discharges. Attaining this goal could contribute significantly to meeting water quality criteria and lowering gas bubble trauma in resident and migrating fish in these rivers. To achieve this goal, the Corps of Engineers is studying various operational and structural alternatives using field investigations and computational modeling tools to simulate the transport of dissolved gas in the river system.

This report summarizes the development and application of a two-dimensional depth-averaged hydrodynamic and water quality model (MASS2) to the Lower Columbia and Snake River system. The report also describes an individual-based model (FINS) that can be used to estimate fish exposure to dissolved gas.

Acknowledgments

Significant editorial and technical contributions were made by the following Battelle staff: Lyle Hibler of the Marine Sciences Group and Kurt Recknagle of the Fluid Dynamics Group, Russ Moursund of the Ecology Group, and Christa Knudson of the Hydrology Group.

Thanks to Rick Emmert, Tom Carlson, Kim Fodrea, and Joe Carroll of the USACE for their assistance in this project.

Contents

1	INTRODUCTION.....	1
2	MASS2 HYDRODYNAMICS AND TRANSPORT MODEL.....	4
2.1	Coordinates and Grid System.....	4
2.2	Hydrodynamics.....	4
2.3	General Scalar Transport.....	7
2.4	Dissolved Gas Transport	7
2.4.1	Governing Equation.....	7
2.4.2	Surface Gas Exchange	9
2.5	Thermal Energy Transport	10
2.5.1	Governing Equation.....	10
2.5.2	Surface Heat Exchange	11
2.6	Discretization	14
2.7	Velocity-Depth Coupling	15
2.8	Initial and Boundary Conditions	15
2.9	Solution Procedure	15
2.10	Model Output	16
2.11	Test Problems.....	16
2.11.1	Mixing of two streams in a straight rectangular channel:	16
2.11.2	Normal Flow in a Straight Channel with a Slope Break	20
3	FINS (FISH INDIVIDUAL-BASED NUMERICAL SIMULATOR) – EXPOSURE MODEL	23
3.1	Background Review.....	23
3.2	Initial Design and Data Structure.....	24
3.3	Release Module	24
3.4	FINS Main Module	26
3.5	Model Testing	28
3.5.1	Dispersion/Diffusion Testing	28
3.5.2	Testing of Numerical Time-Step Effects:.....	29
3.6	Parameter Estimation from PIT Data and Correlated Random Walk Model.....	31
3.6.1	Travel Time Versus Mean Flow.....	32
3.6.2	Parameter Estimation (σ).....	34

3.7	Correlated Random Walk Test:	39
3.7.1	Travel time variability due to velocity variations only.....	41
3.7.2	Possible Concerns.....	42
3.8	Post-Processing Module	42
3.9	Current Status of FINS	44
4	MODEL APPLICATION	45
4.1	Model Grid and Bathymetry	45
4.2	Boundary and Initial Conditions	49
4.2.1	Project Operations	49
4.2.2	Water Quality.....	50
4.2.3	Meteorological Conditions.....	55
4.2.4	Initial Conditions.....	57
5	SUMMARY OF RESULTS	58
5.1	Overview of Simulations	58
5.2	Parameter Selection	59
5.3	Lower Granite (LGR)	59
5.3.1	LGR Hydrodynamics.....	60
5.3.2	LGR Water Quality.....	61
5.3.3	LGR Summary	64
5.4	Little Goose (LGO)	64
5.4.1	LGO Hydrodynamics.....	65
5.4.2	LGO Water Quality	66
5.4.3	LGO Summary	68
5.5	Lower Monumental (LMN)	69
5.5.1	LMN Hydrodynamics.....	70
5.5.2	LMN Water Quality.....	71
5.5.3	LMN Summary.....	74
5.6	Ice Harbor (IHR)	75
5.6.1	IHR Hydrodynamics.....	76
5.6.2	IHR Water Quality.....	77
5.6.3	IHR Summary	78
5.7	McNary (MCN)	79
5.7.1	MCN Hydrodynamics.....	80
5.7.2	MCN Water Quality	80
5.7.3	MCN Summary	83
5.8	John Day (JDA)	85
5.8.1	JDA Hydrodynamics	85
5.8.2	JDA Water Quality.....	86
5.8.3	JDA Summary.....	90

5.9	The Dalles (TDA)	92
5.9.1	TDA Hydrodynamics.....	92
5.9.2	TDA Water Quality	94
5.9.3	TDA Summary	97
5.10	Bonneville (BON)	99
5.10.1	BON Hydrodynamics	99
5.10.2	BON Water Quality.....	100
5.10.3	BON Summary.....	103
5.11	Tidal Reach (TID)	103
5.11.1	TID Hydrodynamics	104
5.11.2	TID Water Quality.....	105
5.11.3	TID Summary.....	108
6	CONCLUSIONS AND RECOMMENDATIONS	109
7	REFERENCES	112

Figures

Figure 1. Geographical domain where MASS2 the two-dimensional hydrodynamic and water quality model was applied. 3

Figure 2. Empirical Transfer Coefficient Relationship. Symbols are field data presented in O’Connor (1982). Red line is a 3rd order polynomial curve-fit..... 10

Figure 3. Longitudinal variation of concentration for Test 1; solid lines are model result and dashed lines are analytical solution (after Fischer et al 1979)..... 18

Figure 4. Lateral variation at x=400 ft and x=1000 ft (top), and x=2000 ft and x=3000ft (bottom); solid lines are numerical solution and dashed lines are analytical solution (after Fischer et al, 1979)..... 19

Figure 5. Horizontal distribution of conservative tracer for Test 1. 20

Figure 6. Velocity (top) and depth (bottom) profiles for Test 2; solid lines are numerical result; dashed lines are analytically derived normal velocity and depths for both upper channel- and lower channel. 22

Figure 7. Generated release points in plan view of 500 smolts in a sample batch. A normal distribution of locations, centered at (100,250) was used. 25

Figure 8. Histogram of generated initial depths for 500 smolts in a sample batch. An exponential distribution with mean depth of 2.0 meters and maximum Depth of 15 meters was specified. 26

Figure 9. Model grid near McNary (above) and John Day (below) dams. 46

Figure 10. Bathymetric data near Ice Harbor dam..... 47

Figure 11. Color representation of The Dalles pool bathymetric surface 48

Figure 12. John Day dam operations during The Dalles Summer 1996 study. 49

Figure 13. The Dalles Dam operations during The Dalles Summer 1996 study period. .. 50

Figure 14. Water temperature at John Day dam during The Dalles Summer 1996 study. 51

Figure 15. TDG pressure at John Day dam during The Dalles Summer 1996 study period. 51

Figure 16. Computed TDG concentration at John Day during The Dalles Summer 1996 study..... 52

Figure 17. Locations, relative to the model grid, of temporary monitors during The Dalles Summer 1996 study period..... 53

Figure 18. Temperatures measured by temporary monitors near John Day dam during The Dalles Summer 1996 study period..... 53

Figure 19. TDG pressures measured by temporary monitors near John Day dam during The Dalles Summer 1996 study period..... 54

Figure 20. TDG concentrations computed from temporary monitor data near John Day dam during The Dalles Summer 1996 study period. 55

Figure 21. Air temperature, dew point, and barometric pressure used during The Dalles Summer 1996 study period. 56

Figure 22. Wind speed used during The Dalles Summer 1996 study period. 56

Figure 23. Net incoming short-wave solar radiation based estimated total radiation used during The Dalles Summer 1996 study period..... 57

Figure 24. Simulated and observed depth-averaged velocities near Lower Granite dam April 4, 1997. 60

Figure 25. Spatial Velocity Distribution in LGR pool near Silcott Island. 61

Figure 26. Temperature and total dissolved gas time series near Snake River mile 123.7 for the LGR Spring 1997 pool study. 62

Figure 27. Total dissolved gas pressure and saturation time series near Snake River mile 123.7 for the LGR Spring 1997 pool study..... 63

Figure 28. Simulated and observed depth-averaged velocities near Lower Granite dam on April 8, 1997. 65

Figure 29. Simulated Spatial Velocity Distribution in LGO pool. 66

Figure 30. Total dissolved gas pressure and saturation time series near at the LGNW fixed monitor during the LGO Spring 1997 pool study (FMS-BC). 67

Figure 31. Total dissolved gas pressure and saturation time series near Snake River Mile 106.7 for the LGO Spring 1997 pool study (FMS-BC)..... 68

Figure 32. Simulated and observed depth-averaged velocities near Snake River Mile 56 on 6-10-1997. 70

Figure 33. Simulated spatial velocity distribution in LMN pool..... 71

Figure 34. Total dissolved gas pressure and saturation time series comparisons near Snake River Mile 59.2 for the LMN Summer 1997 study (TM-BC). 72

Figure 35. Simulated spatial TDG distribution in LMN pool. 74

Figure 36. Simulated and observed depth-averaged velocities near Columbia River Mile 40.5 on 4-28-1997..... 76

Figure 37. Simulated spatial velocity distribution in IHR pool..... 77

Figure 38. Total dissolved gas pressure and saturation time series comparisons near Snake River Mile 010.2 for Spring 1997 study period (TM-BC). 78

Figure 39. Simulated and observed depth-averaged velocities at the confluence of the Columbia and Snake Rivers on 7-11-1996. 80

Figure 40. Temperature and total dissolved gas time series comparisons near Columbia River Mile 323.5 for the Summer 1996 pool study (TM-BC). 81

Figure 41. Total dissolved gas time series comparisons near Columbia River Mile 323.5 for the MCN Summer 1996 pool study (TM-BC)..... 82

Figure 42. Simulated and observed velocities near John Day dam on May 23, 1997. 85

Figure 43. Simulated spatial velocity distribution in JDA pool just downstream from McNary Dam for the Spring 1997 case. 86

Figure 44. Total dissolved gas pressure and saturation time series comparisons near Columbia River Mile 227.7 for the JDA Spring 1997 study (TM-BC)..... 87

Figure 45. Total dissolved gas pressure and saturation time series comparisons near Columbia River Mile 227.7 for the Spring 1997 study (TM-BC). Air/water gas exchange option activated. 89

Figure 46. Simulated and observed depth-averaged velocities near The Dalles dam on June 24, 1997..... 93

Figure 47. Simulated spatial velocity distribution in TDA pool upstream of The Dalles Dam..... 94

Figure 48. Temperature and total dissolved gas time series near Columbia River Mile 201.2 during the Summer 1997 pool study (TM-BC). 95

Figure 49. Total dissolved gas time series comparisons at the river mile 201.2 during the TDA Summer 1997 pool study (TM-BC)..... 96

Figure 50. Simulated and observed depth-averaged velocities near Columbia River Mile 146.5 on 6-26-1997..... 99

Figure 51. Simulated spatial velocity distribution upstream of Bonneville Dam..... 100

Figure 52. Total dissolved gas pressure and saturation time series comparisons near
Columbia River Mile 175.6 for the BON Summer 1996 study period (TM-BC)... 101

Figure 53. Simulated and observed depth-averaged velocities near Columbia River Mile
120.5 on 7-18-1997..... 104

Figure 54. Simulated spatial velocity distribution downstream of Bonneville dam..... 105

Figure 55. Total dissolved gas pressure and saturation time series comparisons near
Columbia River mile 122.6 for the TID Spring 1996 study period (FMS-BC). 106

Tables

Table 1. Gas fractions used to compute gas mass concentrations from gas pressures (Colt, 1984). Mole fractions are for atmospheric air. 9

Table 2 Summary of cases that were simulated..... 58

Table 3. Statistical summary of measurements and simulations at river mile 123.7 during the LGR Spring 1997 pool study..... 64

Table 4. Percentage of time during the simulation where the computed value is within the given variance compared to the measurements at rivermile 123.7 for the LGR Spring 1996 study. 64

Table 5. Summary of model performance compared to field measurements for LGO pool. Table shows the number of occurrences within and outside of the RMS error noted. 69

Table 6. Statistical summary of measurements and simulations at River Mile 059.2 during the LMN Summer 1997 study (TM-BC). 73

Table 7. Percentage of time during the simulation where the computed value is within the given variance compared to the measurements at River Mile 059.2 during the Summer 1997 study (TM-BC). 73

Table 8. Summary of model performance compared to field measurements for LMN pool. Table shows the number of occurrences within and outside of the RMS error noted. 75

Table 9. Summary of model performance compared to field measurements for IHR pool. Table shows the number of occurrences within and outside of the RMS error noted. 79

Table 10. Statistical summary of measurements and simulations for the MCN Summer 1996 pool study (TM-BC)..... 83

Table 11. Percentage of time during the simulation where the computed value is within the given variance compared to the measurements. MCN Summer 1996 pool study (TM-BC). 83

Table 12. Summary of model performance compared to field measurements for MCN pool. Table shows the number of occurrences within and outside of the RMS error noted. 84

Table 13. Statistical summary of measurements and simulations at river mile 227.7 during JDA Spring 1997 pool study. 88

Table 14. Percentage of time during the simulation where the computed value is within the given variance compared to the measurements at river mile 227.7 for the Spring 1997 study (TM-BC). 88

Table 15. Statistical summary of measurements and simulations at river mile 227.7 during Spring 1997 pool study. Air/water gas exchange option activated. 90

Table 16. Percentage of time during the simulation where the computed value is within the given variance compared to the measurements at river mile 227.7 for the JDA Spring 1997 study (TM-BC). Air/water gas exchange option activated. 90

Table 17. Summary of model performance compared to field measurements for JDA pool. Table shows the number of occurrences within and outside of the RMS error noted. 91

Table 18. Statistical summary of measurements and simulations at Columbia River mile 201.2 during the TDA Summer 1997 pool study (TM-BC). 97

Table 19. Percentage of time during the simulation where the computed value is within the given variance compared to the measurements at Columbia river mile 201.2 during the TDA Summer 1997 study (TM-BC)..... 97

Table 20. Summary of model performance compared to field measurements for TDA pool. Table shows the number of occurrences within and outside of the RMS error noted. 98

Table 21. Statistical summary of measurements and simulations near Columbia River mile 175.6 during the BON Summer 1996 study period (TM-BC). 102

Table 22. Percentage of time during the simulation where the computed value is within the given variance compared to the measurements near Columbia River mile 175.6 for the BON Summer 1996 study period (TM-BC). 102

Table 23. Summary of model performance compared to field measurements for BON pool. Table shows the number of occurrences within and outside of the RMS error noted. 103

Table 24. Statistical summary of measurements and simulations near Columbia River mile 122.6 during the TID Spring 1996 study (FMS-BC)..... 107

Table 25. Percentage of time during the simulation where the computed value is within the given variance compared to the measurements at river mile 122.6 for the TID Spring 1996 study (FMS-BC). 107

Table 26. Summary of model performance compared to field measurements for TID. Table shows the number of occurrences within and outside of the RMS error noted. 108

Table 27. Summary of model performance compared to field measurements for all simulated cases. Table shows the number of occurrences within and outside of the RMS error noted. 109

Two-Dimensional Hydrodynamic, Water Quality, and Fish Exposure Modeling of the Columbia and Snake Rivers. Part 1: Summary and Model Formulation

Under Biological Services Contract DACW68-96-D-0002, Delivery Order No. 8, Battelle Pacific Northwest Division developed and applied a two-dimensional hydrodynamic, water quality transport model, and fish exposure model to the Lower Columbia and Snake River systems. This work reported herein is an element of the U.S. Army Corps of Engineers Dissolved Gas Abatement Program (DGAS).

The present document, Part 1 of the report series, presents the mathematical formulation, numerical solution procedures, and also provides a summary and examples of the model application results. The application of the model to each individual reservoir or pool for each field data study period resulted in a very large number of graphics and tabular output. Thus it was determined that a summary document would be helpful to introduce the general features and results of the modeling work. Parts 2 through 10 of the report series (Richmond and Perkins (1998a-i)) provide additional details for each pool in an appendix-style format.

1 Introduction

The principal goal of the U.S. Army Corps of Engineers (USACE) Dissolved Gas Abatement Program (DGAS) is to reduce dissolved gas supersaturation (DGS) associated with the eight federal hydroelectric dams on the Lower Columbia and Snake rivers. Reductions in dissolved gas supersaturation are needed to move toward meeting water quality criteria and might also reduce mortality in both anadromous and resident fish populations caused by gas bubble trauma (GBT). To achieve this goal, the USACE is examining a number of design alternatives that include modifications to dam structures as well as dam operations. To evaluate the effectiveness of the different gas abatement alternatives, the relative reduction in DGS has been chosen as one basis for comparing the various alternatives.

In order to address the complex nature of DGS distributions in the river system and biological exposure, numerical models of gas transport, gas mixing, and dynamic gas bubble trauma were developed. These models couple flow, DGS production, DGS transport, and fish distribution information with a dynamic GBT mortality model. These tools provide the capability to perform comparative evaluations of the various gas abatement alternatives and to identify those alternatives that are most effective in reducing DGS in the river system.

Two models were developed and applied to the Lower Columbia and Snake Rivers in this study. Hydrodynamics (velocities and depths) and transport were numerically simulated using the Modular Aquatic Simulation System two-dimensional (MASS2) model. MASS2 simulates the depth-averaged (plan view) values of water surface elevation, velocity, temperature, and gas concentration. Note that since this is a physics-based

model incorporating the available river bathymetry data, it is capable of simulating both impounded and natural river conditions under drawdown alternatives.

Fish exposure to total dissolved gas and other impacts can be simulated using the Fish Individual-based Numerical Simulator (FINS) model. FINS provides the integration of the physical and biological models by tracking the space-time position and exposure history for groups of fish. The exposure histories, or logs, are then fed into the dynamic GBT Mortality Model described by Fidler (1998). The FINS model runs independently and uses output from MASS2 to define the velocities and lateral gas distribution information to the individual exposure model. FINS can provide a detailed picture of how different gas abatement alternatives affect exposure and the resulting mortality.

The geographic domain that the models were applied to is shown in Figure 1. The upstream limit of the model on the Columbia River is at Clover, Island near Kennewick, Washington. The upstream extent of the models on the Snake River is approximately 1 mile upstream on the Snake-Clearwater confluence near Lewiston, Idaho. The downstream end of the model domain is near Columbia River Mile 110 which is just upstream of the confluence with the Willamette River near Portland, Oregon. The models were applied to each individual reservoir or pool.

The overall report series is divided into a part for each application. The reservoirs or pools are: Lower Granite, Little Goose, Lower Monumental, Ice Harbor, McNary, John Day, The Dalles, and Bonneville. The final geographical section is referred to as the Tidal Reach which covers the area from below Bonneville Dam to Columbia River Mile 110.

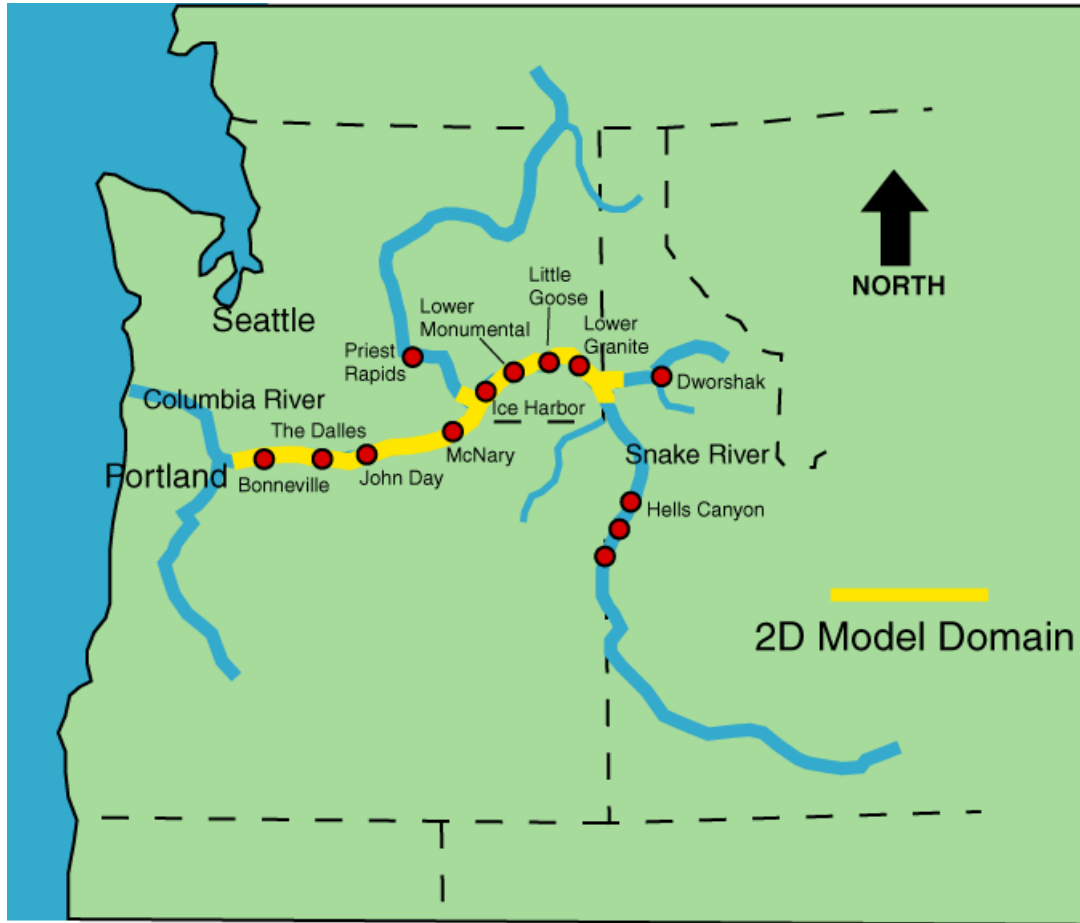


Figure 1. Geographical domain where the MASS2 two-dimensional hydrodynamic and water quality model was applied in this study.

2 MASS2 Hydrodynamics and Transport Model

MASS2 is a two-dimensional-depth averaged hydrodynamics and transport model. The model simulates time-varying distributions of the depth-averaged velocities, water temperature, and total dissolved gas. The model is coded in standard FORTRAN90 and runs on a WindowsNT (compiled with Digital Visual Fortran90) or a Silicon Graphics Unix system (compiled with MIPSpro Fortran90 version 7.2) platform.

The model is an unsteady finite-volume code that is formulated using the general principles described by Patankar (1980). The model uses a structured multi-block scheme on a curvilinear grid system. The coupling of the momentum and mass conservation (continuity) equations is achieved using a variation of Patankar's (1980) SIMPLE algorithm extended to shallow-water flows by Zhou (1995). Spasojevic and Holly (1990) give an example of a two-dimensional model of this type.

2.1 Coordinates and Grid System

The model is formulated using an orthogonal, curvilinear coordinate system. The governing equations are formulated in a conservation form using a full-transformation in the curvilinear system (Richmond, et al. 1986). The physical coordinates (x_1, x_2) are denoted by (x, y) . The orthogonal computational coordinates (ξ_1, ξ_2) are denoted by (ξ, η) . Note that the subscripts 1 and 2 in the following equations refer to the respective coordinate directions.

When the physical coordinate system is Cartesian, the metric coefficients take the form

$$h_1 = \left[\left(\frac{\partial x}{\partial \xi} \right)^2 + \left(\frac{\partial y}{\partial \xi} \right)^2 \right]^{1/2}$$

$$h_2 = \left[\left(\frac{\partial x}{\partial \eta} \right)^2 + \left(\frac{\partial y}{\partial \eta} \right)^2 \right]^{1/2}$$

where

h_1 = metric coefficient in the x_1 or ξ direction

h_2 = metric coefficient in the x_2 or η direction

(x, y) = Cartesian physical coordinates, i.e. State Plane coordinates

(ξ, η) = orthogonal computational coordinates

2.2 Hydrodynamics

Depth-averaged equations for the conservation of mass and momentum are the following:

Continuity (water mass conservation) Equation

$$h_1 h_2 \frac{\partial d}{\partial t} + \frac{\partial(h_2 d U)}{\partial \mathbf{x}} + \frac{\partial(h_1 d V)}{\partial \mathbf{h}} = 0 \quad (1)$$

where

d = water depth

t = time

U = depth-averaged velocity component in the \mathbf{x} direction

V = depth-averaged velocity component in the \mathbf{h} direction

U or \mathbf{x} -direction momentum equation

$$\begin{aligned} h_1 h_2 \frac{\partial(dU)}{\partial t} + \frac{\partial(h_2 d U^2)}{\partial \mathbf{x}} + \frac{\partial(h_1 d V U)}{\partial \mathbf{h}} + d \frac{\partial h_1}{\partial \mathbf{h}} U V - d \frac{\partial h_2}{\partial \mathbf{x}} V^2 = -g h_2 d \frac{\partial(z_b + d)}{\partial \mathbf{x}} \\ \frac{1}{r} \frac{\partial(h_2 d T_{11})}{\partial \mathbf{x}} + \frac{1}{r} \frac{\partial(h_1 d T_{21})}{\partial \mathbf{h}} + \frac{d}{r} \frac{\partial h_1}{\partial \mathbf{h}} T_{21} - \frac{d}{r} \frac{\partial h_2}{\partial \mathbf{x}} T_{22} + \frac{h_1 h_2}{r} (\mathbf{t}_{s1} - \mathbf{t}_{b1}) \end{aligned} \quad (2)$$

where

g = gravitational constant

ρ = fluid density

T_{11}, T_{21}, T_{22} = effective stresses

z_b = channel bottom elevation

\mathbf{t}_{b1} = bottom shear stress in the ξ -direction

\mathbf{t}_{s1} = surface shear stress in the ξ -direction

V or \mathbf{h} -direction momentum equation

$$\begin{aligned} h_1 h_2 \frac{\partial(dV)}{\partial t} + \frac{\partial(h_2 d U V)}{\partial \mathbf{x}} + \frac{\partial(h_1 d V^2)}{\partial \mathbf{h}} + d \frac{\partial h_2}{\partial \mathbf{x}} U V - d \frac{\partial h_1}{\partial \mathbf{h}} U^2 = -g h_1 d \frac{\partial(z_b + d)}{\partial \mathbf{h}} \\ \frac{1}{r} \frac{\partial(h_2 d T_{12})}{\partial \mathbf{x}} + \frac{1}{r} \frac{\partial(h_1 d T_{22})}{\partial \mathbf{h}} + \frac{d}{r} \frac{\partial h_2}{\partial \mathbf{x}} T_{12} - \frac{d}{r} \frac{\partial h_1}{\partial \mathbf{h}} T_{11} + \frac{h_1 h_2}{r} (\mathbf{t}_{s2} - \mathbf{t}_{b2}) \end{aligned} \quad (3)$$

where

T_{11}, T_{21}, T_{22} = effective stresses

z_b = channel bottom elevation

t_{b2} = bottom shear stress in the η -direction

t_{s2} = surface shear stress in the η -direction

The components of the stress tensor, T_{11}, T_{21}, T_{22} , are the so-called effective stresses and these are linearly related to the fluid strain rate in an incompressible fluid through the following equations:

$$\begin{aligned} T_{11} &= 2m e_x e_x \\ T_{22} &= 2m e_h e_h \\ T_{12} &= T_{21} = m e_x e_h \end{aligned} \quad (4)$$

where

$$\begin{aligned} e_x e_x &= \frac{1}{h_1} \frac{\partial U}{\partial \mathbf{x}} + \frac{V}{h_1 h_2} \frac{\partial h_1}{\partial \mathbf{h}} \\ e_h e_h &= \frac{1}{h_2} \frac{\partial V}{\partial \mathbf{h}} + \frac{U}{h_1 h_2} \frac{\partial h_2}{\partial \mathbf{x}} \\ e_x e_h &= \frac{h_2}{h_1} \frac{\partial}{\partial \mathbf{x}} \left(\frac{V}{h_2} \right) + \frac{h_1}{h_2} \frac{\partial}{\partial \mathbf{h}} \left(\frac{U}{h_1} \right) \end{aligned}$$

If a Bousinesq eddy viscosity model is used to represent the turbulence stresses then the viscosity coefficient in (4) is a turbulent eddy viscosity. A two-equation turbulence model could be introduced in the future if necessary.

Bottom shear stress is computed using the following equations:

$$\begin{aligned} t_{b1} &= r C_b U \sqrt{U^2 + V^2} \\ t_{b2} &= r C_b V \sqrt{U^2 + V^2} \end{aligned}$$

where the bed-friction coefficient is calculated based on the Manning n-value roughness using

$$C_b = g \left(\frac{n^2}{1.49 d^{1/3}} \right)$$

Surface shear stress resulting from wind can be computed using formulae similar to those above for bottom shear stress, but using a wind-stress coefficient instead.

2.3 General Scalar Transport

The governing equation for the transport of a scalar is obtained by applying the principle of conservation of mass to a fluid element. In orthogonal curvilinear coordinates the governing equation is

$$h_1 h_2 \frac{\partial(dC)}{\partial t} + \frac{\partial(h_2 dUC)}{\partial \mathbf{x}} + \frac{\partial(h_1 dVC)}{\partial \mathbf{h}} = \frac{\partial}{\partial \mathbf{x}} \left(h_2 \frac{\mathbf{e}_1}{h_1} \frac{\partial C}{\partial \mathbf{x}} \right) + \frac{\partial}{\partial \mathbf{h}} \left(h_1 \frac{\mathbf{e}_2}{h_2} \frac{\partial C}{\partial \mathbf{h}} \right) + h_1 h_2 S \quad (5)$$

where

C = scalar concentration per unit volume

ϵ_1 = turbulent diffusion coefficient in the ξ -direction

ϵ_2 = turbulent diffusion coefficient in the η -direction

S = source term

2.4 Dissolved Gas Transport

2.4.1 Governing Equation

The conservation equation for depth-averaged total dissolved gas is

$$h_1 h_2 \frac{\partial(dC)}{\partial t} + \frac{\partial(h_2 dUC)}{\partial \mathbf{x}} + \frac{\partial(h_1 dVC)}{\partial \mathbf{h}} = \frac{\partial}{\partial \mathbf{x}} \left(h_2 \frac{\mathbf{e}_1}{h_1} \frac{\partial C}{\partial \mathbf{x}} \right) + \frac{\partial}{\partial \mathbf{h}} \left(h_1 \frac{\mathbf{e}_2}{h_2} \frac{\partial C}{\partial \mathbf{h}} \right) + h_1 h_2 S_{TDG} \quad (6)$$

where

C = depth-averaged total dissolved gas concentration (mg/l)

S = sources and/or sinks of total dissolved gas

Calculation of TDG pressures and saturations from a given concentration or vice versa is accomplished using the relationships presented in Colt (1984). The mass concentration of TDG is computed as

$$C_{TDG} = \frac{(P_{TDG} - P_{H_2O}) b_{air}}{A_{air}} \quad (7)$$

where

C_{TDG} = apparent total dissolved gas concentration, mg/L;

P_{TDG} = total dissolved gas pressure, mm Hg;

$P_{\text{H}_2\text{O}}$ = vapor pressure of water, mm Hg;

b_{air} = apparent Bunsen coefficient for air, L/L·atm;

A_{air} = apparent molecular volume of air (with unit conversion), atm ·L/mg·
mm Hg;

Air is assumed to be composed of a limited number, N , of individual gases. These are shown in Table 1. The apparent Bunsen coefficient for air is computed as an aggregate of the Bunsen coefficients for individual gas fractions:

$$b_{\text{air}} = \frac{\sum_{i=1}^N b_i X_i}{\sum_{i=1}^N X_i} \quad (8)$$

where

b_i = Bunsen coefficient for gas fraction i , L/L·atm; and

X_i = mole fraction of gas i ;

The mole fractions used are those for atmospheric air and are shown in Table 1. Individual gas fraction Bunsen coefficients are computed, as functions of temperature and salinity (assumed zero), using relationships presented by Colt (1984, Appendix A), as is water vapor pressure, $P_{\text{H}_2\text{O}}$ ¹. The apparent molecular volume of air is also computed as an aggregate of individual gas fractions:

$$A_{\text{air}} = \frac{760}{1000} \left(\frac{\sum_{i=1}^N b_i X_i}{\sum_{i=1}^N K_i b_i X_i} \right) \quad (9)$$

where K_i is the ratio of molecular weight to molecular volume, g/L, for gas fraction i , the values of which are shown in Table 1.

¹ For brevity, these equations are not presented here.

Table 1. Gas fractions used to compute gas mass concentrations from gas pressures (Colt, 1984). Mole fractions are for atmospheric air.

Gas Fraction	X_i	K_i , g/L
Nitrogen (NO ₂)	0.78084	1.25043
Oxygen (O ₂)	0.20946	1.42903
Argon (Ar)	0.00934	1.78419
Carbon Dioxide (CO ₂)	0.00032	1.97681

2.4.2 Surface Gas Exchange

The source term for air/water gas exchange is of the form

$$S_{TDG} = K_L(C_* - C) \tag{10}$$

where

K_L = surface transfer coefficient (m/day)

C_* = saturation concentration of air at the water surface (mg/l)

The surface transfer coefficient as a function of wind speed is given by a curve fit to empirical data presented in O'Connor (1982, Figure 6 intermediate scale data).

A general cubic polynomial equation is currently implemented in MASS2 and the coefficients are:

$$K_L = -0.0045W^3 + 0.1535W^2 - 0.5026W + 0.6885$$

where

W = wind speed in meters per second (10 m above water surface)

The following figure graphically displays the relationship:

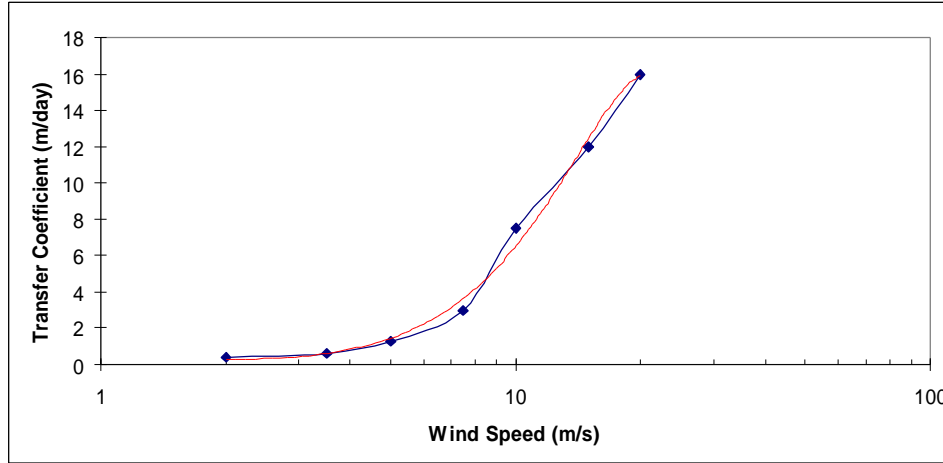


Figure 2. Empirical Transfer Coefficient Relationship. Symbols are field data presented in O'Connor (1982). Red line is a 3rd order polynomial curve-fit.

In the future, it may be desirable to implement a mechanistic surface gas exchange formulation along the lines presented by O'Connor. However, given the uncertainties associated with estimating the wind speed using remote measurements the curve-fit relationship is used in the model at this time.

2.5 Thermal Energy Transport

2.5.1 Governing Equation

Applying the principle of conservation of energy to a fluid volume, relating the internal energy to temperature, and then depth-averaging yields

$$h_1 h_2 \frac{\partial(dT)}{\partial t} + \frac{\partial(h_2 dUT)}{\partial \mathbf{x}} + \frac{\partial(h_1 dVT)}{\partial \mathbf{h}} = \frac{\partial}{\partial \mathbf{x}} \left(h_2 \frac{\mathbf{e}_1}{h_1} \frac{\partial T}{\partial \mathbf{x}} \right) + \frac{\partial}{\partial \mathbf{h}} \left(h_1 \frac{\mathbf{e}_2}{h_2} \frac{\partial T}{\partial \mathbf{h}} \right) + \frac{h_1 h_2 H}{\mathbf{r} c_v} \quad (11)$$

where

T = depth-averaged water temperature (deg C)

H = net heat flux at the water surface (W/m^2)

\mathbf{r} = water density ($= 1000 \text{ kg/m}^3$)

c_v = specific heat of water at 15 C° ($= 4186 \text{ J/kg-C}^\circ$).

2.5.2 Surface Heat Exchange

Heat exchange at the water surface is computed as the net heat flux which is represented as

$$H = H_{sn} + H_{an} - (H_b + H_e + H_c) \quad (12)$$

where

H = net surface heat flux (W/m^2)

H_{sn} = net solar shortwave radiation (W/m^2)

H_{an} = net atmospheric longwave radiation (W/m^2)

H_b = longwave back radiation (W/m^2)

H_e = heat flux due to evaporation (W/m^2)

H_c = heat flux due to conduction (W/m^2)

If measured radiation is available, the net solar shortwave radiation is computed as

$$H_{sn} = H_a(1 - R_s) \quad (13)$$

where

H_{sn} = net incoming short-wave solar radiation flux, W/m^2 ;

H_a = measured short-wave solar radiation, W/m^2 ; and

R_s = albedo or reflection coefficient;

The albedo is computed as (Brown and Barnwell, 1987)

$$R_s = A \left(\frac{180a}{p} \right)^B \quad (14)$$

where

a = solar altitude, radians.

$$A = \begin{cases} 1.18 & \text{for } C_L < 0.1 \\ 2.20 & \text{for } 0.1 \leq C_L < 0.5 \\ 0.95 & \text{for } 0.5 \leq C_L < 0.9 \\ 0.35 & \text{for } C_L > 0.9 \end{cases}$$

and

$$B = \begin{cases} -0.77 & \text{for } C_L < 0.1 \\ -0.97 & \text{for } 0.1 \leq C_L < 0.5 \\ -0.75 & \text{for } 0.5 \leq C_L \leq 0.9 \\ -0.45 & \text{for } C_L > 0.9 \end{cases}$$

When measured radiation is not available, net incoming short-wave solar radiation is estimated using (Brown and Barnwell, 1987)

$$H_{sn} = H_o a_t (1 - R_s) (1 - 0.65 C_L^2) \quad (15)$$

where

H_o = the radiation flux reaching the earth's atmosphere, W/m²;

a_t = atmospheric transmission coefficient; and

C_L = cloudiness as a fraction of sky covered.

H_o in (15) is estimated using (Wigmosta and Perkins, 1997, Appendix C)

$$H_o = H_{sc} \left(1 + 0.033 \cos \left[\frac{360n}{365} \right] \right) \sin a \quad (16)$$

where

H_{sc} = the solar constant, approximately 1360 W/ m²;

n = day of the year;

and the solar altitude is calculated using

$$\sin a = \sin f \sin d + \cos f \cos d \cos h \quad (17)$$

where

f = site latitude, radians;

d = declination of the sun, radians,

$$= 23.45 \frac{p}{180} \sin \left(2p \left[\frac{284 + n}{365} \right] \right); \text{ and} \quad (18)$$

h = hour angle of the sun, radians;

$$= \frac{p}{12}(T_s - 12) \quad (19)$$

T_s is the solar time, in hours, given by

$$T_s = T_l + \frac{12}{p}(L_{st} - L_{loc}) + E \quad (20)$$

where

T_l = local time, hours;

L_{st} = standard longitude for the local time zone ($120p/180$ for the Pacific time zone), radians;

L_{loc} = local longitude, radians; and

E = equation of time, hours

$$= (9.87 \sin 2B - 7.53 \cos B - 1.5 \sin B) / 60 \quad (21)$$

$$B = \frac{2p(n - 81)}{364}.$$

The net atmospheric longwave radiation is computed using formula 2.1.1 in Edinger, Brady, and Geyer (1974):

$$H_a = 4.4 \times 10^{-8} (T_a + 273)^4 [C_a + 0.031 \sqrt{e_a}] \quad (22)$$

where

T_a = air temperature (deg. C)

e_a = air vapor pressure (mm Hg)

C_a = Brunt's coefficient (average value = 0.65)

The longwave backradiation is computed using formula 2.1.4 in Edinger, Brady, and Geyer (1974):

$$H_b = e_w s^* (T_s + 273.15)^4 \quad (23)$$

where

T_s = water surface temperature (deg. C)

e_a = emissivity of water (= 0.97)

s^* = Stephan-Boltzmann constant (= 5.67×10^{-8} W/m²K⁴)

The evaporation heat flux is computed using formula 2.1.5 in Edinger, Brady, and Geyer (1974):

$$H_e = f(W)(e_s - e_a) \quad (24)$$

where

$f(W)$ = wind speed function = $9.2 + 0.46W^2$ (W/(m² mmHg))

W = wind speed (m/s)

e_a = air vapor pressure (mm Hg)

e_s = saturation vapor pressure of air at the water surface at T_s (mm Hg)

The conduction heat flux is computed using formula 2.1.11 in Edinger, Brady, and Geyer (1974):

$$H_c = 0.47 f(W)(T_s - T_a) \quad (25)$$

where

$f(W)$ = wind speed function = $9.2 + 0.46W^2$ (W/(m² mmHg))

W = wind speed (m/s)

e_a = air vapor pressure (mm Hg)

e_s = saturation vapor pressure of air at the water surface at T_s (mm Hg)

2.6 Discretization

The governing equations in the model are discretized using the finite-volume formulation described by Patankar (1980). The power-law scheme is used for the convective-diffusion terms. The time derivative is approximated using an implicit backward difference scheme. The reader is referred to Zhou (1995) for an example of the form of the discretization equations in a Cartesian coordinate system. The orthogonal curvilinear form of the discretization equations used herein reduce to the Cartesian form when the metric coefficients are unity.

It should be noted that the power-law scheme reduces to 1st order accuracy for high values of the grid Peclet number (advection-dominated cases) and therefore introduces artificial diffusion when the computational grid lines and streamlines are not aligned. In

the majority of the river system considered here the artificial diffusion should be minimal since the grid lines and streamlines will be approximately aligned with one another. Higher-order schemes can be used to minimize artificial diffusion but this increased accuracy comes at the price of additional computational effort that Ye and McCorquodale (1997) estimate to be 40-70% more than the power-law scheme. Presently MASS2 uses the power-law scheme, but it could be easily extended to include an option for a higher-order method.

2.7 Velocity-Depth Coupling

The coupling of the momentum and mass conservation (continuity) equations is achieved using a variation of Patankar's (1980) SIMPLE algorithm extended to shallow-water flows by Zhou (1995). Zhou's method has been extended here to orthogonal curvilinear coordinates in the present study. As in Patankar (1980), a staggered numerical grid is employed to avoid the computation of unrealistic depth and velocity fields.

2.8 Initial and Boundary Conditions

To numerically solve the system of governing equations initial and boundary conditions must be specified. Initial conditions for each dependent variable (velocity, depth, and species) are assigned at the start of each simulation either as approximate values or using the results of a previous simulation (i.e., hotstart or restart file). Boundary conditions are specified at each boundary. At the upstream boundary the incoming velocity or discharge is specified as a function of time for each cell and depth is extrapolated from the nearest interior cell. At the downstream boundary the depth for each cell is specified as a function of time and zero gradient conditions are assigned for the velocity. Along the shoreline, a zero gradient or slip condition is applied to the longitudinal velocity component and the normal velocity to the shore is set to zero. The depth is extrapolated from the nearest interior cell to the shore.

2.9 Solution Procedure

The discretization equations are implicit in space and time. The assembly of these equations for each numerical element results in a system of linear equations that are solved using a line-by-line tridiagonal matrix algorithm. Non-linearity and coupling of the equations are handled through an iterative solution procedure.

The overall solution procedure is summarized as follows:

1. Read in general parameters and input/output file specifications.
2. Read in computational grid data files.
3. Set initial conditions or read in a hotstart file from a previous simulation
4. Begin time marching loop

5. Begin hydrodynamic iteration loop
6. Compute discretization coefficients
7. Solve for velocity field
8. Solve for depth-correction field
9. Compute new depth field
10. Update velocity field using depth-corrections
11. Return to step 5 until mass source is reduced to the desired level or the maximum number of iterations for a time step are exceeded.
12. Solve scalar transport equation for each species
13. Write out data to output files
14. Return to step 4 for the next time step or stop if the ending date/time is reached.

2.10 Model Output

Simulation results from MASS2 are output as ASCII files that can be read by plotting and post-processing software. Time-series records can be obtained at any user specified cell location and time-frequency (i.e., every n time-steps). Spatial distributions over the computational domain can also be obtained at a user-specified time-frequency.

Since the output is in the form of ASCII files the user has great flexibility to choose the most appropriate graphics software. The plots in this report were produced using GNUplot (available at no-cost on the internet), TECPLOT from Amtec Engineering, and IDL from Research Systems, Inc.

2.11 Test Problems

Two tests are presented to verify the performance of the model. The first test case is a mixing problem in a short channel for which there is an analytical solution. This test was designed to verify the mass balance and transport equation solution method used in the model. The second test case is a slope break problem designed to test the capability of the model to the transition to uniform conditions in an open channel flow. In this case, comparisons can be made with analytical solutions for normal flow.

2.11.1 *Mixing of two streams in a straight rectangular channel:*

This test was conducted with a rectangular straight channel 4000 feet in length and 100 feet wide (W). At the upper end a constant discharge rate of 1000 cubic feet per second (cfs) was specified and at the downstream end the depth was specified to be 6 ft giving a cross-sectional average velocity (u) of 1.67 fps. The channel was uniformly discretized at

40 feet in the longitudinal (x) direction and 5 feet in the lateral (y) direction giving a grid size of 100 x 20.

A conservative tracer is continuously released at the upper boundary of the channel. The left half ($y < 50$ ft) of the channel has a higher concentration ($C = 200$ units/ft³) than the right half ($y > 50$ ft) at $C = 100$ units/ft³. Lateral mixing of the two plumes occurs downstream. At some location the two plumes are essentially completely mixed ($C = 150$ units/ft³). An analytical solution to this problem is available for model comparison. The analytical solution is made possible by the assumption of complete vertical mixing, homogeneous and isotropic diffusion coefficients, and a temporally and spatially constant flow field. The transverse mixing coefficient was set to 3 ft²/s. Comparison of the modeled plumes with this analytical solution provides the model verification of tracer transport. The analytical solution is (after Fischer et al , 1979):

$$C(x, y) = C_o \sum_{n=-\infty}^{\infty} \left(\operatorname{erf} \frac{y' + 1/2 + 2n}{\sqrt{4x'}} - \operatorname{erf} \frac{y' - 1/2 + 2n}{\sqrt{4x'}} \right) + C_b$$

where:

$$x' = xe_t / uW^2$$

$$y' = y / W$$

For this test problem was $C_o = 100$ units/ft³ and a background concentration (C_b) of 100 units/ft³ is added.

The longitudinal variation in concentration at $y = 40$ ft and $y = 60$ ft is shown in Figure 3. The agreement between the analytical and model solution is quite good. At the end of the channel the completely mixing concentration of 150 units/ft³ is achieved indicating that mass is conserved. Lateral tracer distributions are shown for the upper portion of the channel in Figure 4 for cross-sections at 400 and 1000 ft. Figure 4 shows lateral tracer distributions for the lower portion of the channel at cross-sections located at 2000 and 3000 ft. The numerical and analytical solution compare well; at $x = 2000$ ft the numerical solution underestimates mixing (though this within 0.15% of the analytical solution). The solutions at $x = 3000$ are indicated lateral mixing with a mixed value of 150 units/ft³. The modeled concentration distribution is shown in Figure 5.

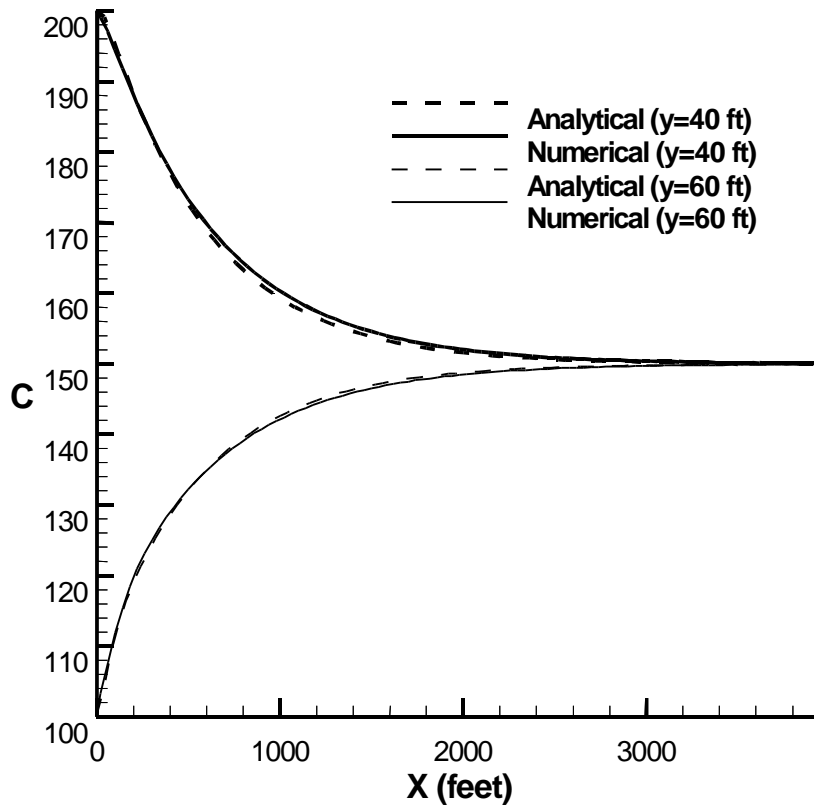


Figure 3. Longitudinal variation of concentration for Test 1; solid lines are model result and dashed lines are analytical solution (after Fischer et al 1979).

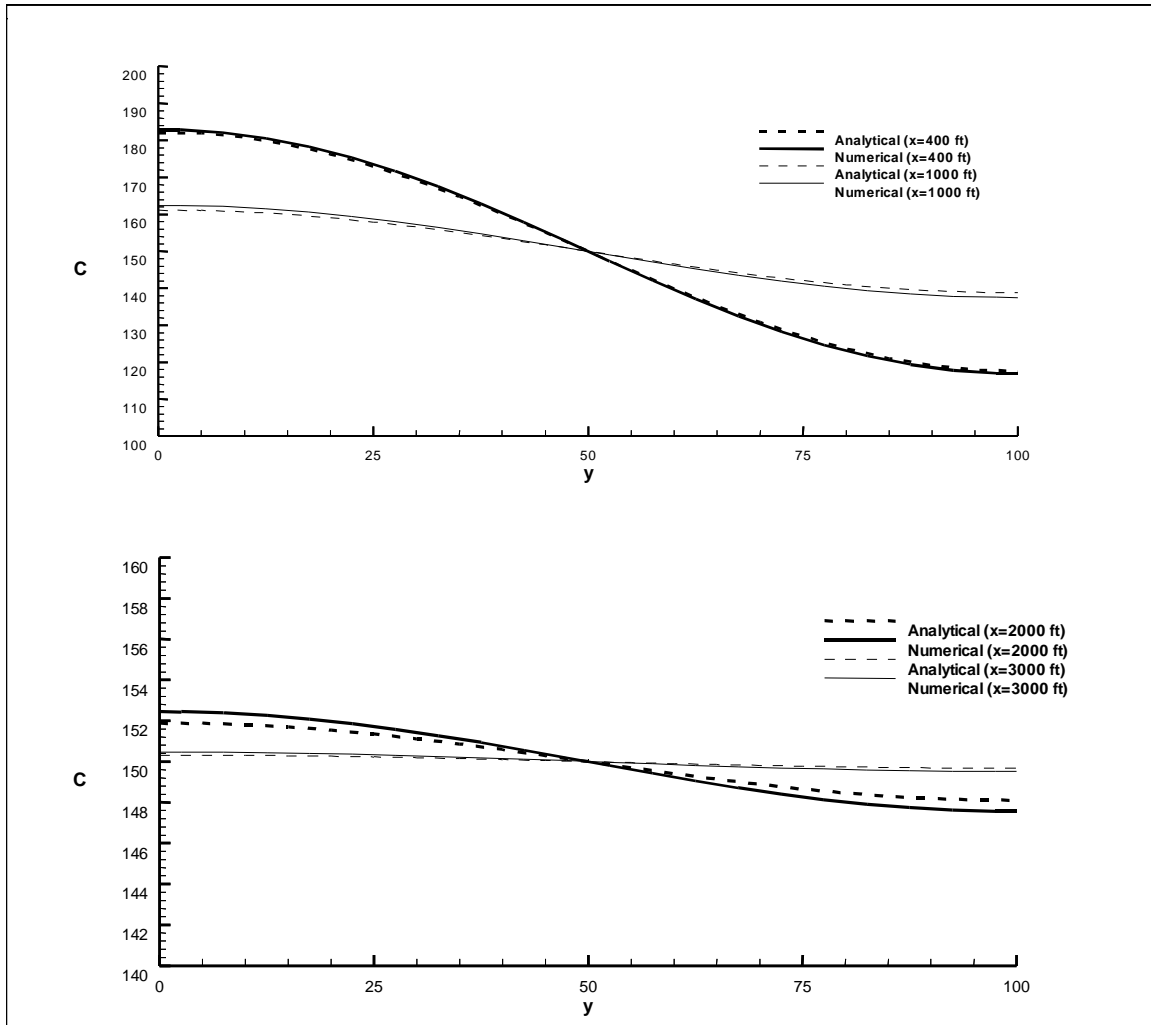


Figure 4. Lateral variation at x=400 ft and x=1000 ft (top), and x=2000 ft and x=3000ft (bottom); solid lines are numerical solution and dashed lines are analytical solution (after Fischer et al, 1979)

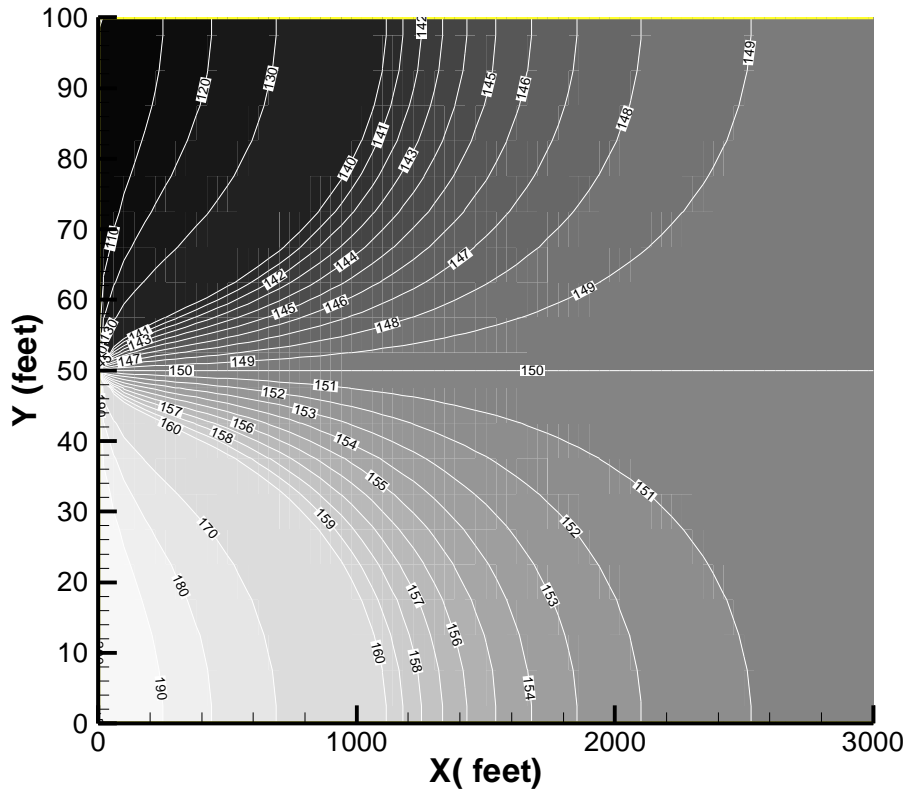


Figure 5. Horizontal distribution of conservative tracer for Test 1.

2.11.2 Normal Flow in a Straight Channel with a Slope Break

In the second problem, the channel is steeper in the upper half end with a slope of 0.0003 and in the lower half the slope eases to 0.0002. This gives a bed elevation drop of 6 feet in the upper half and 4 feet in the lower half for a channel length of 40,000 ft. The channel width was 400 ft. The Manning’s roughness coefficient was set to 0.035. The computational time step was 4 seconds. The uniform longitudinal and lateral discretization was 400 and 20 ft respectively. A 1000 cfs discharge is specified at the upper end of the channel and the downstream depth was held at 2.5 ft.

The analytical solution (in English units and for a wide channel) for the normal depth, y_n , and the normal cross-sectionally averaged velocity, u_n , are:

$$y_n = \left(\frac{Qn}{1.49w\sqrt{s}} \right)^{3/5}$$

$$u_n = \frac{Q}{wy_n}$$

In the upper half of the channel, the normal depth is 2.0804 feet (velocity 1.2017 fps). In the lower half the normal depth is 2.3495 feet (1.0641 fps). The downstream depth is held at 2.5 ft.

Because the downstream boundary depth (2.5 ft) is larger than the normal depth for the lower section of the channel, a backwater curve is expected where depths decrease in the upstream direction. If the channel is long enough, the depth should approach the normal depth for the lower portion of the channel. Where there is a break in the bed slope (i.e. at $x = 20000$ ft), a transition is expected. Further up the channel, the depth should again approach the normal depth for the upper portion of the channel provided that the upstream reach is long enough. Figure 6 shows the velocity profile after the simulation has converged and the depth profile. The analytical solution (using the above equations) for the normal flow are also shown. The agreement between the analytical and numerical solution is very good. The numerical solution at the top of the upper channel is a depth of 2.08 ft with a velocity of 1.202 ft/s; the errors are -.02% and +0.03% of the analytical values respectively. The numerical solution at the top of the lower channel is a depth of 2.35 ft with a velocity of 1.064 ft/s; the errors are -.02% and +0.01% of the analytical values respectively.

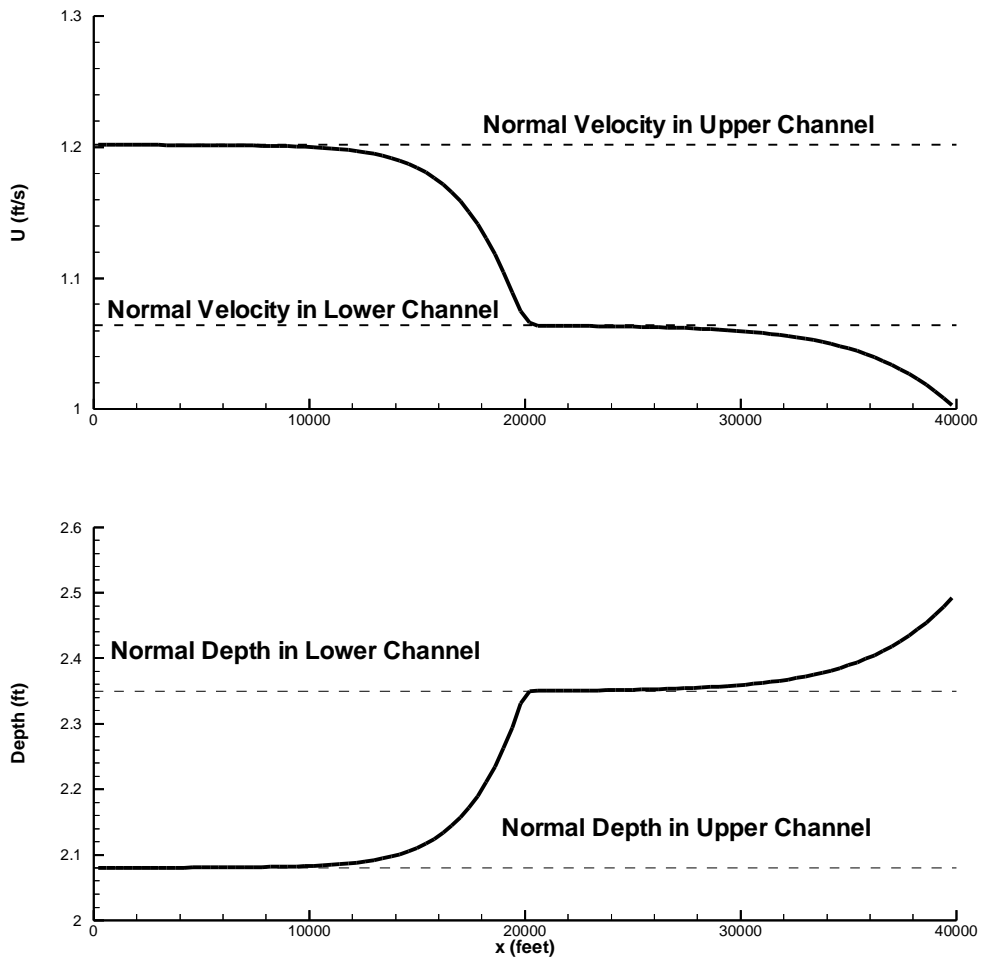


Figure 6. Velocity (top) and depth (bottom) profiles for Test 2; solid lines are numerical result; dashed lines are analytically derived normal velocity and depths for both upper channel- and lower channel.

3 FINS (Fish Individual-based Numerical Simulator) – Exposure Model

The Fish Individual-based Numerical Simulator (FINS) is the integrator of the physical and biological models. FINS works by tracking the space-time position and exposure history for groups of fish (the individual exposure model) and feeding those histories into the dynamic GBT Mortality Model (the biological effect model) developed by Fidler (1998). FINS can be applied pool-by-pool to evaluate the lateral mixing of gas plumes and the specific project details such as changes in spill patterns and the resultant effects on velocities, gas mixing, and fish exposure. FINS can provide a detailed picture of how different gas abatement alternatives affect exposure and the resulting mortality.

FINS tracks large numbers of fish groups through each pool as “particles” moving according to user defined rules. The space-time position of each fish group is recorded and their exposure history to dissolved gas can be logged. These records are called “exposure logs”. The 2D hydrodynamic and transport model provides velocity, temperature, and dissolved gas information that will be used to drive the fish group movement and exposure calculations. This approach is flexible in that different sets of user defined fish behavior rules can be assigned and directly compared using the same physical setting (velocity, temperature, and dissolved gas). Examples of “fish rules” include relative movement versus water particle movement, differences in day/night movement, species dependent behavior, different depth distributions, and site specific behavioral differences.

The exposure logs can then be fed into the dynamic gas bubble trauma mortality model (DBGTM) to assess biological impacts. The DBGTM model is described in Fidler (1998).

FINS is written in Fortran90 using Microsoft’s Visual Development Environment and Digital Fortran90 and runs on a Windows95/NT platform.

3.1 Background Review

A brief review of existing literature was made in two areas:

1. General information on particle-based simulation of individual fish movements
2. Specific information on salmonid smolt migration behavior relevant to simulation of individual fish movements

Based on this review, a number of potential factors that could be considered in simulations, and standard methods of performing such simulations, were identified. Smolt actions that should be considered for inclusion in the simulation approach include:

- Advection with local velocity (2D).
- Active swimming with or against current (1D) as function of degree of smoltification

-
- Change transverse location relative to thalweg (1D), preference for near-bank or mid-channel as function of species and age
 - Change vertical location (1D) as function of species-dependent depth preference, time of day.
 - Random dispersion (2D) to account for variations in individual behavior
 - Correlated dispersion (2D)
 - Reflection off boundaries (riverbank, bottom) (2D)
 - Forebay dam-crossing delay
 - Selection of dam passage route
 - Mortality (predation, dam passage, other)

3.2 Initial Design and Data Structure

The FINS code is modular, with separate modules for initial release, passage through individual reaches, and post-processing of output. Based on the factors and data needs identified in the background review, a data and code structure was developed. Note that FINS is being developed to operate in a stand-alone mode using previously computed and stored hydrodynamic, dissolved gas, and temperature data from the MASS2 model.

3.3 Release Module

The release module establishes the initial conditions for smolts (location, time of release, species type, etc.) at the beginning of the run. This module is written as an interactive, terminal-based application. It prompts the user for a number of input parameters that define the release characteristics for the batch of fish to be simulated, then writes the resulting information in a standard format that is used for initialization of the first reach as well as transfer of information between reaches.

The release module allows for a variety of different conditions for the initial distribution in time and space of released smolts. One or more smolt release batches can be defined, to accommodate multiple releases or multiple species types. The release location is specified in terms of river reach coordinates; fish can be released at a single point, uniformly over a line or rectangle, or randomly over a line or elliptical region. A pseudo-random number generator is used to represent random variability in release points; uniform and normal random distributions are provided as options for release locations. Time of release is specified in terms of hours relative to midnight on a reference date. The time of release of a batch of fish can be a single point in time, uniformly (deterministically or randomly) distributed over a time interval, or normally distributed with specified mean and standard deviation. The initial depth distribution can be all at a

single depth, uniform with depth, normally distributed with mean and standard deviation, or exponentially distributed with mean and maximum depths.

An example case was generated using the release module; selected results are plotted below. In this example, the center release point was 100 meters downstream from the top of the reach, and in the center of the channel. A normal (Gaussian) distribution of locations was specified with mean at the center release point and standard deviation of 25 meters in both downstream and transverse directions, effectively forming a quasi-circular release zone. The generated release points are plotted in Figure 1 below. The initial depth, in this example, was specified as an exponential distribution with mean depth of 2.0 meters and maximum depth of 15.0 meters. A frequency plot (histogram) of initial smolt depths as generated by the release module is shown in Figure 2 below.

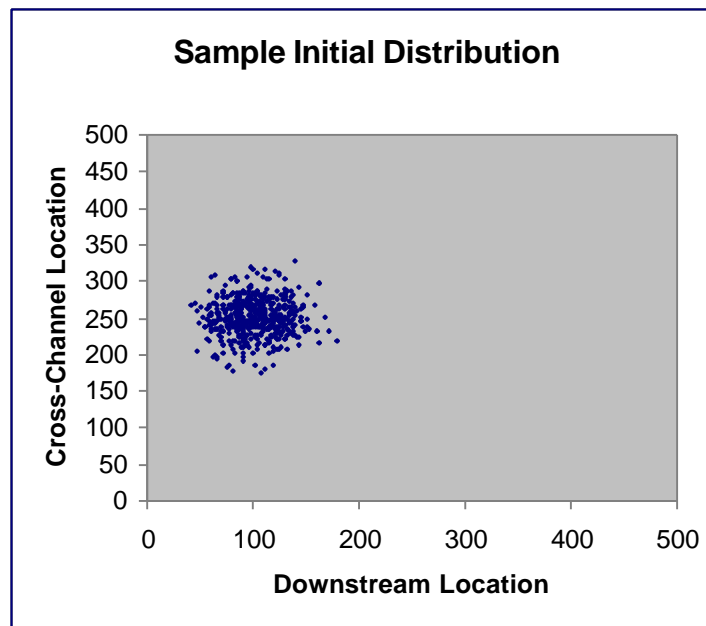


Figure 7. Generated release points in plan view of 500 smolts in a sample batch. A normal distribution of locations, centered at (100,250) was used.

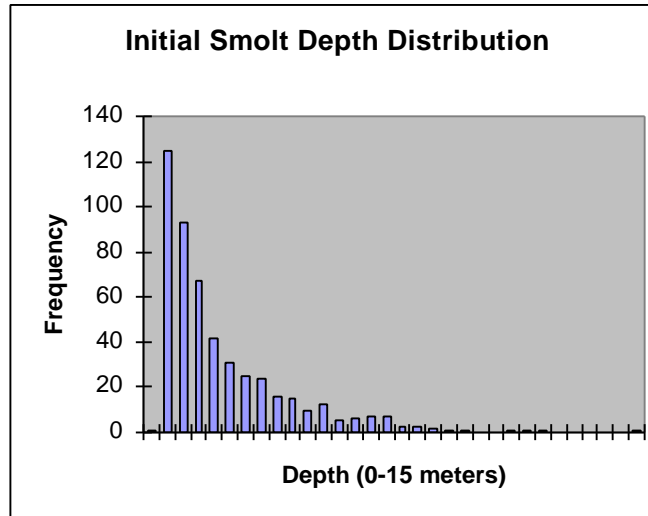


Figure 8. Histogram of generated initial depths for 500 smolts in a sample batch. An exponential distribution with mean depth of 2.0 meters and maximum Depth of 15 meters was specified.

3.4 FINS Main Module

The main module of FINS performs the numerical transport simulation. This module is written as an interactive, terminal-based application. It utilizes as input the initial fish descriptions generated by the release module and a configuration file containing control flags and transport parameters.

Downstream Migration

Downstream migration of smolts is represented by four general processes in FINS:

1. **Advection**: Passive movement with the local water velocity
2. **Dispersion**: Random variations in fish velocity (differing from local water velocity) that are linearly related to local water velocity. This essentially represents the apparent effects of water velocity variations at scales smaller than that explicitly modeled in the hydrodynamic simulation.
3. **Diffusion**: Random variations in fish velocity (differing from local water velocity) that are unrelated to local water velocity. This represents random velocity variations due to fish swimming and allows fish to move out of low velocity areas that they would otherwise be "stuck" in.

4. **Correlated Random Walk:** Both the diffusion and dispersion mechanisms are uncorrelated in space and time. However, it is reasonable to imagine that if a fish is swimming faster than the local water velocity at one time, it will probably also be doing so at the next time step. This is represented in the correlated random-walk model by a probabilistic correlation between the random velocity variations from one time step to the next.

The dispersion and diffusion processes are combined into a single diffusion-like process, where the effective diffusion coefficient is the sum of the specified diffusion coefficient and the product of the specified dispersivity and the local water velocity.

These processes are represented using three parameters. The advection process does not require any parameterization, since it is purely determined by the local water velocities as computed in the hydrodynamic code. The dispersion process is parameterized by the *dispersivity* (units of feet). The value of the parameter, since it represents sub-grid-scale velocity variations, should theoretically be smaller than the average grid spacing. The diffusion process is parameterized by the *dispersion coefficient* (units of ft²/sec). An overall diffusion coefficient (denoted D below) is obtained by combining the dispersivity and diffusion coefficient as follows:

$$D = D' + \alpha V$$

Where D' is the specified diffusion coefficient, α is the dispersivity, and V is the local water velocity. The values of dispersivity and diffusion coefficient are specified in terms of lateral (parallel to local flow direction) and transverse (perpendicular to local flow direction) components, and can be species-dependent.

Simulation of Changes in Depth

The hydrodynamic simulation is depth-averaged, two-dimensional. Therefore, modeled water velocity varies only in the plan view coordinates and cannot be used to drive changes in smolt depth. Three alternative processes have been implemented to allow variations in smolt depth (which in turn affects the depth-compensated total gas pressure even though dissolved gas concentrations do not vary vertically in the model). These three processes are:

1. **Linear preference model:** This model assumes that smolts are generally surface-oriented and have a specific preferred migration depth (distance from the water surface). This function provides a "driving force" to move fish toward the preferred depth at a rate that depends linearly on their current deviation from that depth. Note that this model does not provide any means of moving away from the preferred depth, so if used alone will lead to a constant smolt depth equal to the preferred depth (once the initial release conditions have been overcome). This model is parameterized by two parameters: 1) the preferred depth (in feet), and 2) the linear preference coefficient that scales the vertical velocity as a function of deviation from the preferred depth.

2. Exponential preference model: This model is similar to the linear preference model, but assumes that the strength of the vertical velocity toward the preferred depth is an exponential function of the deviation. This model is along the lines of that derived from principles of light dissipation with depth and preference of smolts for a particular level of light (see Zabel 1994). This model has three parameters: 1) the preferred depth (in feet), 2) a constant coefficient "psi", and 3) an exponent "alpha". Again, this model alone will not lead to any variation in depth.
3. Random vertical velocity model: This model used random vertical velocities generated in each time step. It is parameterized by a mean vertical velocity (drift), generally taken as zero, and a variance in vertical velocity. Random vertical velocities are assumed to be normally distributed, with the specified mean and variance. This model will usually be combined with models 1 or 2 above to generate random movements about a preferred depth, but can also be used alone to generate a purely random depth history.

3.5 Model Testing

3.5.1 Dispersion/Diffusion Testing

A rectangular model domain with a uniform velocity field was constructed as a test case for the dispersion and diffusion functions. Because the velocity is uniform and known, all spreading of particles is due to the dispersion/diffusion, and analytical descriptions of expected behavior are available. Based on advection/diffusion theory, the spatial variance of particle locations should increase linearly with time as:

$$s^2 = 2Dt$$

where D is the dispersion coefficient and t is time. Diffusion and dispersion function are combined into an overall dispersion coefficient D:

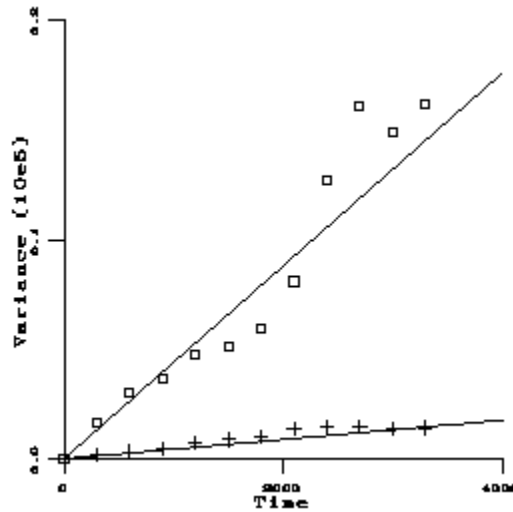
$$D = d_{loc} + \alpha V$$

where d_{loc} is the local diffusion coefficient (random fish behavior) and α is the dispersivity, V is the local velocity.

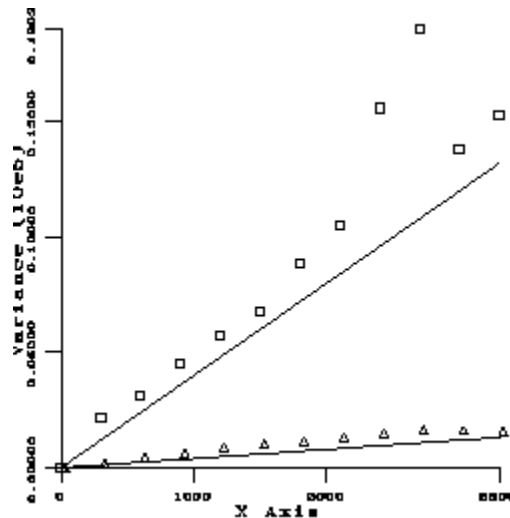
In contrast to the hydrodynamic dispersion, d_{loc} is not dependent on the local water velocity, but is purely random. This allows fish to "escape" from stagnant areas. Note that the hydrodynamic dispersion represents the effects of small-scale water velocity variations, below the scale of the computational grid, whereas the diffusion function represents random fish behavior.

For the tests, 100 particles were released into the field and tracked for 1 hour. The spatial variance of the particle locations parallel and transverse to the mean flow was computed every 5 minutes. The following plot shows the particle variances (longitudinal and transverse) as symbols, and the predicted linear relationship (based on the known

velocity and the imposed longitudinal and transverse dispersivities). This case is computed using only the dispersion (velocity-dependent diffusion) function. It can be seen from this plot that the particle behavior tracks well with the expected behavior, especially given the relatively small number of particles used to compute the simulation variances.



A second case was run using only the purely diffusive model (non-velocity-dependent). Again, as shown below, the model results and theoretical prediction are in good agreement.

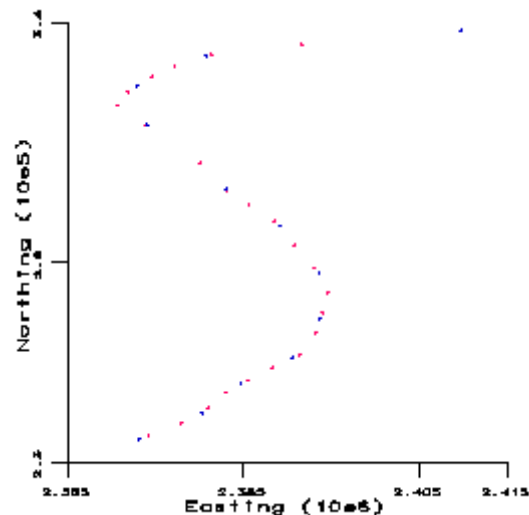


3.5.2 Testing of Numerical Time-Step Effects:

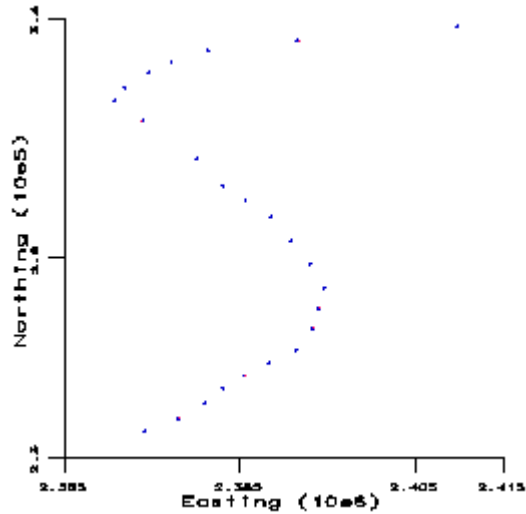
A series of model runs were made, using advection only (no diffusion or dispersion), with variable numerical time steps. The advection algorithm uses the local velocity experienced by a particle at the beginning of a time step to move it over that time step. In

the actual velocity field, velocities vary spatially, and therefore a small amount of numerical error is introduced by applying the velocity at the beginning of the time step over the whole time step. As the time step is decreased arbitrarily small, the error diminishes to zero. These tests were made to demonstrate that the time step being used is sufficiently small so as not to introduce significant numerical error into the model solution.

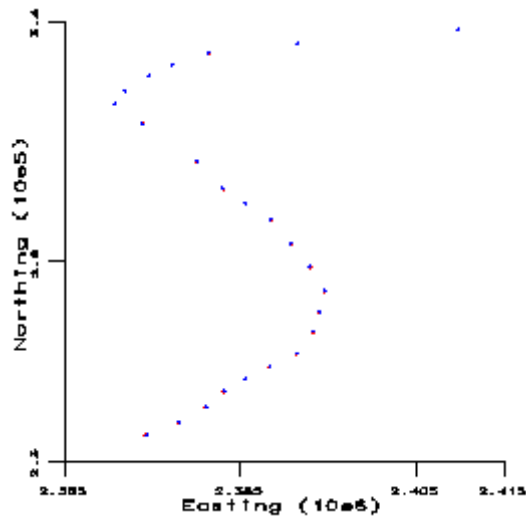
In the examples previously run, we have been using a time step (dt) of 50 seconds, chosen based on judgement of the relevant time scale of velocity variation spatially and temporally. Note that this is the same time step typically used for the transient hydrodynamic simulations on which the particle simulations are based. To test the validity of this time step, the same case was run at time steps of 12.5, 25, 50, and 100 seconds, and the resulting model predictions compared graphically. The graph below compares the results for $dt = 50$ seconds (red dots) and 100 seconds (blue dots). The dots represent the simulated locations of a single fish released at a specified point, at various times as it moves through the McNary pool. Since the two solutions do not directly overlie one another, there is clearly a noticeable effect introduced by increasing the time step from 50 to 100 seconds.



The next graph compares solutions for $dt = 50$ seconds (red dots) and $dt = 25$ seconds (blue dots). Here the two solutions nearly overlie one another, indicating that decreasing the time step to 25 seconds does not significantly improve the solution.



The final graph compares solutions at time steps of 12.5 seconds (red dots) and 25 seconds (blue dots). Again the two solutions are nearly coincident, indicating that no significant gain in solution accuracy is achieved by refining the time step further.



Based on these tests, it appears that a time step of 50 seconds provides an accurate solution while minimizing the computational demands of the model simulations.

3.6 Parameter Estimation from PIT Data and Correlated Random Walk Model

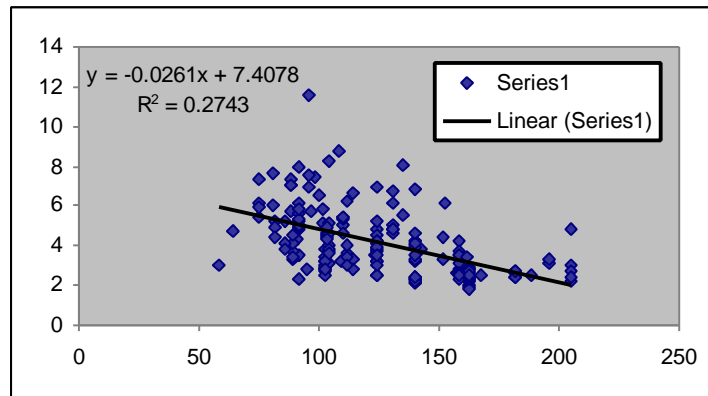
In this section we perform a preliminary travel time analysis based on 1996 PIT Tag data. PIT data was downloaded from the Pacific States Marine Fisheries Commission ftp site

(ftp.psmfc.org). Daily river flow data was downloaded from the University of Washington DART website (<http://www.cqs.washington.edu/dart/dart.html>).

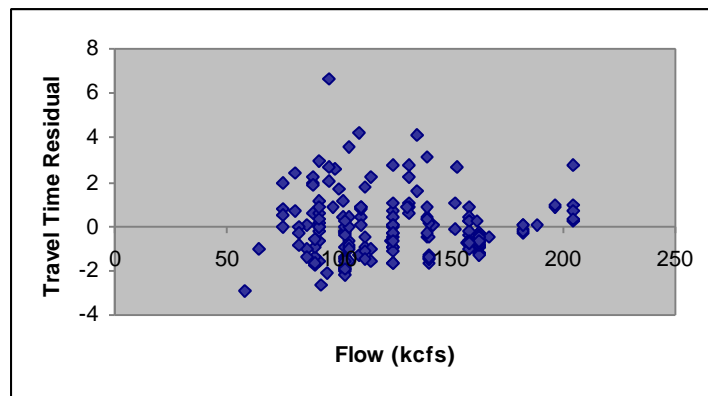
Scripts were developed to extract PIT records for which fish were observed both at Lower Monumental (LMN) and McNary (MCN) Dams (unfortunately there is no PIT tag interrogation facility at Ice Harbor Dam). Information stored in these extracted records includes the daily average flow at LMN on the day the fish passed LMN (kcfs), the daily average flow at LMN on the day the fish passed MCN (kcfs), the fish's recorded length in the LMN and MCN records, and the travel time between projects in days (computed from the date and time the fish was observed at each of the two projects).

3.6.1 Travel Time Versus Mean Flow

171 records were found in the 1996 PIT data for fish in this class observed at both LMN and MCN. The observed travel time (days) was first plotted against the flow rate at LMN on the date the fish passed LMN (kcfs):

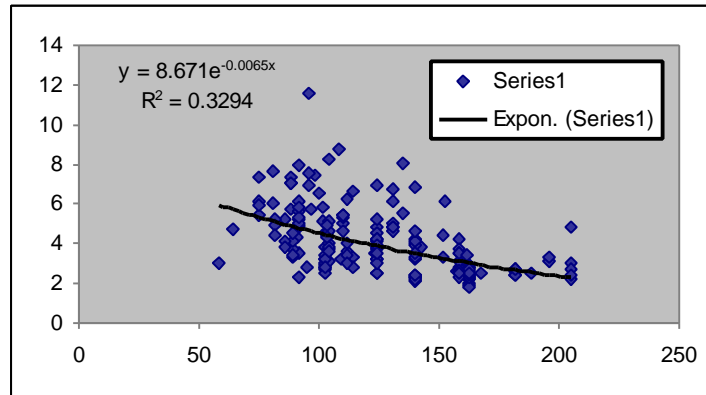


A linear trend line was fit to the scatter data, as shown on the graph above. To test the validity of this relationship, residuals (observed - estimated travel times) were computed and plotted versus flow:

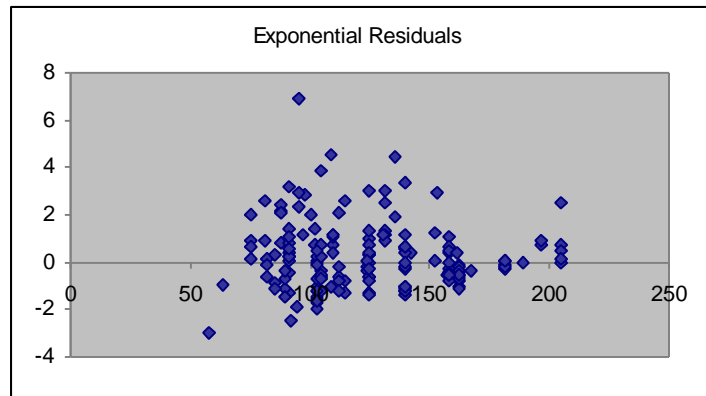


This plot indicates that variations from the linear model are fairly random (do not exhibit any systematic pattern), and that the linear model therefore explains well the portion of variability in travel time that is due to flow variability.

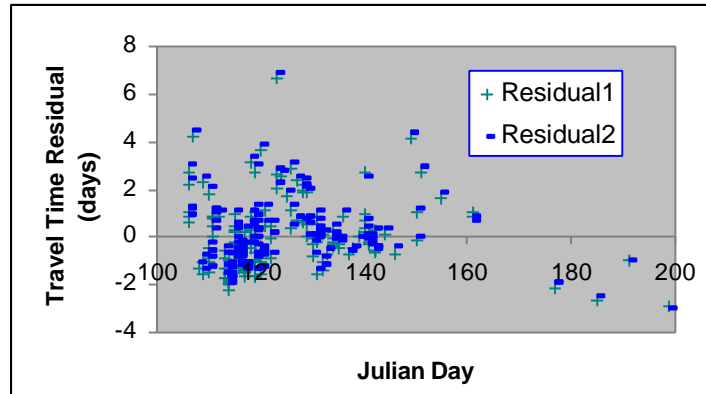
A slightly higher R^2 was obtained using an exponential model with a small degree of non-linearity:



The corresponding residuals are plotted versus flow below, and again do not exhibit any systematic pattern.



To determine whether any of the remaining variability can be explained by the start date, the residuals were plotted against start date. Below is a plot of start date (in Julian day) versus the linear and exponential residuals.



While the pattern doesn't appear to be totally random, it is difficult to identify any clear relationship.

"Clusters" of fish released at or passing LMN at very similar flows (probably on the same day) can be clearly identified in the flow vs. travel time plots above. Within these groups, there appears to be fairly consistent distribution of travel time with a range of ± 2 days around the mean travel time for the group. The mean travel time for each group is related to flow according to the regression equations (linear or exponential) defined above. Therefore, the largest proportion of variability not explained by total flow variations appears to be due to individual behavioral variations. These individual variations are represented in the FINS model in part by dispersion and/or diffusion mechanisms, characterized by a diffusion parameter.

3.6.2 Parameter Estimation (\hat{s})

From Zabel [1994, p.52], the maximum likelihood estimator (MLE) for \hat{s} (representing diffusion in the advection-diffusion equation representation of fish migration) is:

$$\hat{s} = L \sqrt{\frac{1}{N} \sum_{i=1}^N \left(\frac{1}{t_i} - \frac{1}{\bar{t}} \right)^2}$$

Where L is the distance between upstream and downstream observation points, N is the number of fish observed, t_i is the travel time of the i th fish, and \bar{t} is the mean travel time of the group. The distance from Lower Monumental to McNary dams is the difference between their location in river kilometers (measured from the mouth of the Columbia River):

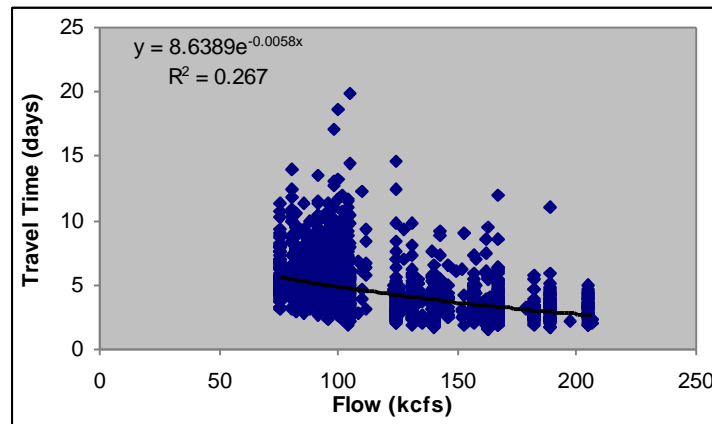
$$(599-470)*1000/0.3048 = 423230 \text{ feet}$$

Case 1: Wild Spring Chinook

The mean travel time between LMN and MCN for the 171 PIT tag records considered above (1996, wild spring chinook) is 4.136 days, which corresponds to an average travel velocity of approximately 1.18 feet/second. The estimated parameter \hat{S} , based on the method of Zabel [1994], is approximately 80,300 ft/day^{1/2}. This corresponds to a value of 24.5 km/day^{1/2}, which is consistent with the range of estimates reported by Zabel [1994, Table 4.2, p. 69]. In our representation of the advection-diffusion equation, the dispersion coefficient D corresponds to $\sigma^2/2$ in Zabel's equation 4.3. Therefore, we estimate $D = 3.22 (10^9) \text{ ft}^2/\text{day}$. If we consider only the velocity-dependent portion of D , $D = \alpha V$ where V is the mean velocity and α is the "dispersivity". This leads to an α of approximately 31,500 feet. Note that this is the longitudinal dispersivity; no estimate of transverse dispersivity can be obtained from PIT data. Also, the value of D or α for use in a fully two-dimensional model with varying velocity should be smaller than those derived for a one-dimensional model, because the effects of lateral, along-stream, and temporal velocity variations (lumped into the one-dimensional dispersion coefficient) are explicitly represented in the two-dimensional model.

Case 2: Hatchery Spring Chinook

In this case, there are many more observations (2013) available. The results in terms of the MLE parameter estimates are very similar to Case 1 ($D = 3.31 (10^9)$ and mean velocity = 1.03 feet/second). The relationship between flow and travel time (shown in the plot below) is also very similar to Case 1.

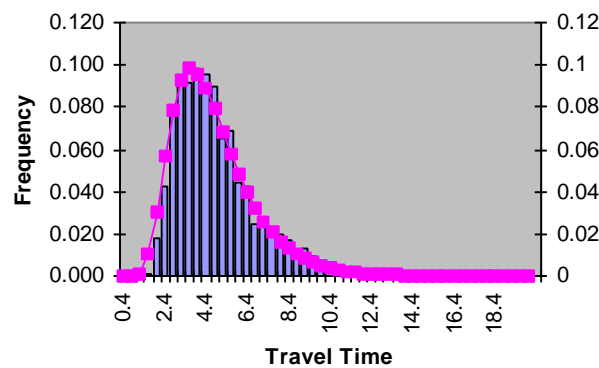


However, the variability in travel time is smaller at higher flow rates, perhaps representing the fact that under high flows there are fewer slack water areas in the river, and therefore less opportunity for individual fish behavior to affect the travel times. The individual variability appears to be larger for hatchery fish than for wild fish, with travel times for groups of fish passing on the same day varying by as much as 12 days or more.

The arrival time distribution can be derived from the basic advection-diffusion model to give (from Zabel, 1994, p. 49):

$$g(t) = \frac{L}{\sqrt{2ps^2t^3}} \exp\left(\frac{-(L-rt)^2}{2s^2t}\right)$$

Using the MLE parameter estimates derived from the data ($r = 27.21$ km/day; $\sigma = 24.78$ km/day^{1/2}; $L = 129$ km), the arrival time distribution predicted by the model can be computed and compared to the actual histogram of arrival time data, as in the graph to the left (bars = data; line/symbols = model):



Although we have not performed a rigorous model test, the data and the model visually appear to conform quite well.

Relationship to FINS Model:

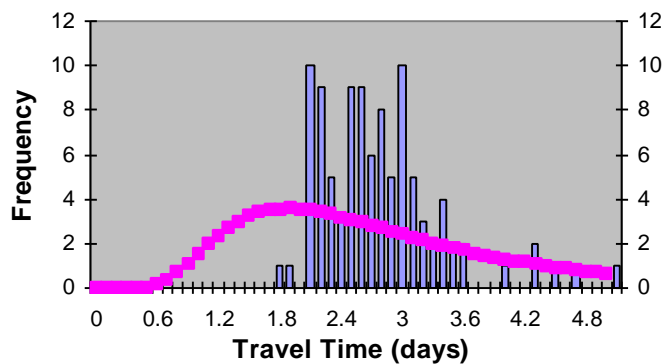
In the FINS model, the average rate of fish migration (r) is not specified in this "lumped parameter" fashion. Instead, fish move with the local flow velocity, as provided from the hydrodynamic model results. There is an ensuing mean migration rate for any particular simulation run, but it results from the combined effects of all the local velocities experienced by each fish, rather than being specified *a priori*. However, the dispersion is modeled using a random-walk procedure, and therefore an *a priori* estimate of σ (or actually D or α in our formulation) is required. Because some of the variability reflected in the estimate of σ above will be explicitly accounted for by virtue of variable local velocities, we expect that the appropriate value of σ to use in the FINS model will be something smaller than that derived directly from the PIT data. The FINS model was executed using 100 fish and a variety of trial values of σ , and the results compared to the lumped model prediction using the parameters derived from the PIT data and the PIT data histogram itself, therefore providing a calibration of the FINS model parameterization to the PIT data.

The FINS model is configured to simulate fish movement from Ice Harbor Dam (IHR) to McNary Dam (MCN), a distance of 78 km (48.5 miles). Flow conditions used were from

the hydrodynamic model simulation corresponding to time: 07-08-1996 12:00:00. Combined "dispersion" and "diffusion" effects were simulated with parameters as follows:

α_L	1000	ft
α_T	100	ft
D_L	1000	ft ² /se c
D_T	100	ft ² /se c

Even using these unreasonably large parameter values (see discussion below), the model is unable to reproduce the degree of variability in travel times observed in the PIT tag data. The graph to the right shows the histogram of simulated travel times (in days) as vertical bars, and the distribution as predicted using the 1D advection-diffusion with parameters estimated from the PIT tag data as the curve with square symbols.



Comparing the FINS simulation results to the lumped-parameter model fitted to the PIT data, we observe two things:

1. The degree of variability (spread) in travel times is smaller in the FINS results, and
2. The peak is slightly later in the FINS results (indicating a slower mean fish velocity).

The mean fish velocity from the PIT data is 27.2 km/day, and that derived from the FINS simulation is 28.4. However, considering that there is no explicit control of the rate parameter "r" in FINS, this is a fairly good correspondence. Also, there is likely to be some variation of "r" as a function of flow rate (see Zabel [1994]) which has not been

considered in the parameter estimate used here. Therefore, the reasonably good correspondence lends support to the conceptualization of passive advection of fish with the local water velocity as the dominant mode of average migration.

The variability in arrival times, on the other hand, is problematic. Consider the implications of a longitudinal diffusion coefficient (diffx) of $1000 \text{ ft}^2/\text{sec}$:

$$dx = \text{DSQRT}(24.0 * \text{diffx} * dt)$$

The maximum displacement in a single time step is given by $dx/2$ where dx is defined in the line of code above. (Note: in the FINS code, the calculations are performed on a transformed grid, which requires scaling dx by a metric coefficient, not shown in this code fragment. However, this part represents the corresponding displacement in the real coordinate system.) Assuming a time step dt of 50 seconds, the maximum displacement is approximately 550 feet, which would require a sustained swimming velocity of 11 feet/second for 50 seconds. Combine this with a velocity-dependent dispersion of another $1000 \text{ ft}^2/\text{sec}$ (assuming a local flow velocity of 1 ft/sec), and the fish now has to swim more than 20 ft/sec for 50 seconds to achieve the maximum dispersive displacement. And even under these unrealistic conditions, the simulated results do not have the degree of variability required to match the PIT tag observations. We conclude, therefore, that while a 1D lumped-parameter model based on a simple advection-diffusion approach can reproduce observed travel time distributions well in a population sense, the individual behavior implied by this model is entirely unrealistic.

As a point of reference, we used the FINS simulated arrival times using the parameters above as input to the MLE parameter estimation methods and obtained a value of $9.9 \text{ km/day}^{1/2}$, which can be compared to a value of $25.8 \text{ km/day}^{1/2}$ estimated from the 1996 PIT tag data as well as values ranging from 15.7 to 39.6 reported by Zabel [1994, p.69]. Again, these values imply local dispersive displacements that are unrealistic given actual fish swimming abilities.

There are several possible approaches that could help to bring FINS simulation results and PIT tag observations into agreement while maintaining realistic fish swimming velocities:

1. Use a velocity preference model wherein some fish preferentially seek low velocity flows and others seek high velocity flows. The degree of preference could be related to fish age or length, with more mature fish tending to stay in high velocity areas of the river. Because a given fish would consistently experience high (or low) velocities, the cumulative effect over time would be to reduce (or increase) the overall travel time relative to other fish, and thereby increase the variability in travel times without requiring high swimming velocities at any particular time step.
2. Introduce a deterministic swimming function that would be added on to (or subtracted from) the local water velocity, again perhaps as a function of fish maturity. With a negative (against the flow) swimming function, a fish could

actually "hold up" in low-velocity regions for some time; a positive swimming function would allow some fish to arrive at the downstream point significantly ahead of the corresponding water packet.

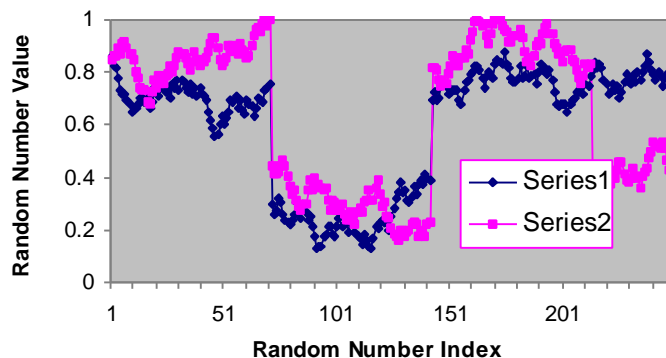
3. Introduce a dam-passage delay at the MCN endpoint (since PIT tags are not interrogated until the fish has entered the bypass facility). If the delay time were variable (probabilistic), overall travel time variability would be enhanced.
4. Use a correlated random-walk approach, wherein the dispersive component of migration at any particular time step is correlated to that in the previous time step. This is intuitively sensible, since a fish moving fast relative to flow in one time step is likely to continue in the same manner in the next time step. In fact, this is similar to items 1 and 2 above, both of which would have the effect of correlated behavior over extended periods of time.

3.7 Correlated Random Walk Test:

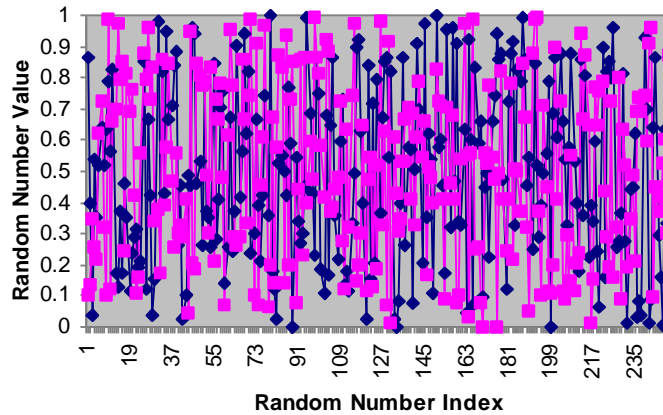
FINS contains a subroutine (random number module) to generate a correlated sequence of random numbers (as dispersive displacements). The input configuration file allows the user to select whether to use a correlated or uncorrelated random walk method. The actual dispersion code (behavior module, subroutine "disperse") is the same in either case; the only difference is that the random number series in the correlated case is modified to introduce temporal correlation. The method used to introduce correlation is:

$$r_i = r_{i-1} + a(x_i - 0.5)$$

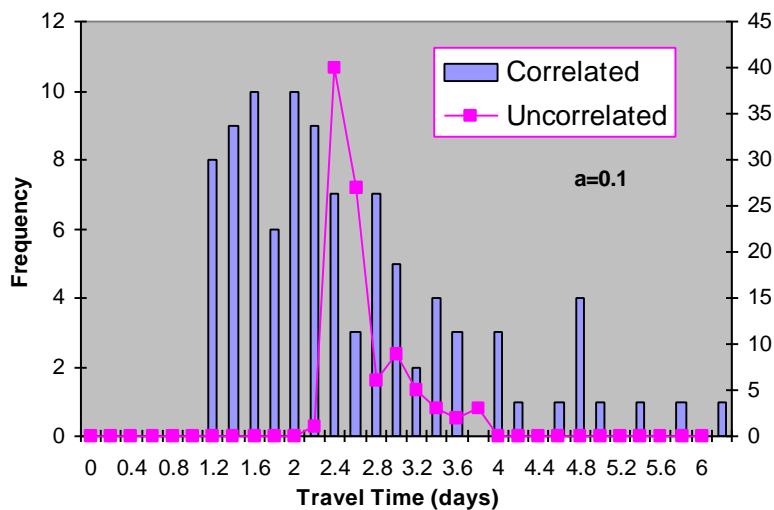
where r_i represents the sequence of random variates to be generated, x_i is a uniform pseudo-random variate on the interval [0,1] (generated using IMSL library functions), and a is a parameter that controls the degree of correlation. Intuitively, a represents the degree of change in the random number allowed from one time step to the next (if $a = 1$, the maximum possible change is 0.5). If a is zero, the sequence is perfectly correlated. This approach is along the lines of a first-order mixed autoregressive-moving average (ARMA) model (e.g., Payne (1982), p. 201). In this implementation, the values of r_i are further constrained to the interval [0,1] by truncating any values outside that range. An example sequence generated using $a=0.1$ is shown in the figure below:



In this example, each fish is moved for 72 time steps (1 hour), requiring two sequences of random variates of length 72 (one for longitudinal and one for transversal dispersion). Three series, and part of a fourth, are shown. For comparison, the corresponding sequence of completely uncorrelated random numbers is shown below.

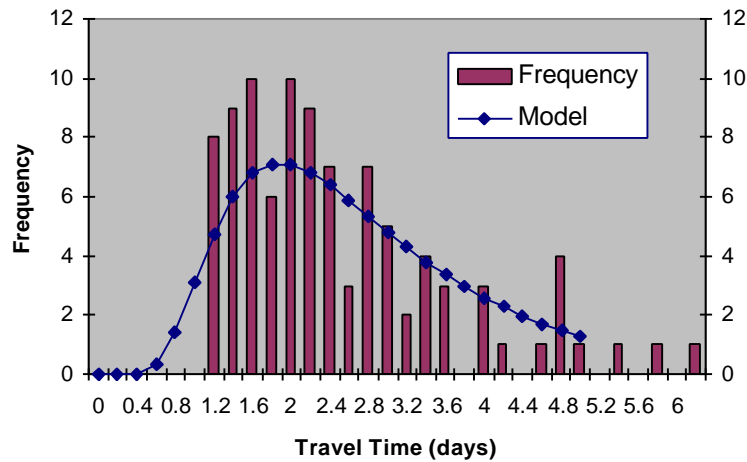


The same test case as described in the above sections was run, this time using both uncorrelated and correlated ($a=0.1$) sequences of random numbers. However, the overall dispersion coefficient was set to a value of $75 \text{ ft}^2/\text{sec}$ (corresponding to a maximum fish sustained swimming velocity of $3 \text{ ft}/\text{sec}$), divided between velocity-dependent ($25 \text{ ft}^2/\text{sec}$) and velocity-independent ($50 \text{ ft}^2/\text{sec}$) components. Note that these values are 1) much smaller than the values used above to try to match the PIT tag data using uncorrelated displacements, and 2) physically plausible. A comparison between the arrival time distributions under the correlated and uncorrelated cases is shown below.



As expected, the correlated random walk method leads to a much wider distribution of arrival times (note that uncorrelated is plotted on the right vertical axis; correlated on the left vertical axis).

The graph below shows the comparison between the modeled arrival distribution from FINS (using correlated random walk) and the arrival distribution from the 1D lumped-parameter model fitted to the PIT tag data. The fit is much better than the uncorrelated random walk results, and employs parameters that have plausible physical interpretation. Therefore, the correlated random-walk method appears to be a much superior representation to the pure advection-dispersion method with uncorrelated local displacements.



Using the 100 simulated (FINS) travel times as input to the MLE parameter estimate method of Zabel [1994], the corresponding σ is $23.3 \text{ km/day}^{1/2}$, close to the value of 24.8 derived from the PIT data and within the range of values reported by Zabel [1994].

3.7.1 Travel time variability due to velocity variations only

The correlated random walk quantifies an aspect of fish behavior -- how a fish moves relative to the local velocity it is experiencing. However, some of the variation in travel time observed is due simply to the different local velocities experienced by fish at different locations in the river. To evaluate the contribution of hydrodynamic velocity variations on travel time distribution, we ran the FINS model with a small transverse diffusion coefficient of $2 \text{ ft}^2/\text{sec}$ (using only non-velocity dependent "diffusion"), and no longitudinal diffusion or dispersion, which allows fish released at the same point in time and space to spread out laterally and thereby sample different velocities within the velocity field but does not affect their downstream position.

The simulated travel time distribution is very narrow, with all fish arriving in 2.2 to 2.6 days (as opposed to the 1 to 6 day range suggested by the PIT data). The MLE estimate of σ derived from the simulated travel times is $1.0 \text{ km/day}^{1/2}$, much smaller than that derived from the PIT data. The mean travel rate is 33.0 km/day , as opposed to 32.4 km/day using the correlated random walk and 27.2 km/day estimated from the PIT data; these deviations are probably within the range of variability caused by large-scale flow fluctuations and may not be significant.

This result suggests that the "average" fish is passive in its migration (as suggested by Smith, 1982), moving with the bulk river flow. However, individual fish vary widely in their behavior in a way that cannot be explained by passive movement with locally-varying velocities; some fish consistently move more slowly than the average flow and others swim rapidly downstream. This behavior appears to be represented fairly well by the correlated random walk method.

3.7.2 Possible Concerns

Although the correlated random walk leads to adequate representation of the population arrival times (based on PIT data), and does so while employing a parameterization that is consistent with fish swimming abilities, there remain some practical concerns that may significantly impact dissolved gas exposure histories. Foremost among these is the likelihood that "slow" fish will tend to frequent shallow, slow-moving areas of the river for extended periods of time, and "fast" fish will tend to frequent the main channel areas where flow rates are high. While this behavior is well-represented macroscopically (i.e., in terms of population arrival times) by the correlated random walk, the actual positions of "slow" and "fast" fish in the river at various times is not directly controlled by this method. That is, a "slow" fish in the model could be in a fairly high velocity area and be exhibiting strong swimming against the flow (not a likely scenario in the river, at least over a sustained time period). Or a "fast" fish in the model could be swimming rapidly through low-velocity areas, again probably not a physically realistic scenario over a sustained time period. To alleviate this problem, we should consider adding a behavioral component to the model that is related to velocity- or depth-preference, varying by individual (perhaps as a function of age or length).

3.8 Post-Processing Module

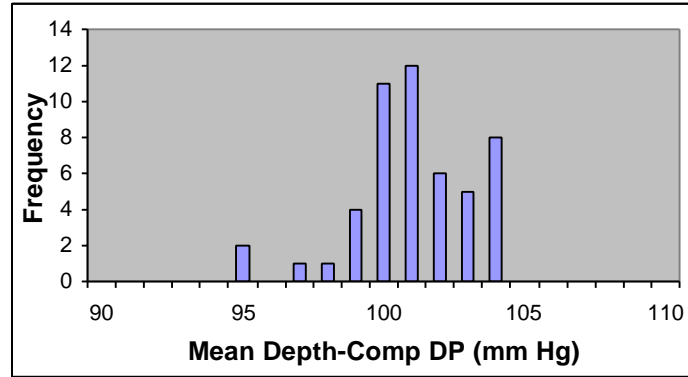
A large number of particles over a long period of time can be simulated without experiencing problems with memory or computer time limitations. A test run using 1000 particles moving over a two-day simulation period was made successfully. Because of the large size of the output data files resulting from larger runs, a binary output format was adopted for printing gas, temperature, and depth histories to disk.

A post-processing module (FINS PostPro) was developed. This code, written as an interactive, terminal-based application, reads in the binary output file created by the FINS main module, and summarizes the individual fish histories in two ways:

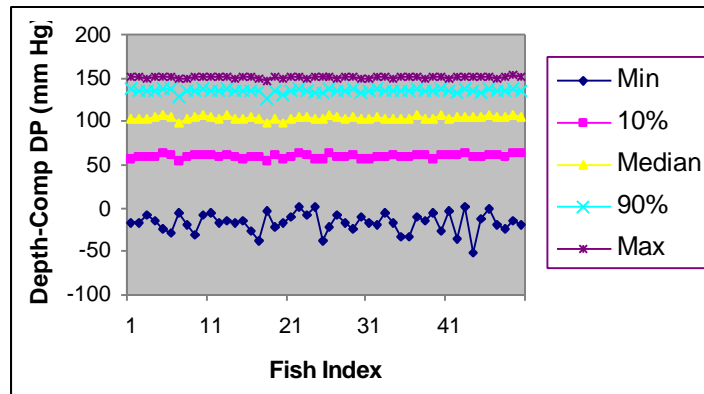
1. Average of dissolved gas, temperature and depth over all fish at each time step (ensemble averaging), and
2. Average and specified quantiles of dissolved gas exposure levels for each individual simulated fish. The mean and median dissolved gas level experienced by each fish is computed, along with the minimum and maximum observed by each fish and the 10th and 90th quantiles.

In both cases, the user can specify with an input flag which measure of dissolved gas level is desired (e.g., TDG in mg/L, TDG Pressure in mm Hg, Depth-compensated delta-P (mm Hg), etc.)

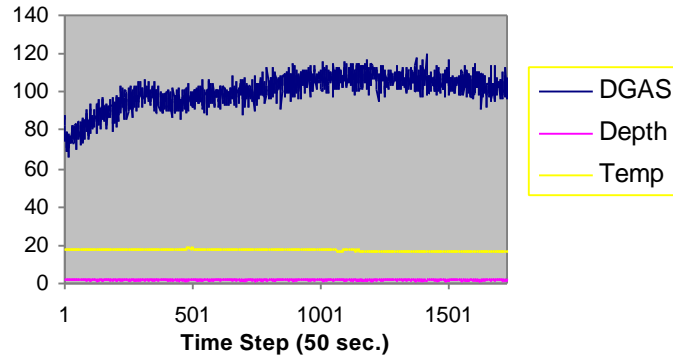
Example graphs using the output from the post-processor are shown below:



Histogram of the mean depth-compensated delta-P (mm Hg) experienced by each of 50 simulated fish "particles".



Quantiles of depth-compensated delta-P levels experienced by each of 50 simulated fish particles.



Average history of depth, temperature, and dissolved gas level (depth-compensated delta-P), averaged over all 50 fish.

3.9 Current Status of FINS

The field data necessary to complete the parameterization and verification of FINS were not available in time to complete those tasks. Thus there are no example applications at this time that compare the simulated fish movement to radio tracked or hydro-acoustically monitored fish. The necessary data will become available in late 1998 for McNary pool and FINS can then be parameterized and verified using those data.

4 Model Application

The section discusses the general aspects of the application of the models to the eight reservoirs and the tidal reach. Typical examples are provided of the procedures, data types, and data sources that were used in each application.

4.1 Model Grid and Bathymetry

The computational grids were generated using the Gridgen 9.1 code. Gridgen 9.1 is software for the generation of 3D, multiple block, structured grids. The code was developed for NASA Ames Research Center (Steinbrenner and Chawner, 1995).

To create the grid, a data file containing discrete geographical locations that outline the river shoreline was imported to Gridgen. In Gridgen, curves containing the data points were created and joined to enclose 2-dimensional flow regions. Grid spacing was set in each flow region and the grids were smoothed using the Gridgen elliptic solver. The elliptic solver was used to minimize grid twist and skew. The flow regions were then joined end to end in the downstream direction to make up the entire flow domain and the entire 2-dimensional grid was written to file. Typical model grids are shown in Figure 9.

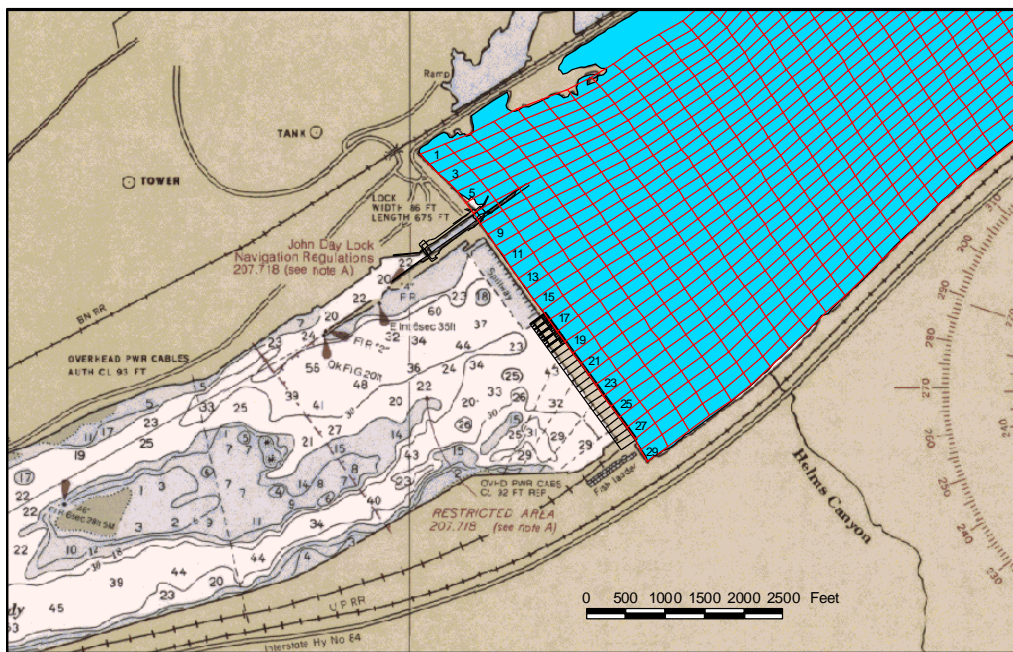
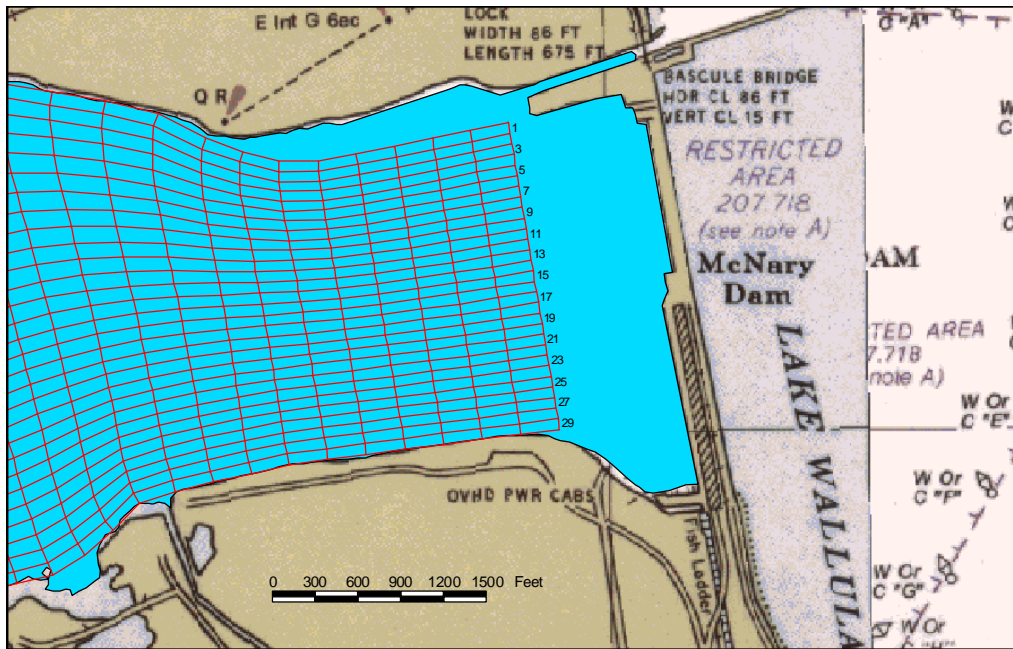


Figure 9. Model grid near McNary (above) and John Day (below) dams.

Once the grid was created three-dimensional representations of the river bottom and surrounding shoreline were used to generate bottom elevations for the hydrodynamic

model. Bathymetric data for the Columbia and Snake Rivers was gathered from the various sources; data were primarily obtained from USACE Portland and Walla Walla Districts and NOAA navigational charts. Figure 10 shows a typical set of bathymetric survey data near Ice Harbor Dam. Using the Arc/Info® GIS software system, the data was converted to a consistent coordinate system and datum, and combined to build a triangular irregular network (TIN), which represented the river bottom and shore as a three-dimensional surface. An example of a bathymetric surface for The Dalles pool is shown in Figure 11. Once the surface was produced, it was “sampled” at the necessary grid locations to produce the bathymetry required by the hydrodynamic model grid.

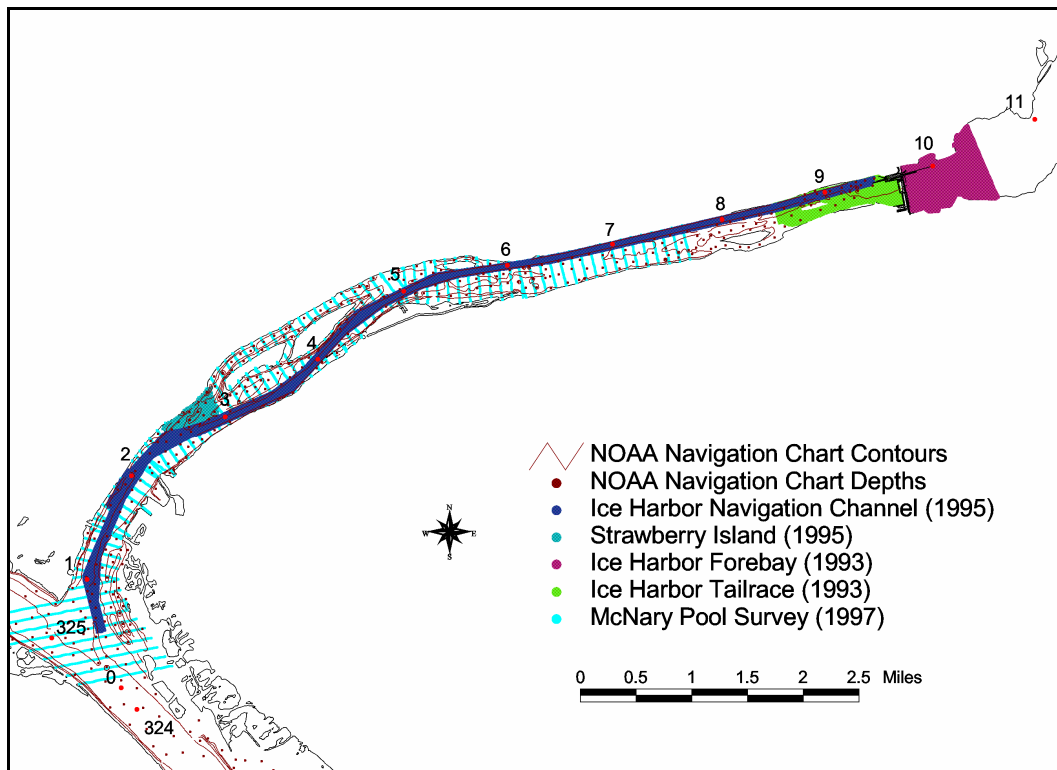


Figure 10. Bathymetric data near Ice Harbor dam.

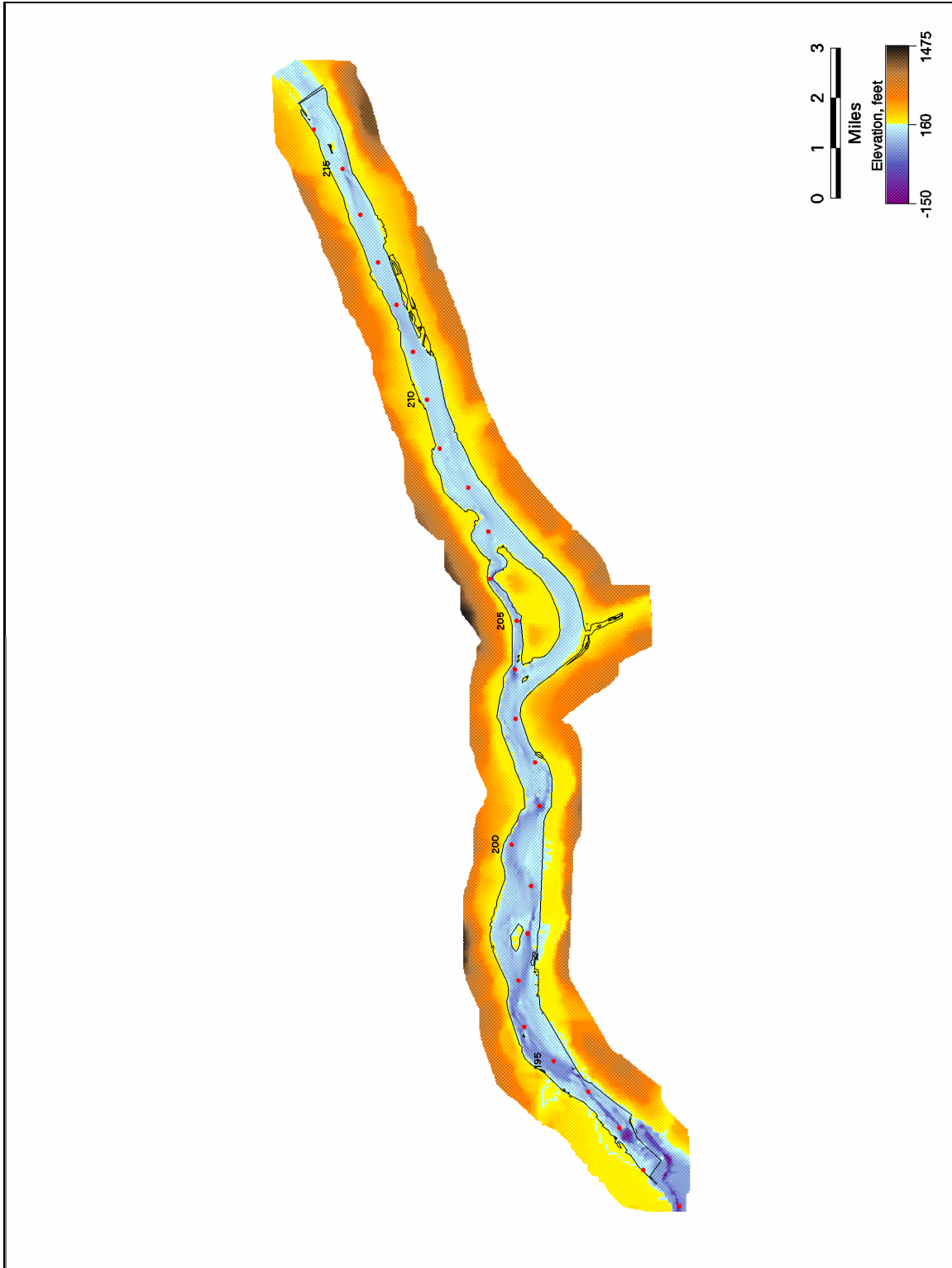


Figure 11 Color representation of The Dalles pool bathymetric surface

4.2 Boundary and Initial Conditions

Once the model grid has been developed for a particular case, the next step in the application process is to develop the boundary and initial conditions. Initial conditions are the starting or initial values of the dependent variables throughout the model grid domain. Boundary conditions are values of the dependent variables or source terms (i.e. surface heat transfer) that are assigned at the upstream, downstream, and water surface boundaries of the model. A steady-state simulation can be performed by holding the boundary conditions constant in time and running the model until the dependent variables no longer change as a function of time. Assigning time-varying boundary conditions yields an unsteady simulation. All of the simulations are unsteady unless otherwise noted.

4.2.1 Project Operations

Project operations data from CHROMS were used to establish the inflow discharges and forebay elevation at the upstream and downstream model boundaries. These data provided hourly spillway flow, power house flow, and forebay elevation. The Dalles Pool Summer 1996 study period provides an example (shown in Figure 12 and Figure 13) of a typical set of hourly total spill powerhouse flows, and forebay elevation conditions. These flows and elevations were uniformly distributed across the corresponding part of the model grid.

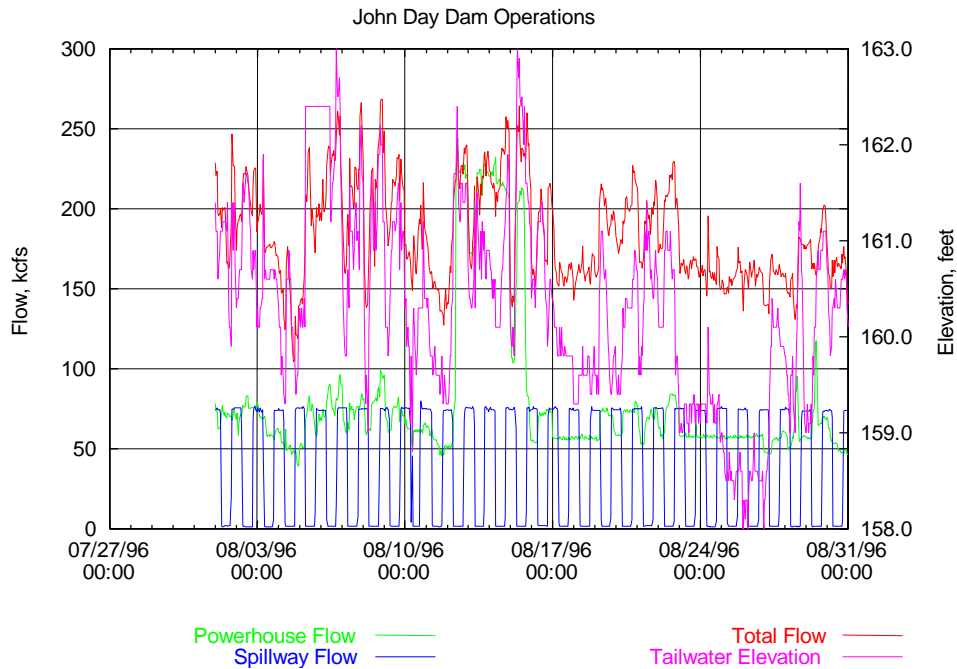


Figure 12. John Day dam operations during The Dalles Summer 1996 study.

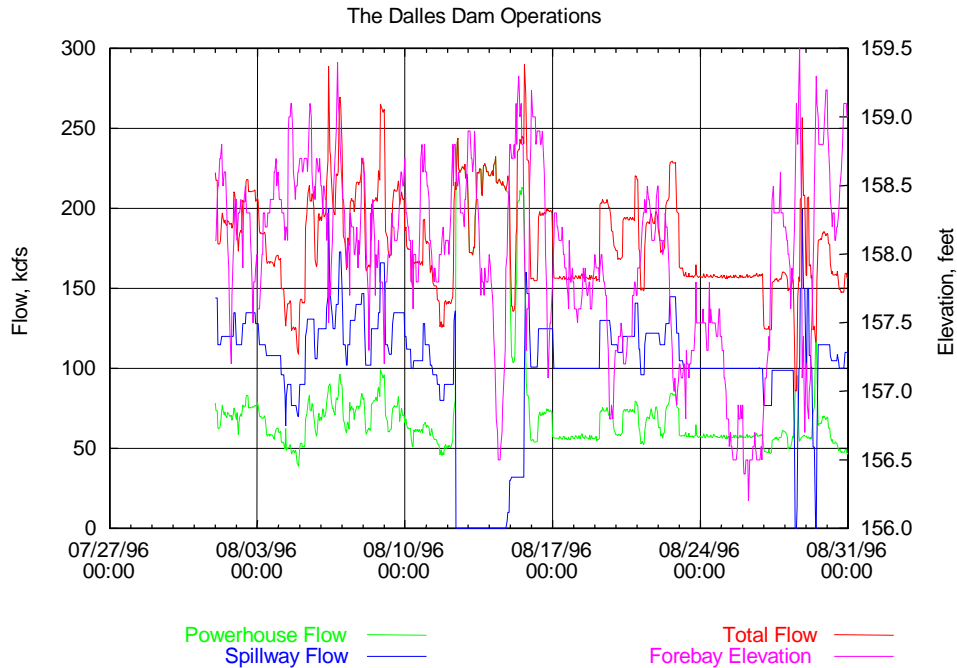


Figure 13. The Dalles Dam operations during The Dalles Summer 1996 study period.

4.2.2 Water Quality

In each case an initial set of simulations were done using the latest regression equations relating TDG production to spillway discharge and forebay fixed monitor (FMS) data for temperature and turbine TDG levels to assign inflow boundary conditions. These cases are identified as FMS-BC.

Data from the permanent fixed monitor located at the upstream dam forebay was used to establish temperature at the upstream model boundary. Station data were taken from the FMS database. Temperatures measured by the station (example shown in Figure 14) were used for both spillway and powerhouse flow. TDG pressures measured by the station (example shown in Figure 15) was used to compute TDG concentrations (example shown in Figure 16) for the power house flow. Spillway TDG gas pressures and concentrations (examples also shown in Figure 15 and Figure 16, respectively) were estimated using the TDG sourcing function (gas production equation) for the upstream dam.

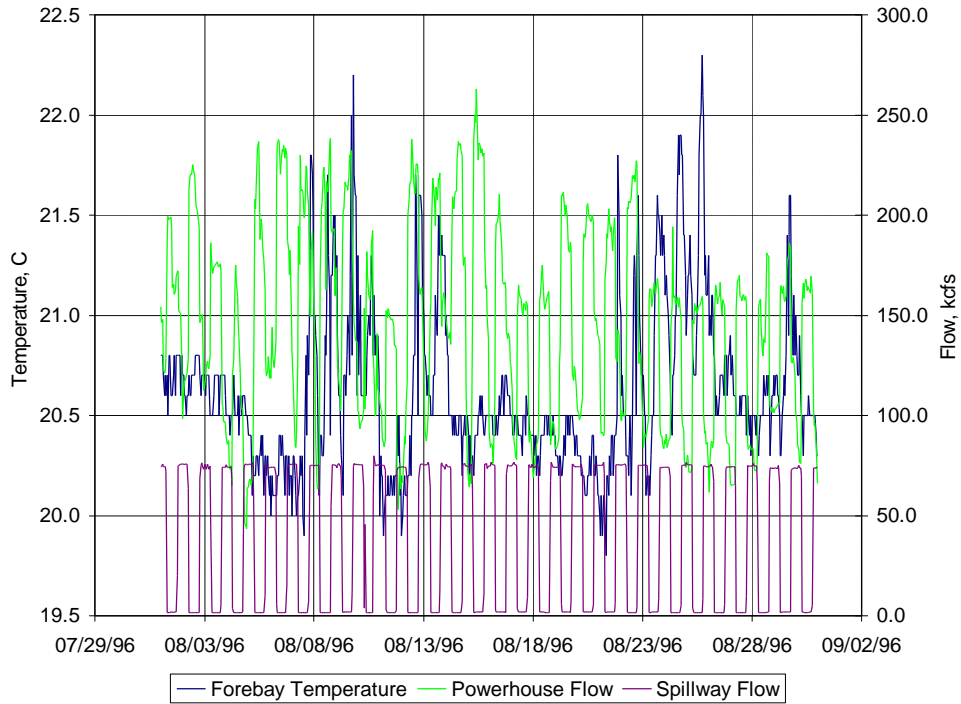


Figure 14. Water temperature at John Day dam during The Dalles Summer 1996 study.

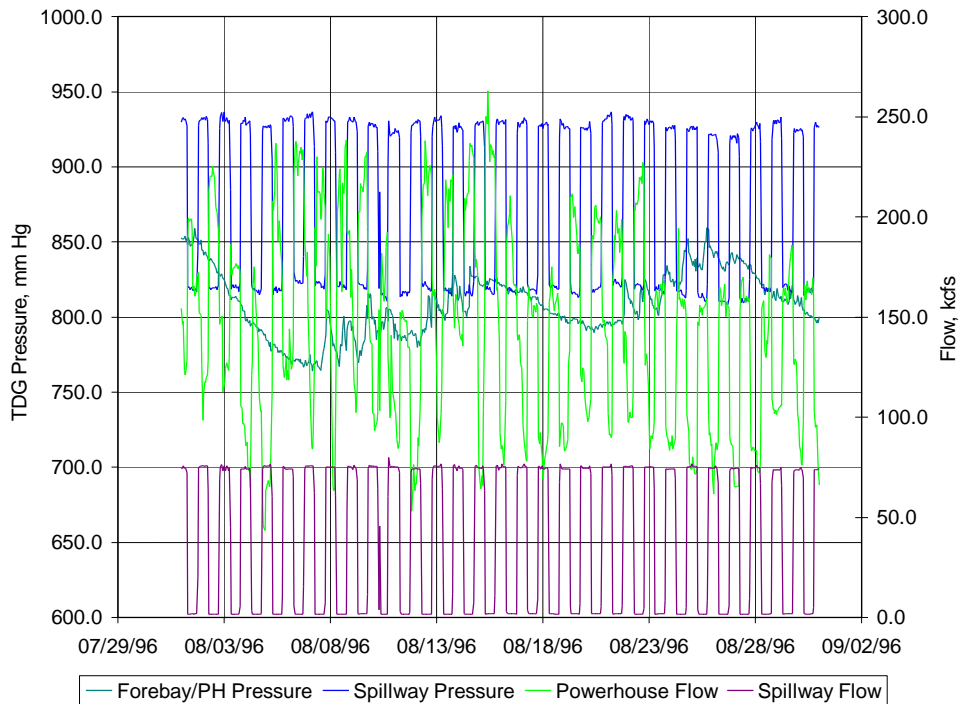


Figure 15. TDG pressure at John Day dam during The Dalles Summer 1996 study period.

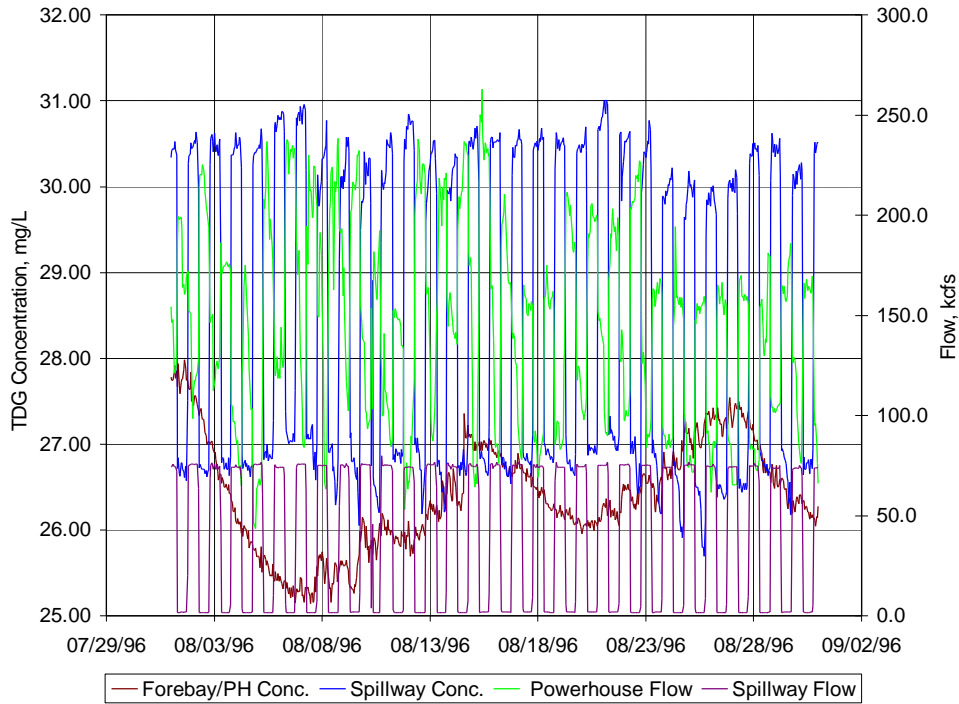


Figure 16. Computed TDG concentration at John Day during The Dalles Summer 1996 study.

In each case a second set of simulations were done using model boundary temperature and dissolved gas concentrations that were established at the upstream boundary using the temporary pool study monitors (TM). These cases are identified as TM-BC.

For example, five temporary monitors were located in the John Day tailrace during the Summer 1996 study period, as shown in Figure 17 (station TDA21585P was not used for establishing boundary conditions). The temperatures and TDG pressures recorded by these monitors are shown in Figure 18 and Figure 19, respectively. TDG concentrations computed from the measured TDG pressures and temperatures are shown in Figure 20. The transport simulation boundary was established at grid row 19 of block 1 (shown in red in Figure 20). Temporary monitor TDG concentrations and temperatures as follows along the model grid:

- TDA21639P: columns 1 to 3;
- TDA21604P: columns 4 to 6;
- TDA21603P: columns 7 to 9;
- TDA21602P: columns 10 to 14; and
- JDADTDP: columns 15 to 24.

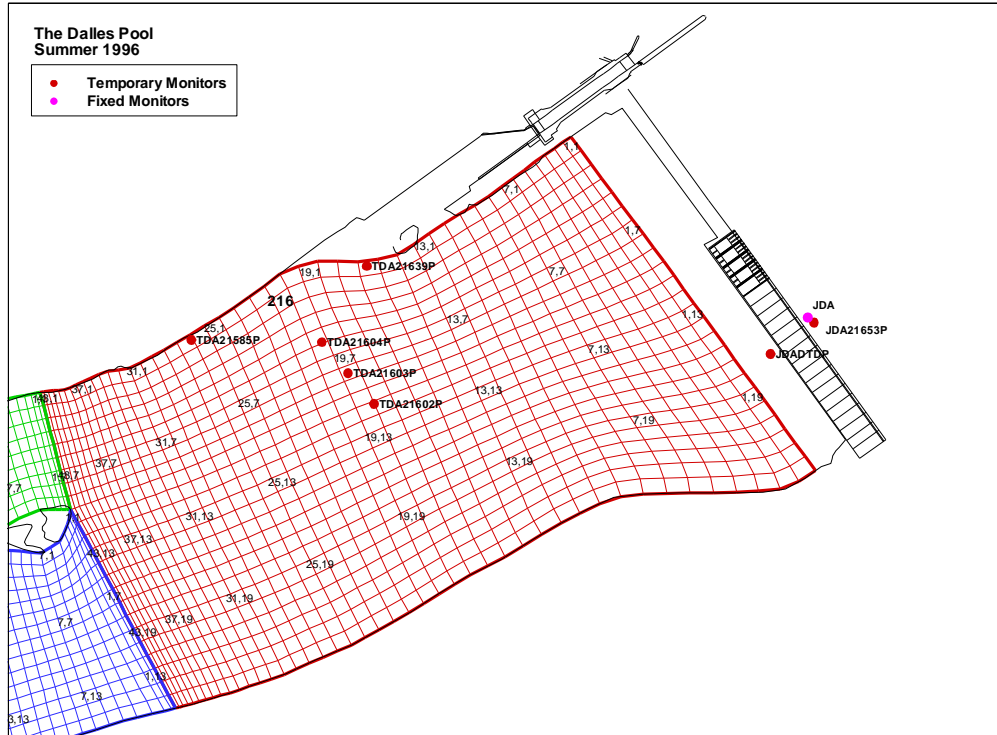


Figure 17. Locations, relative to the model grid, of temporary monitors during The Dalles Summer 1996 study period.

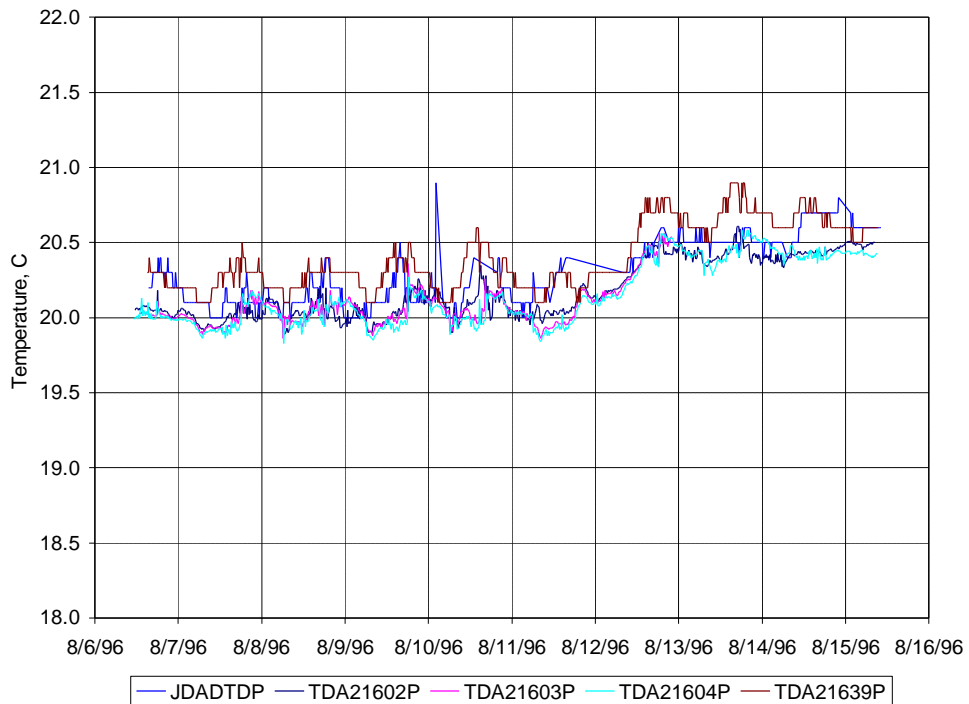


Figure 18. Temperatures measured by temporary monitors near John Day dam during The Dalles Summer 1996 study period.

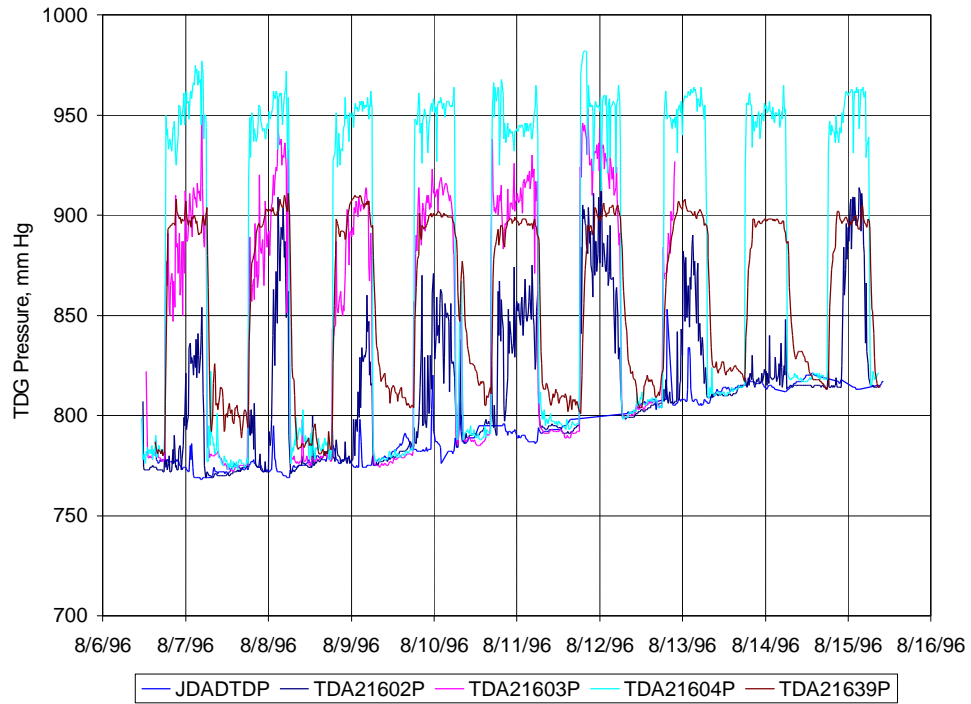


Figure 19. TDG pressures measured by temporary monitors near John Day dam during The Dalles Summer 1996 study period.

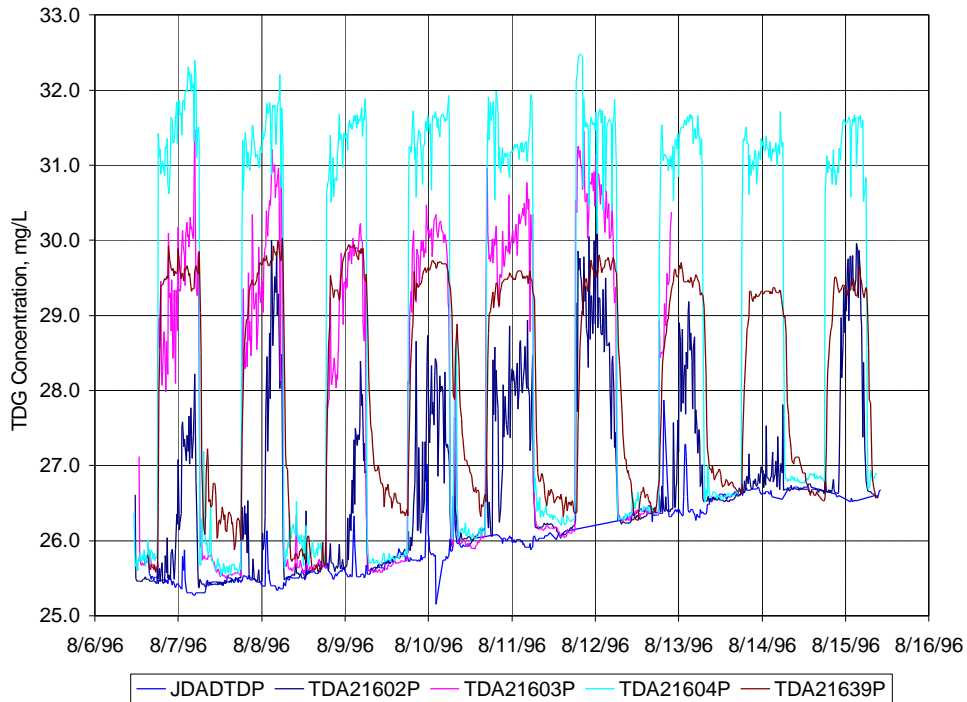


Figure 20. TDG concentrations computed from temporary monitor data near John Day dam during The Dalles Summer 1996 study period.

4.2.3 Meteorological Conditions

Atmospheric conditions were considered constant over the entire pool in each simulation case. Data from the nearest National Weather Service (NWS) station were used to assign air temperature, dew point temperature, cloud cover, and wind speed unless otherwise noted. The barometric pressure measured at fixed monitor station was applied within the pool. Net incoming short-wave solar radiation was assigned using the WeatherPak database collected by the DGAS field team or using the equations in Section 2.5 if field data were not available.

The Summer 1996 study in The Dalles Pool provides a set of example meteorological boundary condition data used in the model. The Dalles, Oregon, air and dew point temperature (Figure 21) and wind speed (Figure 22) were used from the NWS weather database. Barometric pressure (also shown in Figure 21), measured at the TDA FMS, was considered to apply over the entire modeled area. Measured short-wave radiation was available from the WeatherPak database for a short time during the Summer 1996 study. That record was extended by estimating total incoming radiation using NWS The Dalles dew point and cloud cover data. Cloud cover was assumed to be zero (clear skies) if cloud cover data was missing from the The Dalles record. Net incoming solar radiation based both on the estimated total solar radiation (Section 2.5) is shown in Figure 23.

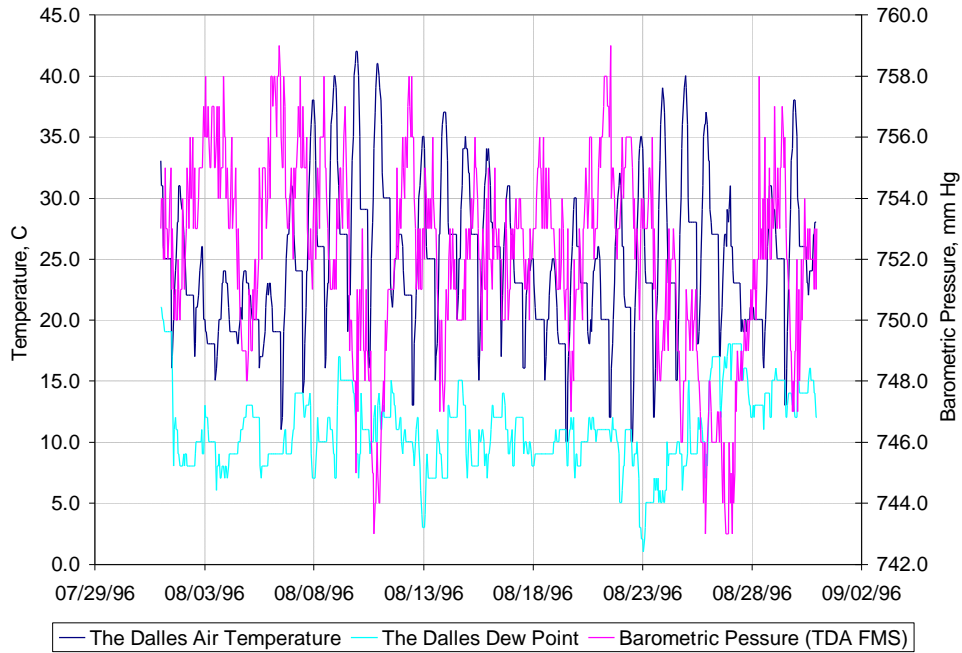


Figure 21. Air temperature, dew point, and barometric pressure used during The Dalles Summer 1996 study period.

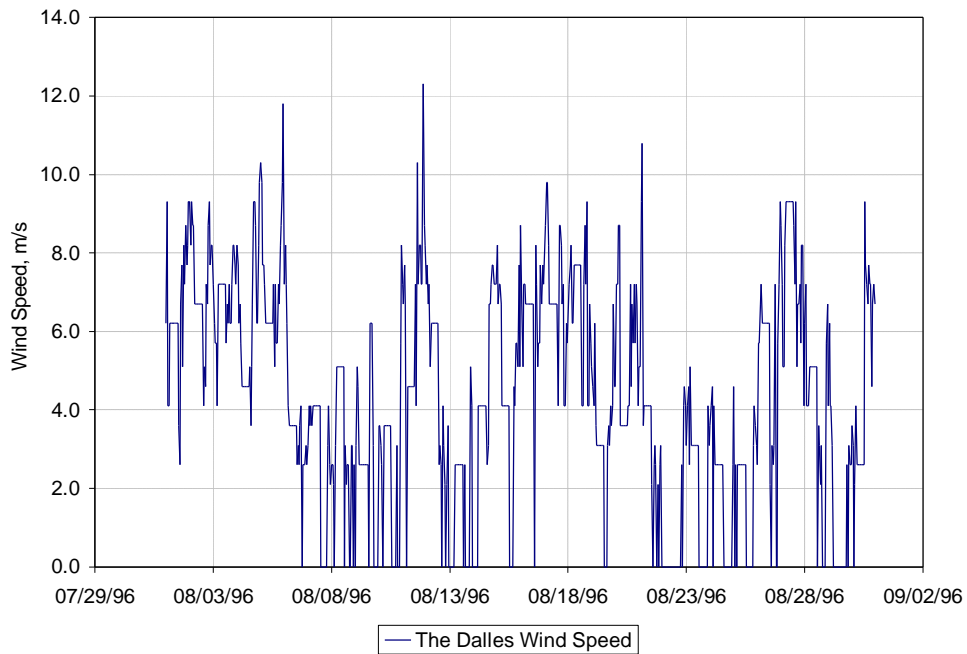


Figure 22. Wind speed used during The Dalles Summer 1996 study period.

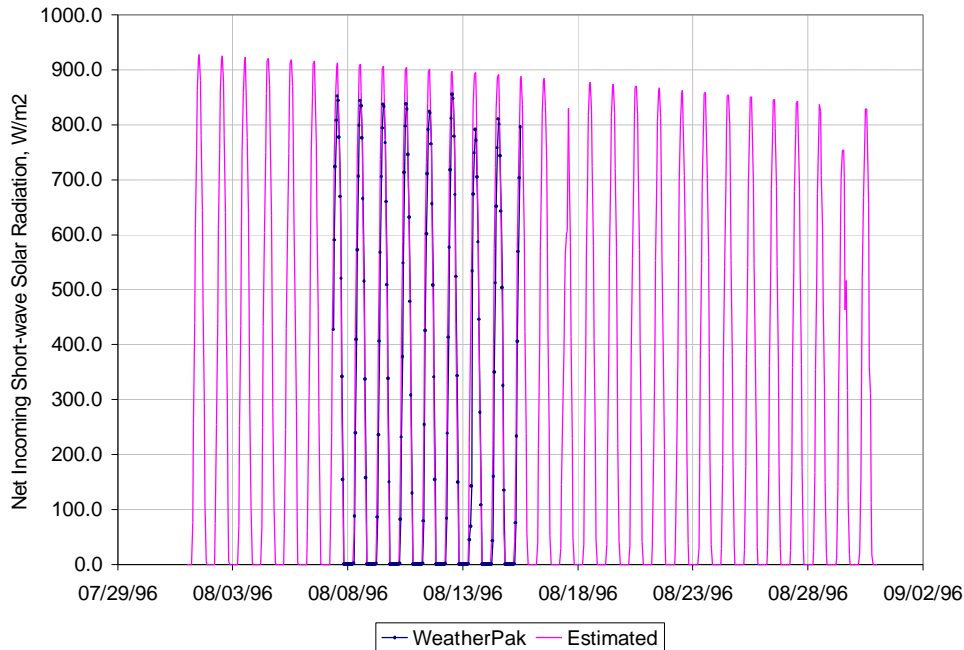


Figure 23. Net incoming short-wave solar radiation based estimated total radiation used during The Dalles Summer 1996 study period.

4.2.4 Initial Conditions

In all cases the model was started from somewhat arbitrary water depth, velocity, temperature, and dissolved gas initial conditions. The model was run for several days using the operations boundary conditions prior to the start of the field data-sampling period to allow it to “spin-up” to a consistent set of dependent variable distributions.

5 Summary of Results

5.1 Overview of Simulations

To verify the performance of the hydrodynamic and transport model, simulations were done that corresponded to the DGAS field data collection studies. Simulated velocities were compared with field measurements collected with an acoustic doppler current profiler (ADCP). Total dissolved gas and water temperature simulations are compared with corresponding measurements using temporary monitoring (TM) instruments and to the permanent, fixed-monitor system (FMS) dissolved gas monitoring stations. The field studies were conducted during the Spring and Summer time period when spillway discharges occur due to high-runoff or as required by fish passage criteria. As noted in Table 2, a total of 17 and 22 cases were performed to verify hydrodynamics and water quality, respectively. In the water quality cases simulations were done using both FMS and TM boundary conditions (with the exception of Lower Granite pool).

Table 2 Summary of cases that were simulated.

Simulation	Hydrodynamics Cases	Water Quality Cases
Lower Granite Pool	Spring 1997	Spring 1997
Little Goose Pool	Spring 1997 Summer 1997	Spring 1997 Summer 1997
Lower Monumental Pool	Spring 1997 Summer 1997	Spring 1996 Spring 1997 Summer 1997
Ice Harbor Pool	Spring 1996 Spring 1997	Spring 1996 Spring 1997
McNary Pool	Summer 1996 Spring 1997	Spring 1996 Summer 1996 Spring 1997
John Day Pool	Spring 1997 Summer 1997	Spring 1997 Summer 1997
The Dalles Pool	Spring 1996 Summer 1997	Spring 1996 Summer 1996 Summer 1997
Bonneville Pool	Spring 1996 Summer 1997	Spring 1996 Summer 1996 Summer 1997
Tidal Reach	Spring 1996 Summer 1997	Spring 1996 Summer 1996 Summer 1997
	17 Total Cases	22 Total Cases

5.2 Parameter Selection

The key model parameters are the time-step, Manning roughness coefficient (n-value), turbulent eddy-viscosity, turbulent diffusion coefficient, and the allowable residual mass error. In general, the time-step used in the model was 50 seconds. Certain periods of low flow in the Tidal Reach required a time step of 30 seconds. Bonneville pool required a 25 second time step due to the complex, shallow bathymetry in The Dalles tailrace region. Manning n-values were established for each pool by comparing the simulated tailwater elevations to that measured at the upstream dam. Turbulent mixing for mass and momentum were adequately represented by constant mixing coefficients of 0.5 ft²/sec and 0.2 ft²/sec, respectively.

Various sources of uncertainty prevented using a traditional model calibration/validation exercise to establish optimal parameters. The primary source of uncertainty is the rate of TDG mass influx at the upstream boundary. Concurrent concentration and velocity measurements at the upstream model boundaries were not available except for very brief periods. Additional sources of uncertainty arise from several sources, including: shoreline locations, vertical and horizontal error in the bathymetry, project operations, extrapolating remote meteorological data to each pool (most of which are in narrow canyons), horizontal location and compass bearing errors in the ADCP data, and horizontal location and instrument error in the TDG measurements. Note that the instrument error in the TDG measurements is estimated to be +/-2% in saturation.

Since the principal intended use of the models is to evaluate relative differences between alternatives the present approach of using a consistent set of mixing parameters for all pools is adequate and preferred over tuning the model to any particular set of data. It is important to maintain a consistent basis for comparisons. In addition, the results show that the absolute performance of the model compared to the field data is very good in most of the cases. The fact that the model water quality simulations do compare well in most cases is due in large part to the strong dependency on the upstream influx condition and that the methods used to assign that influx to the model are reasonable.

5.3 Lower Granite (LGR)

Lower Granite pool extends from the forebay of Lower Granite Dam (LGR) near Snake River Mile 107.5 up the Snake and Clearwater Rivers until the backwater influence from the dam fades away. The confluence of the Snake and Clearwater Rivers is at Snake River Mile 139.2. The MASS2 model domain extended from LGR to approximately Clearwater River Mile 0.9 and Snake River Mile 141.8; the upstream boundaries of the model are at those locations.

This section only shows examples from the complete set of simulations. Additional details in the form of plots and summary tables are presented in Part 2 of the report series (Richmond and Perkins, 1998a).

5.3.1 LGR Hydrodynamics

Simulations to compare the model hydrodynamics with measured ADCP data were performed for the Spring 1997 case. That was the only DGAS collected field data available. Upstream water discharge boundary conditions were developed using the one-dimensional MASS1 unsteady flow model (Richmond and Perkins, 1998j). Using hourly discharge data further upstream on the Clearwater and Snake Rivers, MASS1 was used to route those flows downstream to the MASS2 upstream boundaries. An example of the comparison between modeled and measured depth-averaged velocities is shown in Figure 24 in the forebay area of LGR. A snapshot of the simulated velocity distribution is shown in Figure 25 for the area near Silcott Island.

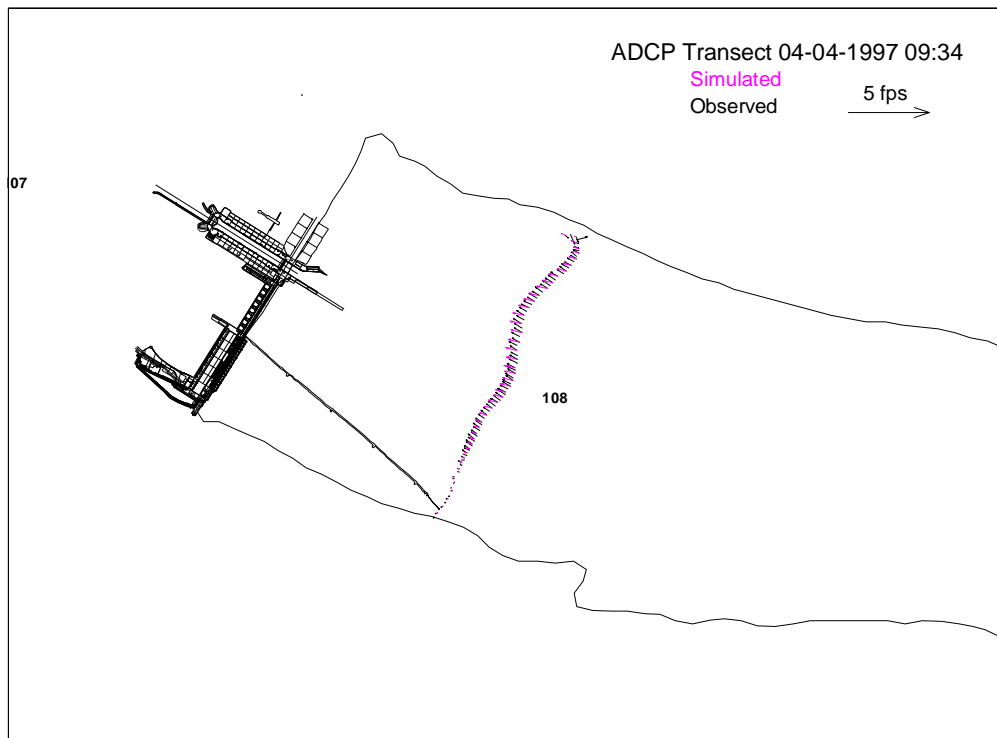


Figure 24. Simulated and observed depth-averaged velocities near Lower Granite dam April 4, 1997.

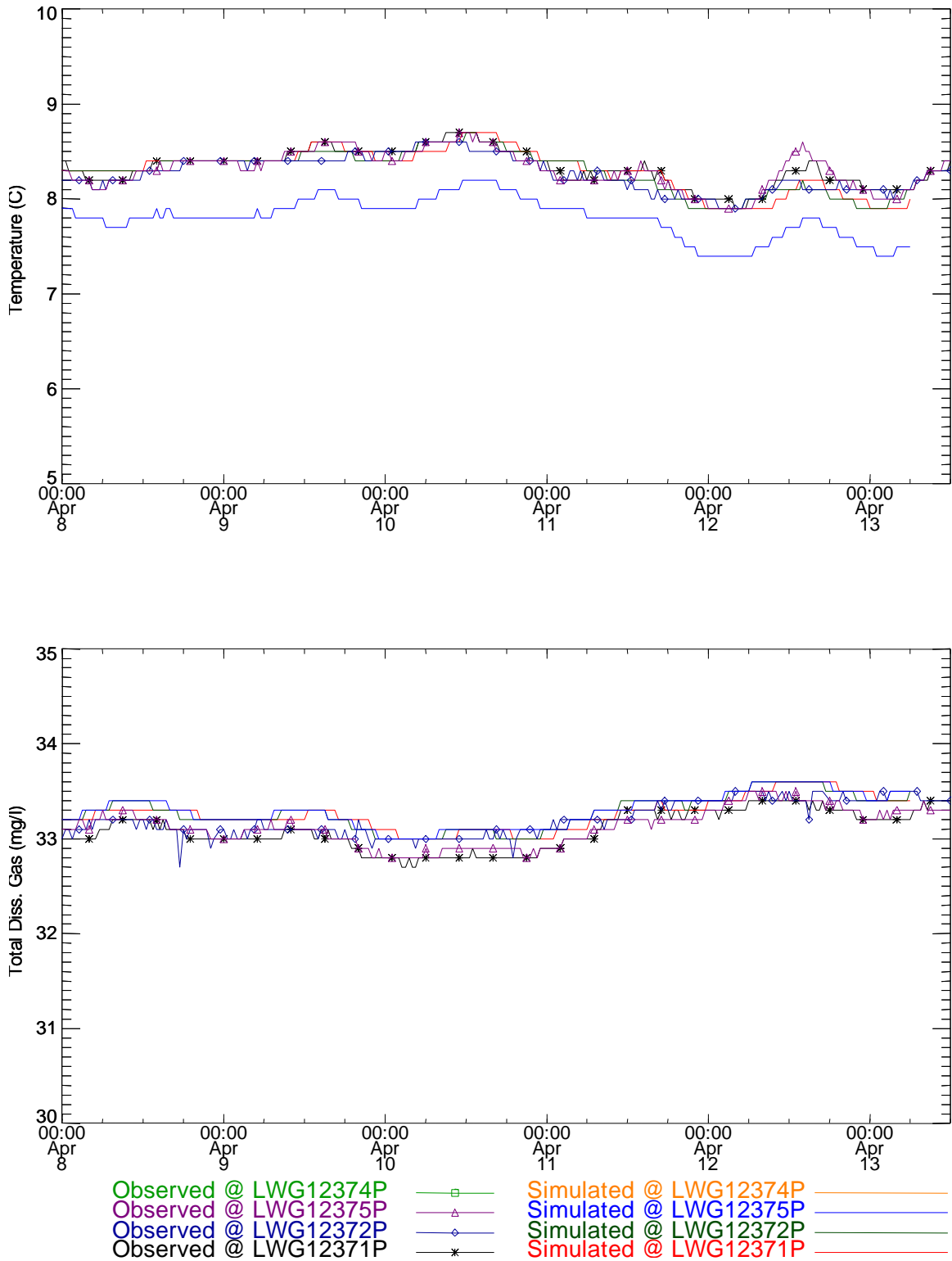


Figure 26. Temperature and total dissolved gas time series near Snake River mile 123.7 for the LGR Spring 1997 pool study.

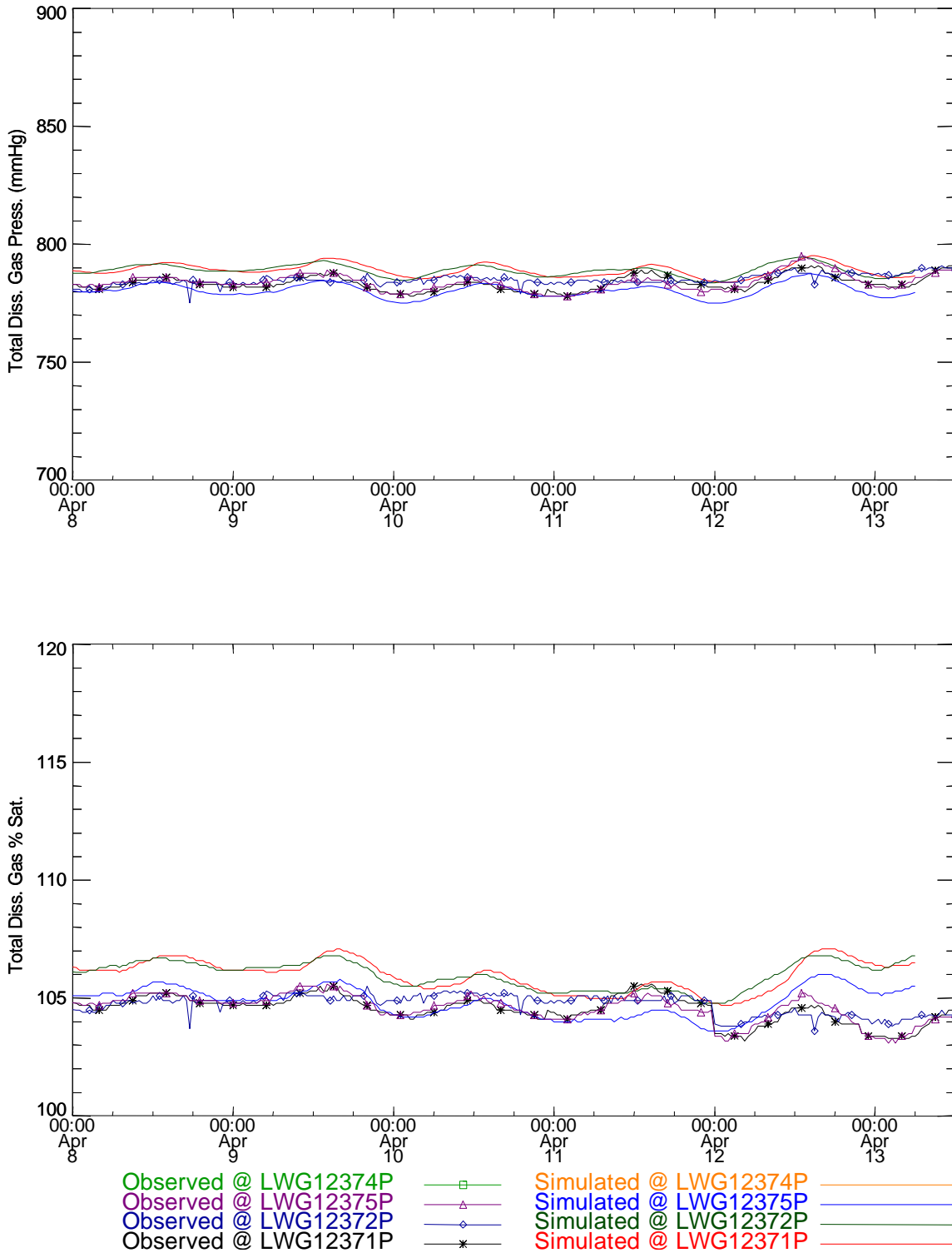


Figure 27. Total dissolved gas pressure and saturation time series near Snake River mile 123.7 for the LGR Spring 1997 pool study.

A statistical summary of the model performance is shown in Table 3. The table shows the average and standard deviation for the model and measurements over the comparison time period. The root mean square error (RMS) is also computed. Table 4 shows the

percentage of time the model is within the performance (plus or minus) criteria noted in the table.

Table 3. Statistical summary of measurements and simulations at river mile 123.7 during the LGR Spring 1997 pool study.

Station	Measured Ave.	Simulated Ave.	Measured Std.Dev	Simulated Std.Dev.	RMS Error
Temperature					
LWG12371P	8.33	8.3	0.19	0.23	0.1
LWG12372P	8.27	8.29	0.19	0.22	0.09
LWG12375P	8.31	7.8	0.2	0.21	0.52
Concentration					
LWG12371P	33.08	33.26	0.2	0.17	0.2
LWG12372P	33.19	33.28	0.18	0.18	0.13
LWG12375P	33.12	33.29	0.19	0.17	0.18
Gas Pressure					
LWG12371P	783.34	789.05	2.93	2.67	6.1
LWG12372P	784.88	789.03	2	2.46	4.97
LWG12375P	783.85	780.51	3.48	2.85	3.76
% Saturation					
LWG12371P	104.55	105.97	0.57	0.66	1.61
LWG12372P	104.75	105.97	0.41	0.58	1.42
LWG12375P	104.62	104.82	0.57	0.62	0.68

Table 4. Percentage of time during the simulation where the computed value is within the given variance compared to the measurements at rivermile 123.7 for the LGR Spring 1996 study.

Station	1.00 C	1.00 mg/l	38.00 mmHg	5.00% Sat.
LWG12371P	100	100	100	100
LWG12372P	100	100	100	100
LWG12375P	100	100	100	100

5.3.3 LGR Summary

All the model simulations had a RMS error of less than 1 degree C and 5% saturation for all the LGR cases. This is not surprising given the use of TM-BC and since the simulation and data collection periods did not overlap the spill season.

5.4 Little Goose (LGO)

Little Goose pool extends from the forebay of Little Goose Dam (LGO) near Snake River Mile 70 to the tailrace of Lower Granite Dam at River Mile 107.5. The MASS2 model domain extended from over the entire pool between the two dams.

This section only shows examples from the complete set of simulations. Additional details in the form of plots and summary tables are presented in Part 3 of the report series (Richmond and Perkins, 1998b).

5.4.1 LGO Hydrodynamics

Hydrodynamics simulations were performed for the Spring 1997 and Summer 1997 ADCP data collection periods. An example comparison from the LGO Spring 1997 case is shown in Figure 28. This figure also shows the errors in horizontal coordinate position that was present in many of the ADCP transects. The data are still useful for qualitative evaluation of the model performance. Figure 29 shows a snapshot of the simulated velocity distribution for a reach downstream of Lower Granite Dam.

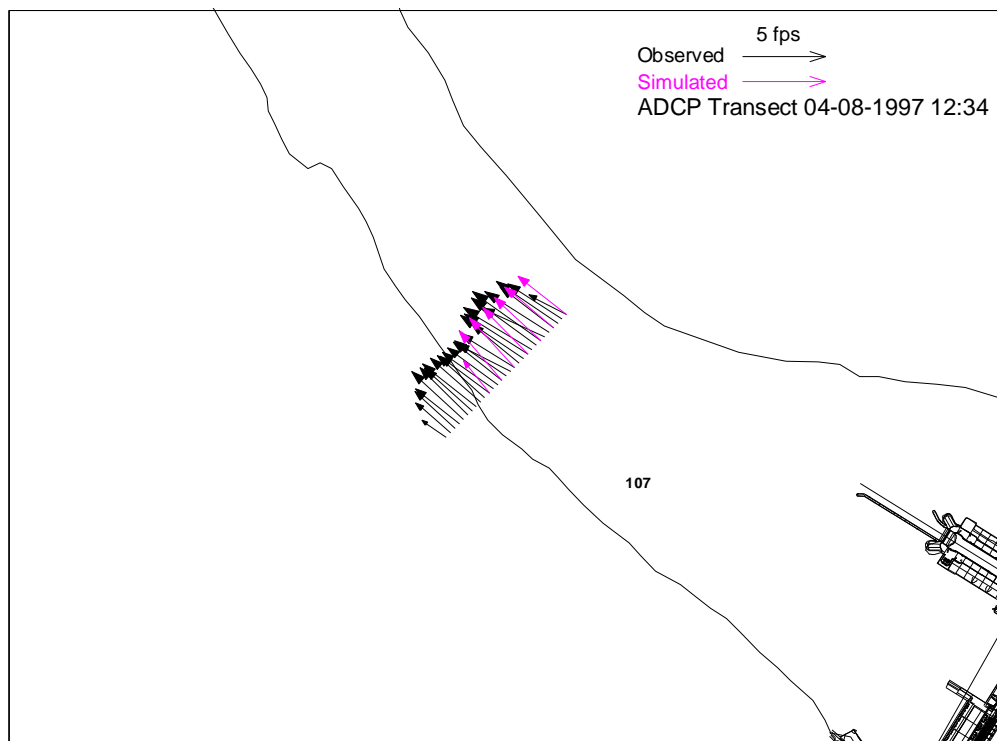


Figure 28. Simulated and observed depth-averaged velocities near Lower Granite dam on April 8, 1997.

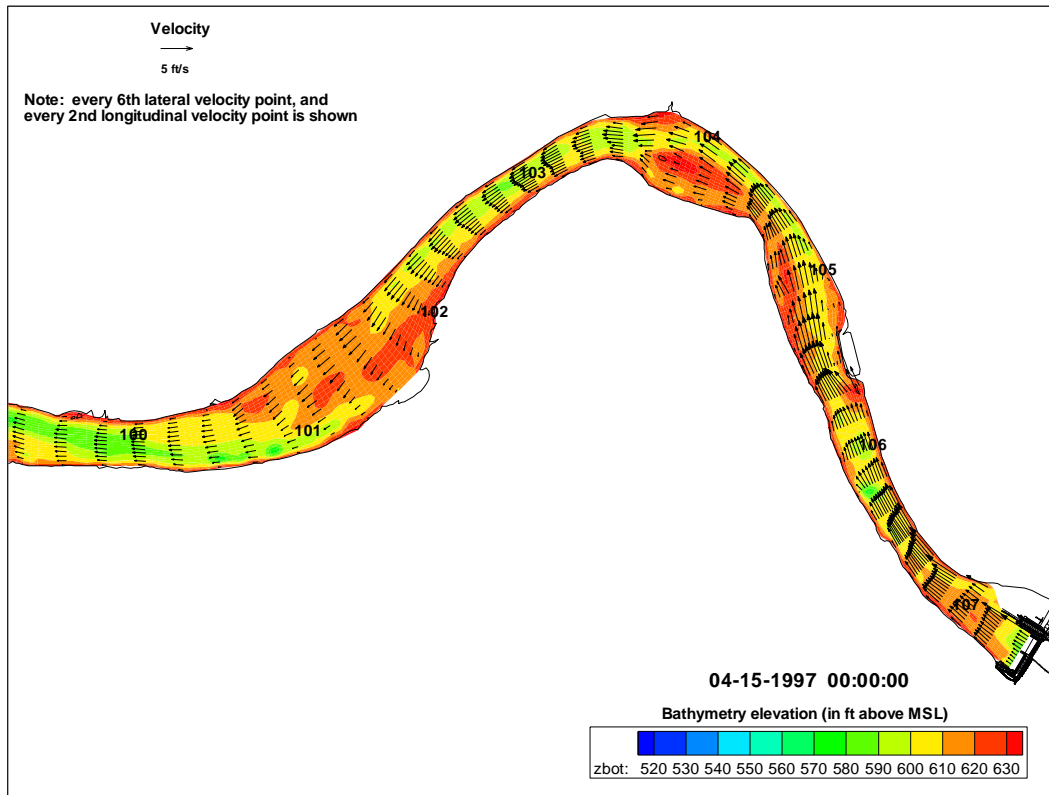


Figure 29. Simulated Spatial Velocity Distribution in LGO pool.

5.4.2 LGO Water Quality

Comparison simulations were done for the LGO Spring 1997 and Summer 1997 water quality sampling periods. Figure 30 shows the simulated and measured dissolved gas pressure and saturation just downstream of Lower Granite Dam at the fixed monitoring site. This simulation used the FMS-BC and since the gas production equation was developed using the FMS data the model performs well. This general trend was observed in the other pools as well. However, as shown in Figure 31, use of the FMS-BC underestimates the TDG mass loading compared to the TM data. This trend was also consistently observed in the downstream comparison locations. This supports the conclusions from the field and physical model studies that a fairly large percentage of the powerhouse discharge is being entrained into the spillway flow and being supersaturated. Estimates of this effect need to be incorporated into the specification of any gas abatement alternative; appropriate gas production algorithms will have to be developed for the model boundary conditions.

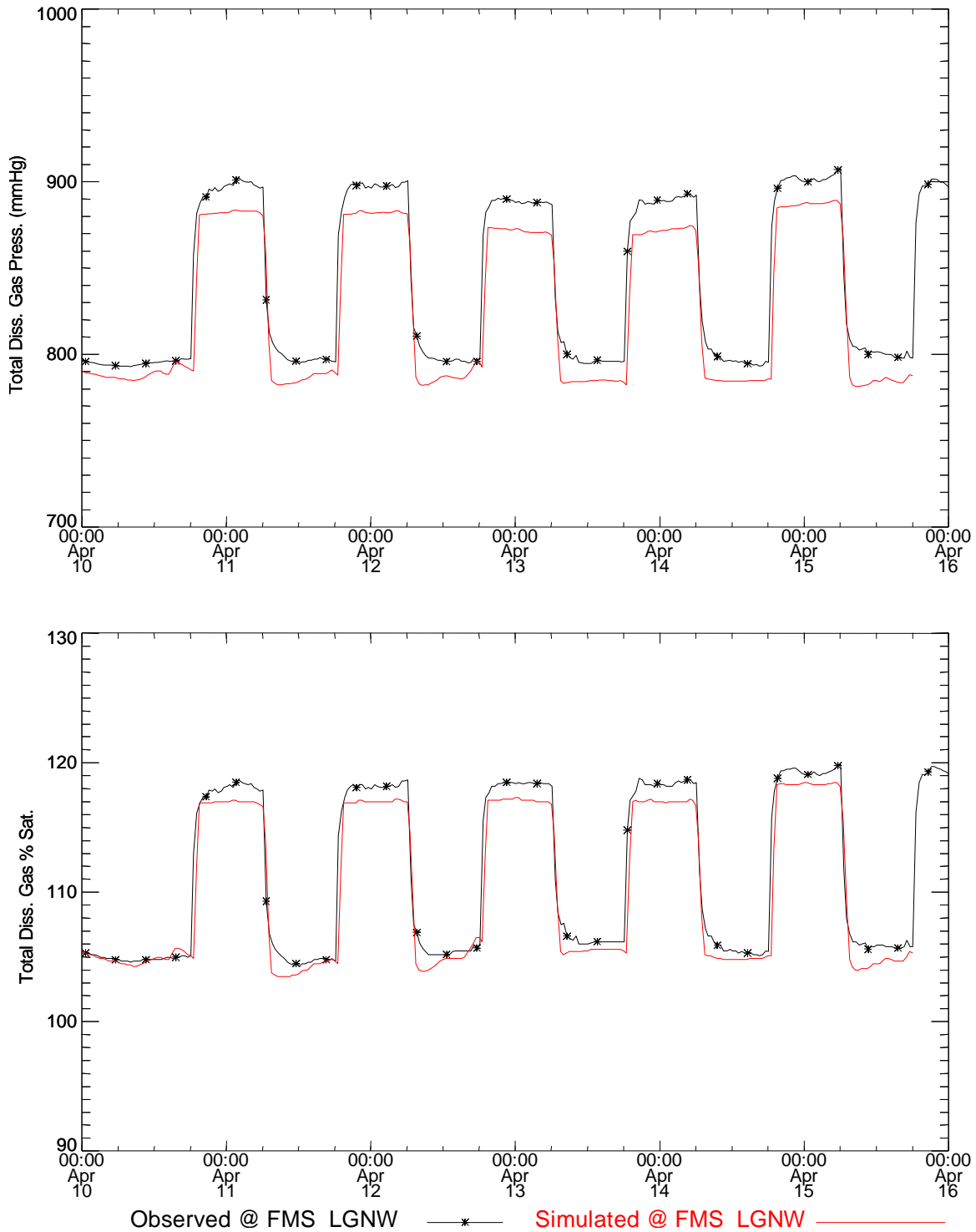


Figure 30. Total dissolved gas pressure and saturation time series near at the LGNW fixed monitor during the LGO Spring 1997 pool study (FMS-BC).

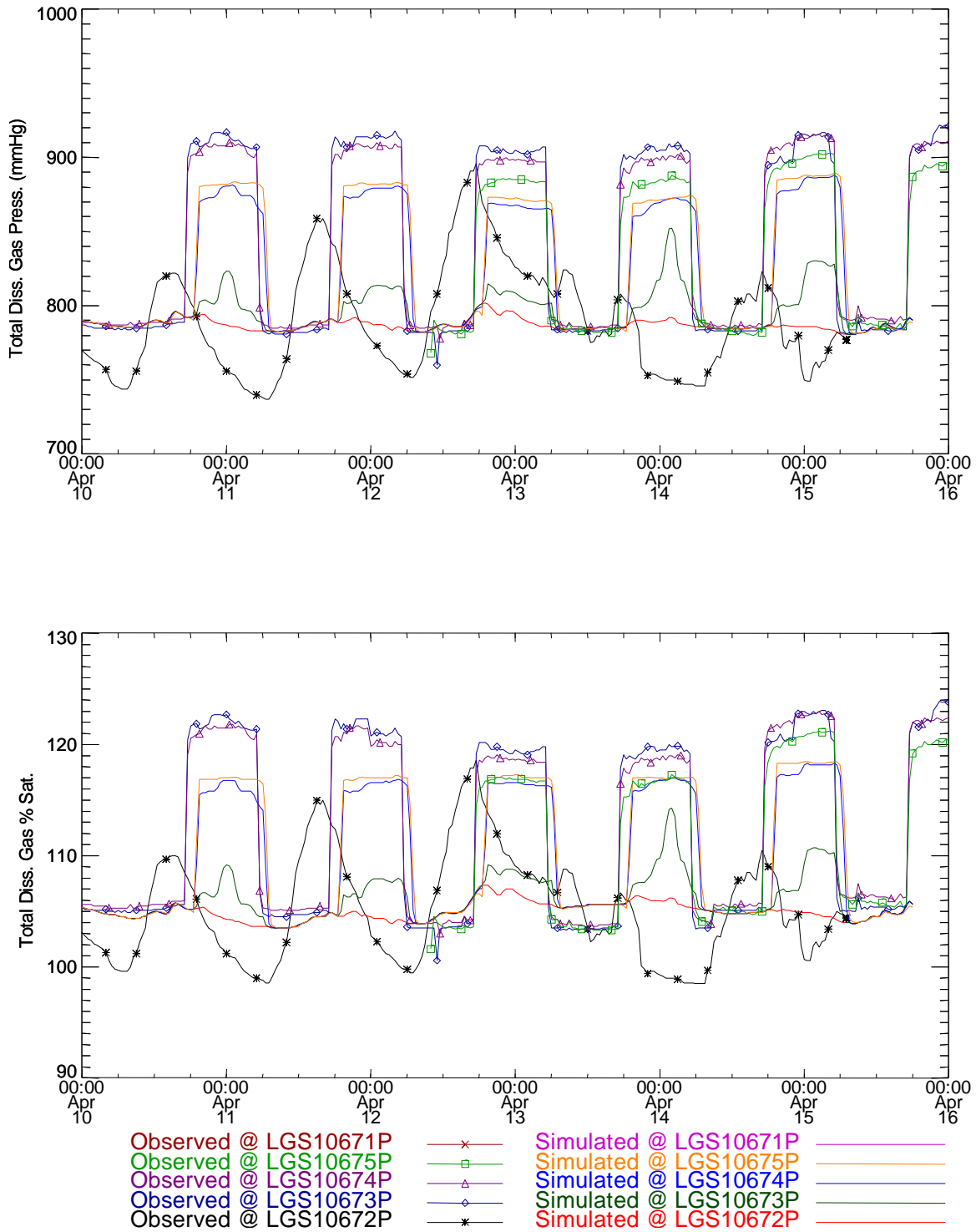


Figure 31. Total dissolved gas pressure and saturation time series near Snake River Mile 106.7 for the LGO Spring 1997 pool study (FMS-BC).

5.4.3 LGO Summary

Table 5 compares the performance of the model to the measured field data. The table shows the number of times the model was within or outside of the stated RMS error. This

was calculated by summing over the total number of field measurement stations for a given study period. For LGO, the table shows that the use of the temporary monitor data for the upstream boundary condition yields a large improvement in the %saturation. The number of occurrences when the model was outside of the 5% RMS range went from 20 in the FMS-BC cases to 2 in the TM-BC cases.

Table 5. Summary of model performance compared to field measurements for LGO pool. Table shows the number of occurrences within and outside of the RMS error noted.

Little Goose Pool				
Fixed Monitor BC				
		Spring 1997	Summer 1997	Total
Total # Stations		19	20	39
Temperature (RMS Error +/- 1.00 C)	# Within	16	19	35
	# Outside	3	1	4
Concentration (RMS Error +/- 1.00 mg/l)	# Within	10	0	10
	# Outside	9	20	29
Gas Pressure (RMS Error +/- 38.00 mmHg)	# Within	14	3	17
	# Outside	5	17	22
% Saturation (RMS Error +/- 5.00% Sat.)	# Within	13	6	19
	# Outside	6	14	20
Temporary Monitor BC				
Total # Stations		19	20	39
Temperature (RMS Error +/- 1 C)	# Within	18	20	38
	# Outside	1	0	1
Concentration (RMS Error +/- 1.00 mg/l)	# Within	14	17	31
	# Outside	5	3	8
Gas Pressure (RMS Error +/- 38.00 mmHg)	# Within	18	19	37
	# Outside	1	1	2
% Saturation (RMS Error +/- 5.00% Sat.)	# Within	18	19	37
	# Outside	1	1	2

5.5 Lower Monumental (LMN)

Lower Monumental pool extends from the forebay of Lower Monumental Dam (LMN) near Snake River Mile 40.5 to the tailrace of Little Goose Dam at River Mile 70. The MASS2 model domain extended from over the entire pool between the two dams.

This section only shows examples from the complete set of simulations. Additional details in the form of plots and summary tables are presented in Part 4 of the report series (Richmond and Perkins, 1998c).

5.5.1 LMN Hydrodynamics

Hydrodynamics simulations were performed for the Spring 1997 and Summer 1997 ADCP data collection periods. Comparisons with the Spring 1997 ADCP data could not be done at this time due to errors in the horizontal coordinates and compass bearing. An example comparison from the LMN Summer 1997 case is shown in Figure 32. Figure 33 shows a snapshot of the simulated velocity distribution for a reach downstream of Lower Granite Dam.

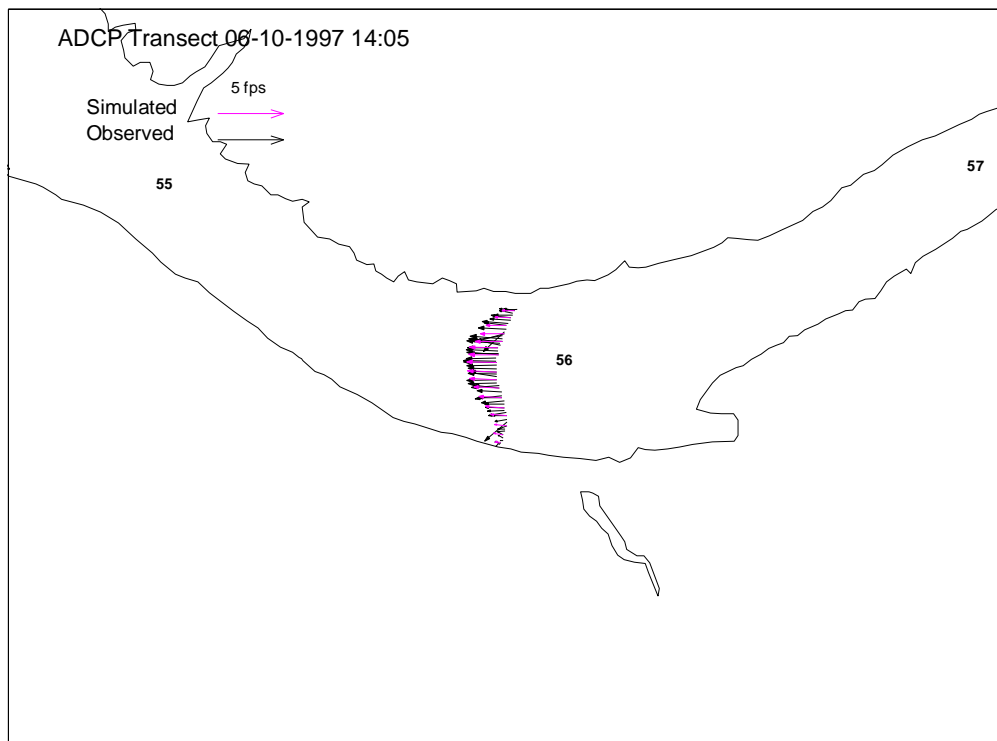


Figure 32. Simulated and observed depth-averaged velocities near Snake River Mile 56 on 6-10-1997.

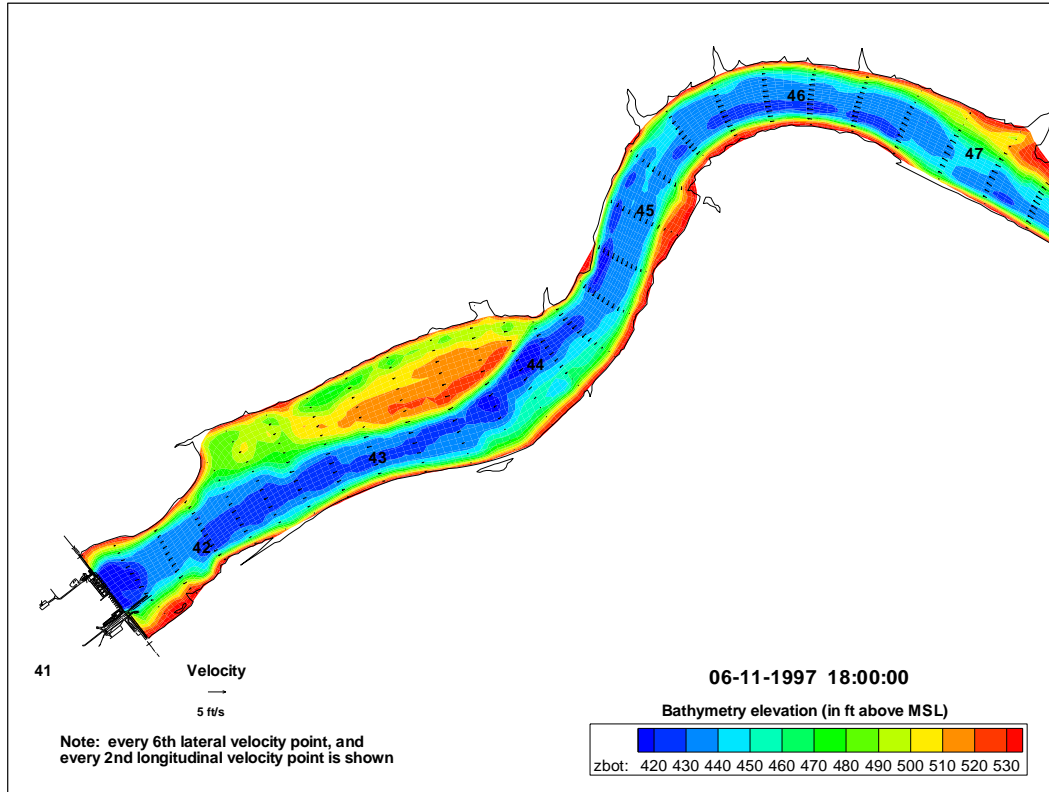


Figure 33. Simulated spatial velocity distribution in LMN pool.

5.5.2 LMN Water Quality

Water quality cases were simulated for the LMN Spring 1996, Spring 1997, and Summer 1997 cases. Use of the FMS-BC led to poor results in most all cases. An example time series using the TM-BC for the Summer 1997 case at a location about 10 miles downstream of Little Goose Dam is shown in Figure 34.

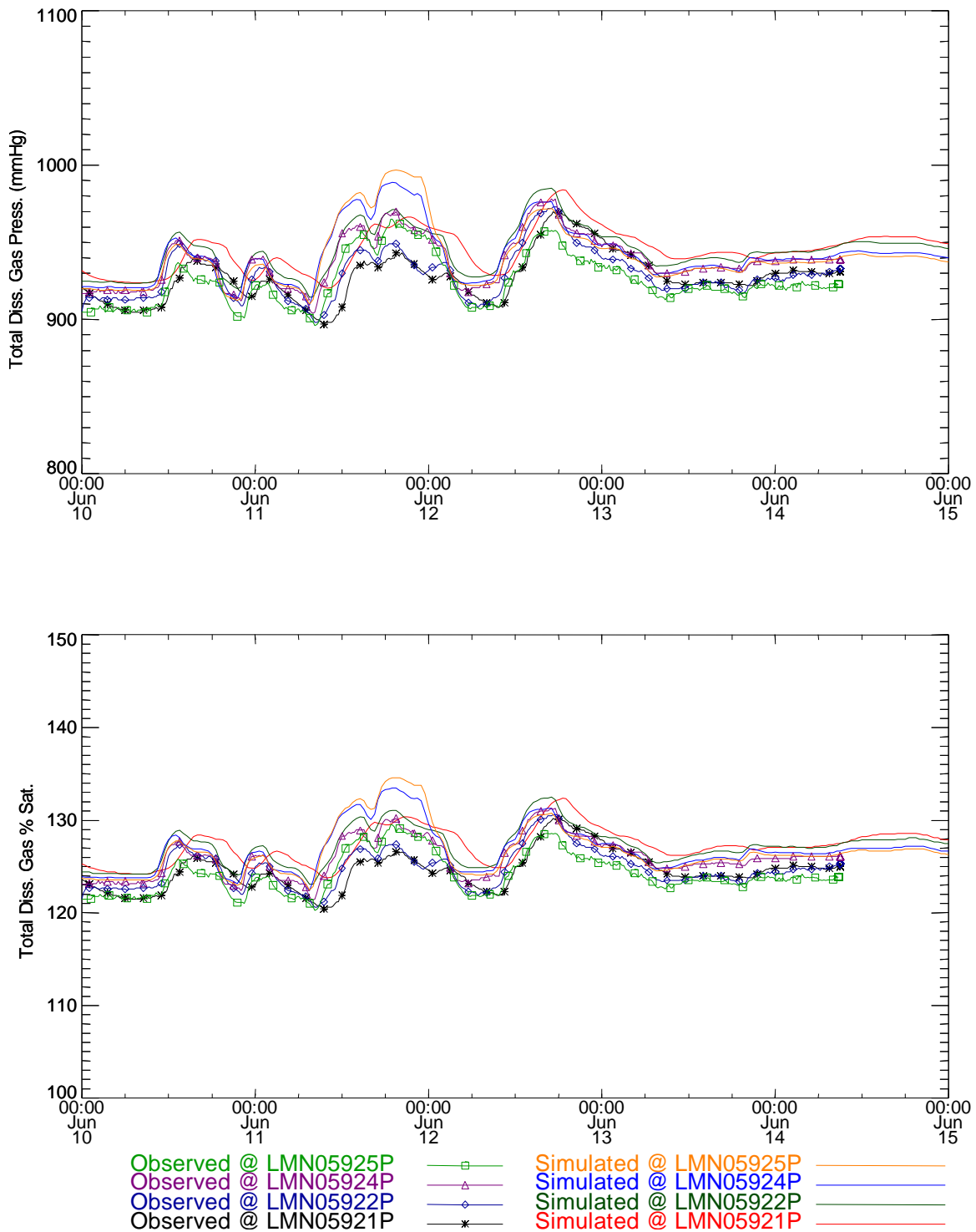


Figure 34. Total dissolved gas pressure and saturation time series comparisons near Snake River Mile 59.2 for the LMN Summer 1997 study (TM-BC).

A statistical summary of the model performance is shown in Table 6. The table shows the average and standard deviation for the model and measurements over the comparison time period. The root mean square error (RMS) is also computed. Table 7 shows the

percentage of time the model is within the performance (plus or minus) criteria noted in the table.

Table 6. Statistical summary of measurements and simulations at River Mile 059.2 during the LMN Summer 1997 study (TM-BC).

Station	Measured Ave.	Simulated Ave.	Measured Std.Dev	Simulated Std.Dev.	RMS Error
Temperature					
LMN05921P	13.5	13.47	0.39	0.42	0.12
LMN05922P	13.48	13.45	0.37	0.38	0.07
LMN05924P	13.51	13.46	0.37	0.37	0.09
LMN05925P	13.62	13.46	0.37	0.38	0.19
Concentration					
LMN05921P	34.98	35.59	0.47	0.41	0.64
LMN05922P	35.07	35.59	0.5	0.47	0.55
LMN05924P	35.37	35.48	0.48	0.58	0.28
LMN05925P	34.77	35.43	0.49	0.66	0.71
Gas Pressure					
LMN05921P	928.02	945.37	14.61	14.06	18.2
LMN05922P	929.68	944.83	14.47	14.93	15.93
LMN05924P	938.44	942.4	15.21	17.89	7.84
LMN05925P	924.72	941.32	15.33	19.78	18.15
% Saturation					
LMN05921P	124.59	127.27	1.96	1.92	2.82
LMN05922P	124.81	127.2	1.94	2.02	2.49
LMN05924P	125.99	126.87	2.04	2.44	1.33
LMN05925P	124.14	126.73	2.05	2.71	2.8

Table 7. Percentage of time during the simulation where the computed value is within the given variance compared to the measurements at River Mile 059.2 during the Summer 1997 study (TM-BC).

Station	1.00 C	1.00 mg/l	38.00 mmHg	5.00% Sat.
LMN05921P	100	96.68	100	100
LMN05922P	100	100	100	100
LMN05924P	100	100	100	100
LMN05925P	100	90.04	98.34	93.78

The initial mixing of the TDG plume for a snapshot in time for LMN is shown in Figure 35. This figure also shows the location of the upstream water quality boundary condition for a typical TM-BC. Discharge boundary conditions are still assigned near the dam, Little Goose in this case, because measured velocities were not available at the monitor location, except for very brief time periods.

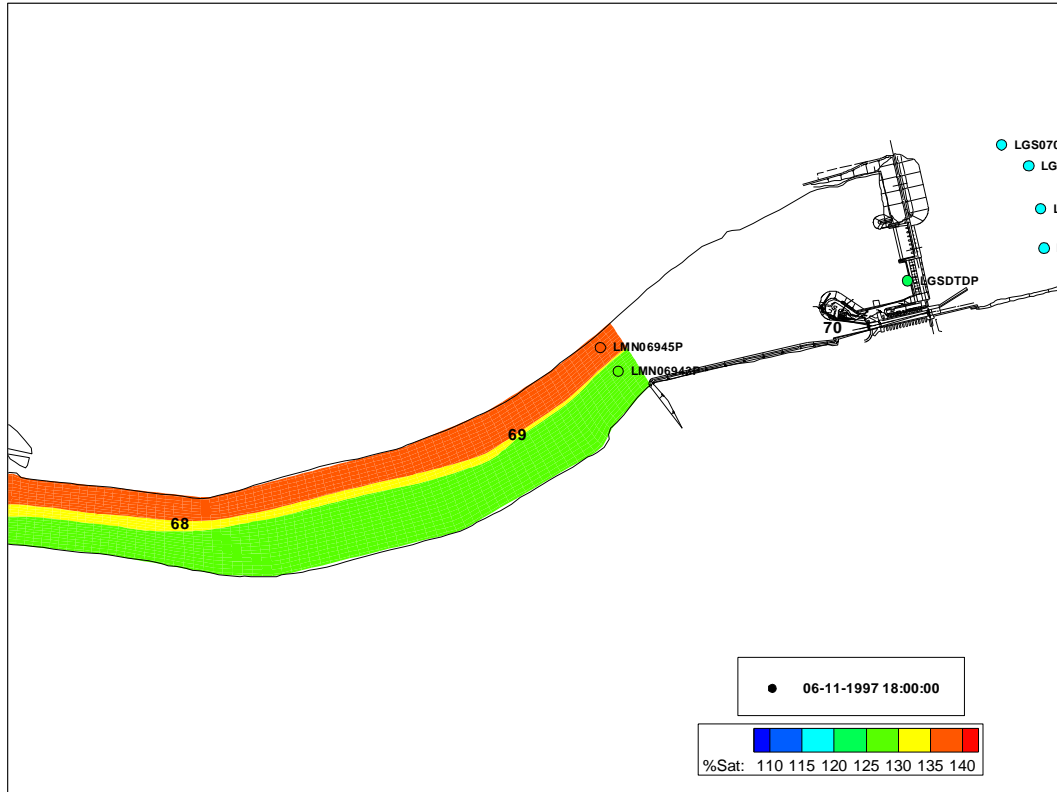


Figure 35. Simulated spatial TDG distribution in LMN pool.

5.5.3 LMN Summary

Table 8 compares the performance of the model to the measured field data. The table shows the number of times the model was within or outside of the stated RMS error summed over the total number of field measurement stations for a given study period. For LMN, the table shows that the use of the temporary monitor data for the upstream boundary condition yields a large improvement in the %saturation. The number of occurrences when the model was outside of the 5% RMS range went from 20 in the FMS-BC cases to 3 in the TM-BC cases.

Table 8. Summary of model performance compared to field measurements for LMN pool. Table shows the number of occurrences within and outside of the RMS error noted.

Lower Monumental Pool					
Fixed Monitor Locations					
		Spring 1996	Spring 1997	Summer 1997	Total
Total # Stations		11	12	11	34
Temperature (RMS Error +/- 1.00 C)	# Within	11	10	10	31
	# Outside	0	2	1	3
Concentration (RMS Error +/- 1.00 mg/l)	# Within	0	0	4	4
	# Outside	11	12	7	30
Gas Pressure (RMS Error +/- 38.00 mmHg)	# Within	1	8	9	18
	# Outside	10	4	2	16
% Saturation (RMS Error +/- 5.00% Sat.)	# Within	1	4	9	14
	# Outside	10	8	2	20
Temporary Monitor Locations					
Total # Stations		11	7	11	29
Temperature (RMS Error +/- 1 C)	# Within	11	6	11	28
	# Outside	0	1	0	1
Concentration (RMS Error +/- 1.00 mg/l)	# Within	7	4	11	22
	# Outside	4	3	0	7
Gas Pressure (RMS Error +/- 38.00 mmHg)	# Within	9	6	11	26
	# Outside	2	1	0	3
% Saturation (RMS Error +/- 5.00% Sat.)	# Within	9	6	11	26
	# Outside	2	1	0	3

5.6 Ice Harbor (IHR)

Ice Harbor pool extends from the forebay of Ice Harbor Dam (IHR) near Snake River Mile 9.8 to the tailrace of Lower Monumental Dam at River Mile 40.5. The MASS2 model domain extended from over the entire pool between the two dams.

This section only shows examples from the complete set of simulations. Additional details in the form of plots and summary tables are presented in Part 5 of the report series (Richmond and Perkins, 1998d).

5.6.1 IHR Hydrodynamics

Hydrodynamics simulations were performed for the Spring 1996 and Spring 1997 ADCP data collection periods. An example comparison from the IHR Spring 1997 case is shown in Figure 36. Figure 37 shows a snapshot of the simulated velocity distribution for a reach mid-way in the IHR pool.

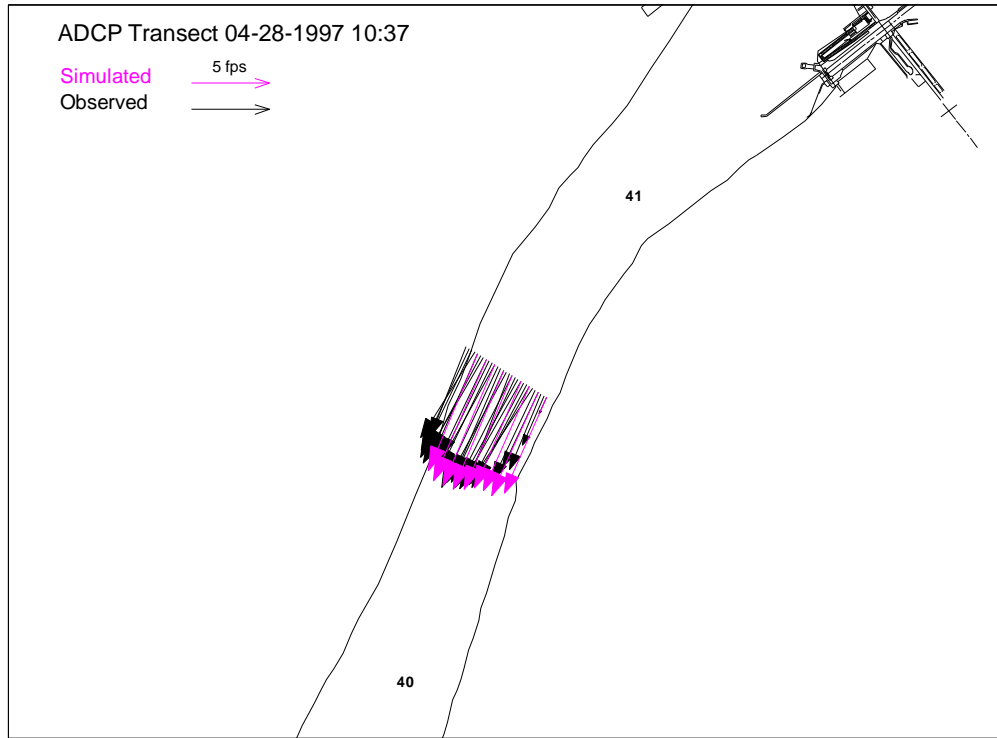


Figure 36. Simulated and observed depth-averaged velocities near Columbia River Mile 40.5 on 4-28-1997.

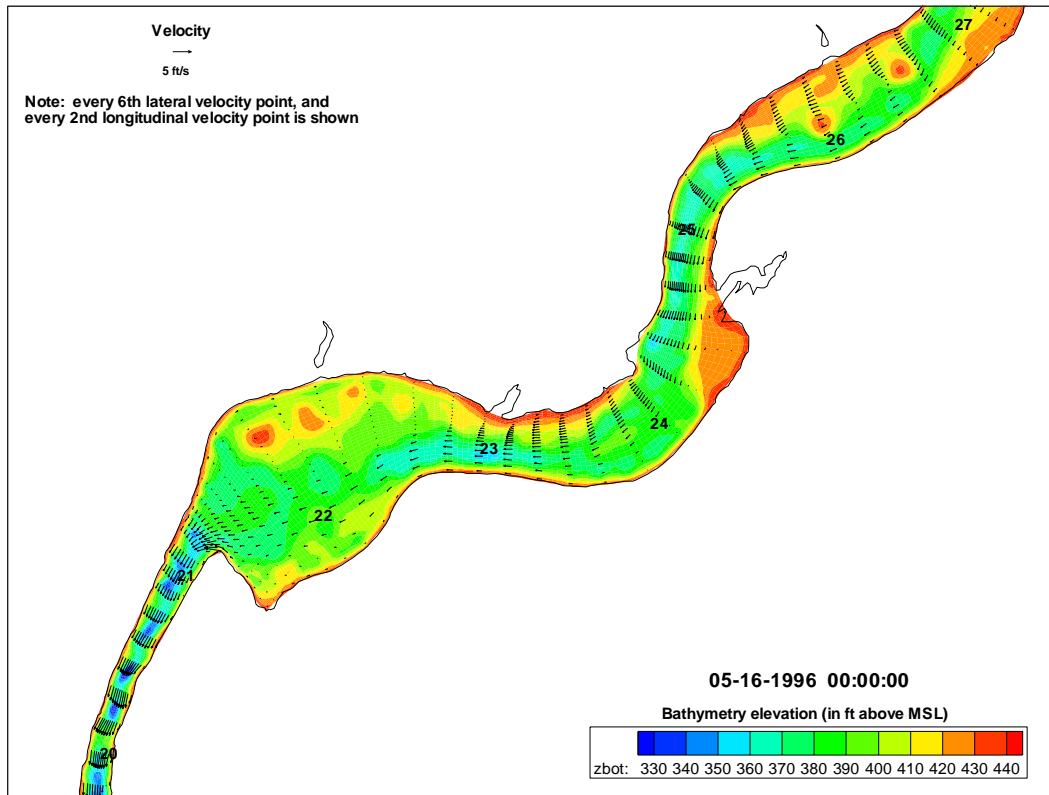


Figure 37. Simulated spatial velocity distribution in IHR pool.

5.6.2 IHR Water Quality

Water quality cases were simulated for IHR Spring 1996 and Spring 1997 cases. Use of the FMS-BC led to poor results in most all cases. An example time series using the TM-BC for the Spring 1997 case at a location in the IHR forebay is shown in Figure 38. This shows the apparent effect of air/water gas exchange (not included in this simulation) on the results. See the John Day pool section for a test of a model simulation that includes gas exchange.

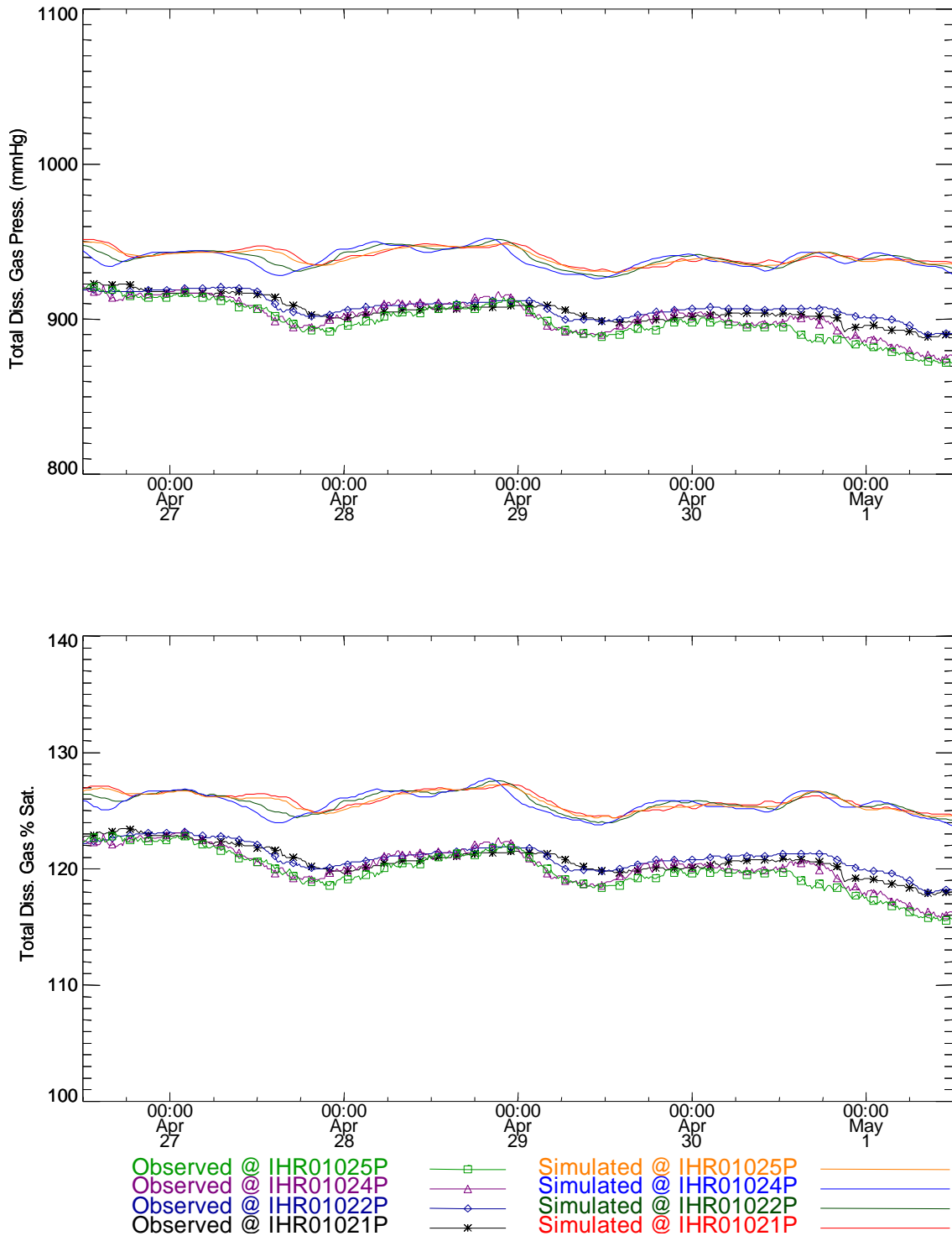


Figure 38. Total dissolved gas pressure and saturation time series comparisons near Snake River Mile 010.2 for Spring 1997 study period (TM-BC).

5.6.3 IHR Summary

Table 9 compares the performance of the model to the measured field data. The table shows the number of times the model was within or outside of the stated RMS error

summed over the total number of field measurement stations for a given study period. For IHR, the table shows that the use of the temporary monitor data for the upstream boundary condition did not yield a large improvement in the %saturation. Use of the temporary monitor conditions did improve the temperature simulation in IHR for the Spring 1996 case.

Table 9. Summary of model performance compared to field measurements for IHR pool. Table shows the number of occurrences within and outside of the RMS error noted.

Ice Harbor Pool				
Fixed Monitor Locations				
		Spring 1996	Spring 1997	Total
Total # Stations		18	16	34
Temperature (RMS Error +/- 1 C)	# Within	0	16	16
	# Outside	18	0	18
Concentration (RMS Error +/- 1.00 mg/l)	# Within	4	9	13
	# Outside	14	7	21
Gas Pressure (RMS Error +/- 38.00 mmHg)	# Within	17	16	33
	# Outside	1	0	1
% Saturation (RMS Error +/- 5.00% Sat.)	# Within	16	16	32
	# Outside	2	0	2
Temporary Monitor Locations				
Total # Stations		17	15	32
Temperature (RMS Error +/- 1 C)	# Within	16	15	31
	# Outside	1	0	1
Concentration (RMS Error +/- 1.00 mg/l)	# Within	15	6	21
	# Outside	2	9	11
Gas Pressure (RMS Error +/- 38.00 mmHg)	# Within	16	13	29
	# Outside	1	2	3
% Saturation (RMS Error +/- 5.00% Sat.)	# Within	16	12	28
	# Outside	1	3	4

5.7 McNary (MCN)

McNary pool extends from the forebay of McNary Dam (MCN) near Columbia River Mile 292.5 up the Columbia until the backwater influence from the dam fades away just upstream of Richland, Washington and up the Snake River to Ice Harbor Dam. The confluence of the Columbia and Snake Rivers is at Columbia River Mile 325. The MASS2 model domain extended from MCN to approximately Columbia River Mile 328

(near Clover, Island) and up the Snake River to Ice Harbor Dam; the upstream boundaries of the model are at those locations.

This section only shows examples from the complete set of simulations. Additional details in the form of plots and summary tables are presented in Part 6 of the report series (Richmond and Perkins, 1998e).

5.7.1 MCN Hydrodynamics

Hydrodynamics simulations were performed for the Summer 1996 and Spring 1997 ADCP data collection periods. An example comparison from the MCN Spring 1997 case is shown in Figure 39. This location is at the confluence of the Columbia and Snake Rivers.

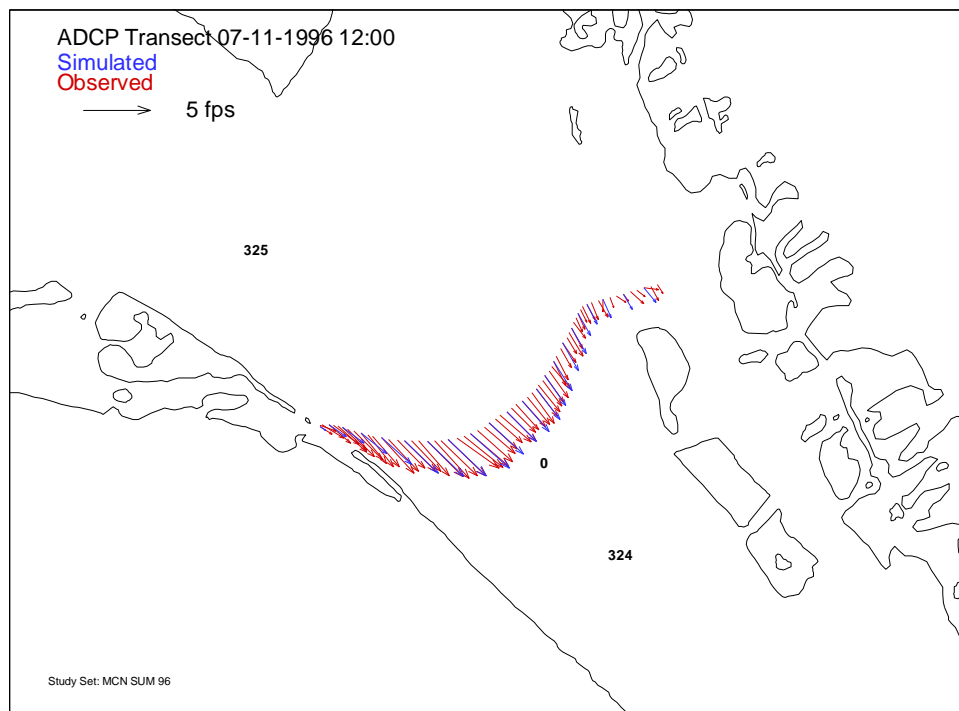


Figure 39. Simulated and observed depth-averaged velocities at the confluence of the Columbia and Snake Rivers on 7-11-1996.

5.7.2 MCN Water Quality

Three water quality cases for MCN were simulated: Summer 1996, Spring 1996, and Spring 1997. Figure 40 shows a time series during the Summer 1996 case using TM upstream boundary conditions. This location is at the railway bridge causeway at River Mile 323. The increase in temperature and TDG concentration during late July 10 occurs from the upstream influx of Snake River water at that location.

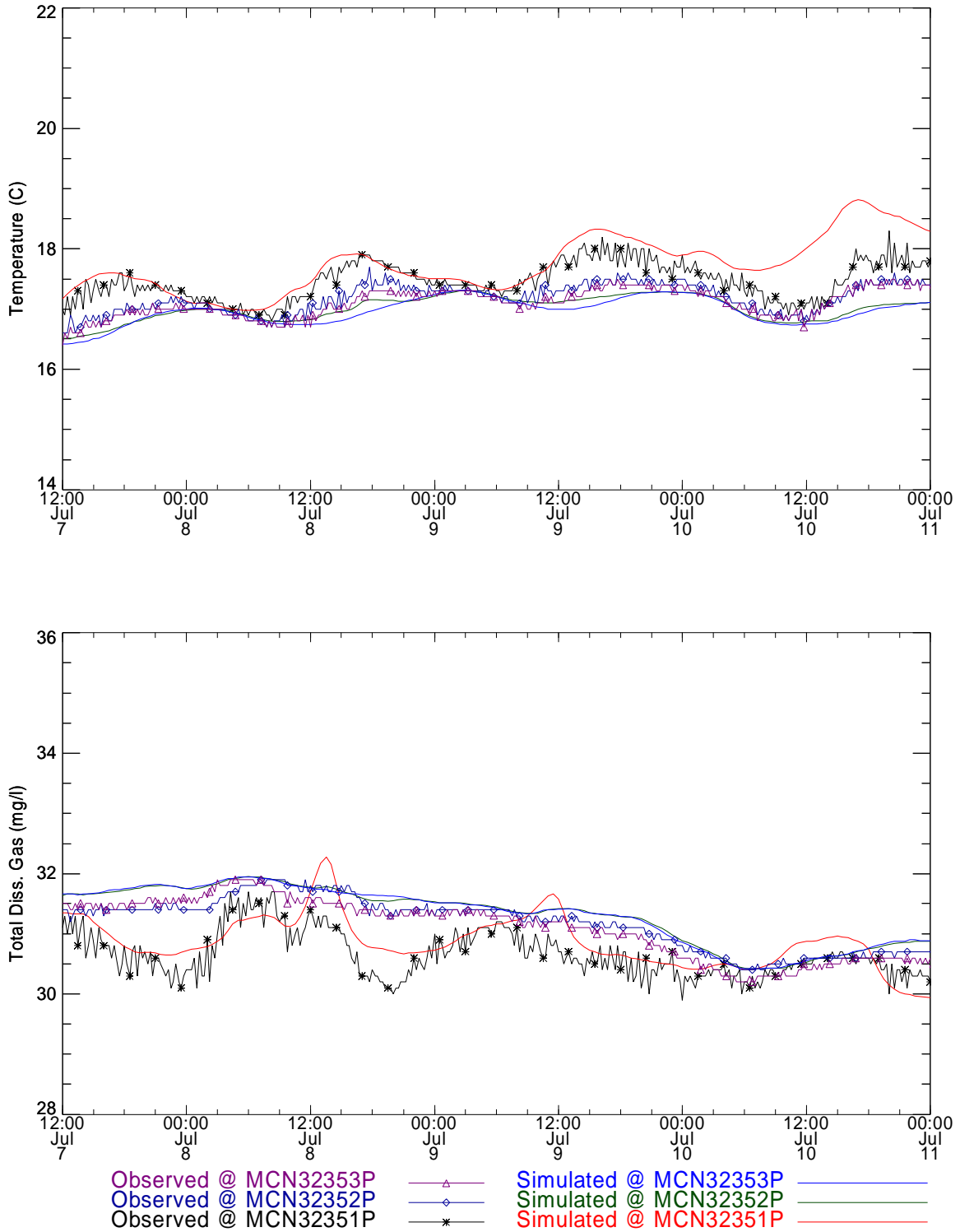


Figure 40. Temperature and total dissolved gas time series comparisons near Columbia River Mile 323.5 for the Summer 1996 pool study (TM-BC).

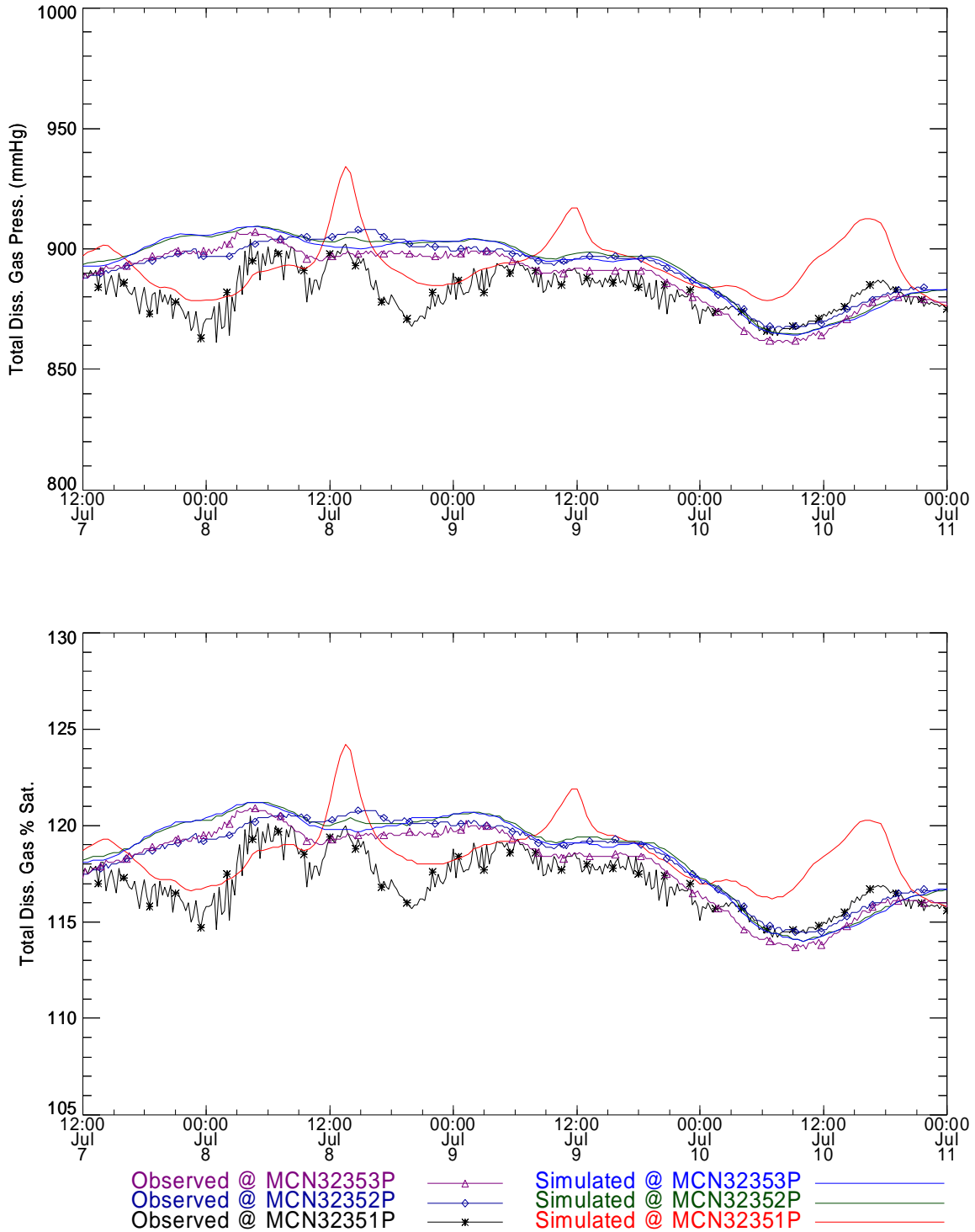


Figure 41. Total dissolved gas time series comparisons near Columbia River Mile 323.5 for the MCN Summer 1996 pool study (TM-BC).

A statistical summary of the model performance is shown in Table 10. The table shows the average and standard deviation for the model and measurements over the comparison time period. The root mean square error (RMS) is also computed. Table 11 shows the

percentage of time the model is within the performance (plus or minus) criteria noted in the table.

Table 10. Statistical summary of measurements and simulations for the MCN Summer 1996 pool study (TM-BC).

Station	Measured Ave.	Simulated Ave.	Measured Std.Dev	Simulated Std.Dev.	RMS Error
Temperature (°C)					
MCN32353P	16.92	16.79	0.34	0.32	0.20
MCN32352P	17.01	16.85	0.32	0.30	0.22
MCN32351P	17.25	17.53	0.39	0.65	0.54
Concentration (mg/l)					
MCN32353P	30.91	31.08	0.52	0.55	0.22
MCN32352P	31.06	31.09	0.39	0.53	0.23
MCN32351P	30.57	30.78	0.42	0.43	0.40
Gas Pressure (mmHg)					
MCN32353P	879.71	883.06	16.73	18.44	5.65
MCN32352P	885.47	884.23	12.66	17.78	6.82
MCN32351P	875.84	887.24	12.88	13.58	14.86
% Saturation					
MCN32353P	116.46	116.90	2.67	2.90	0.75
MCN32352P	117.22	117.05	2.15	2.81	0.90
MCN32351P	115.94	117.45	2.08	2.05	1.96

Table 11. Percentage of time during the simulation where the computed value is within the given variance compared to the measurements. MCN Summer 1996 pool study (TM-BC).

Station	±1.00 C	±1.00 mg/l	±38.00 mmHg	±5.00% Sat.
MCN32353P	100	100	100	100
MCN32352P	100	100	100	100
MCN32351P	90.81	98.94	98.23	98.23

5.7.3 MCN Summary

Table 12 compares the performance of the model to the measured field data. The table shows the number of times the model was within or outside of the stated RMS error summed over the total number of field measurement stations for a given study period. For

MCN, the table shows that the use of the temporary monitor and fixed-monitor data for the upstream boundary condition performed similarly at the 5% criteria level.

Table 12. Summary of model performance compared to field measurements for MCN pool. Table shows the number of occurrences within and outside of the RMS error noted.

McNary Pool					
Fixed Monitor Locations					
		Spring 1996	Summer 1996	Spring 1997	Total
Total # Stations			25	23	48
Temperature (RMS Error +/- 1.00 C)	# Within		24	23	47
	# Outside		1	0	1
Concentration (RMS Error +/- 1.00 mg/l)	# Within		15	18	33
	# Outside		10	5	15
Gas Pressure (RMS Error +/- 38.00 mmHg)	# Within		21	21	42
	# Outside		4	2	6
% Saturation (RMS Error +/- 5.00% Sat.)	# Within		22	21	43
	# Outside		3	2	5
Temporary Monitor Locations					
Total # Stations		24	24	22	70
Temperature (RMS Error +/- 1 C)	# Within	22	22	22	66
	# Outside	2	2	0	4
Concentration (RMS Error +/- 1.00 mg/l)	# Within	18	16	15	49
	# Outside	6	8	7	21
Gas Pressure (RMS Error +/- 38.00 mmHg)	# Within	23	20	19	62
	# Outside	1	4	3	8
% Saturation (RMS Error +/- 5.00% Sat.)	# Within	23	20	19	62
	# Outside	1	4	3	8

5.8 John Day (JDA)

John Day pool extends from the forebay of John Day Dam (JDA) near Columbia River Mile 217 to the tailrace of McNary Dam at River Mile 292.5. The MASS2 model domain extended from over the entire pool between the two dams.

This section only shows examples from the complete set of simulations. Additional details in the form of plots and summary tables are presented in Part 7 of the report series (Richmond and Perkins, 1998f).

5.8.1 JDA Hydrodynamics

Hydrodynamics simulations were performed for the Spring 1997 and Spring 1997 ADCP data collection periods. An example comparison from the JDA Spring 1997 case is shown in Figure 42 at a location in the forebay. Figure 43 shows a snapshot of the simulated velocity distribution for a reach downstream of McNary Dam.



Figure 42. Simulated and observed velocities near John Day dam on May 23, 1997.

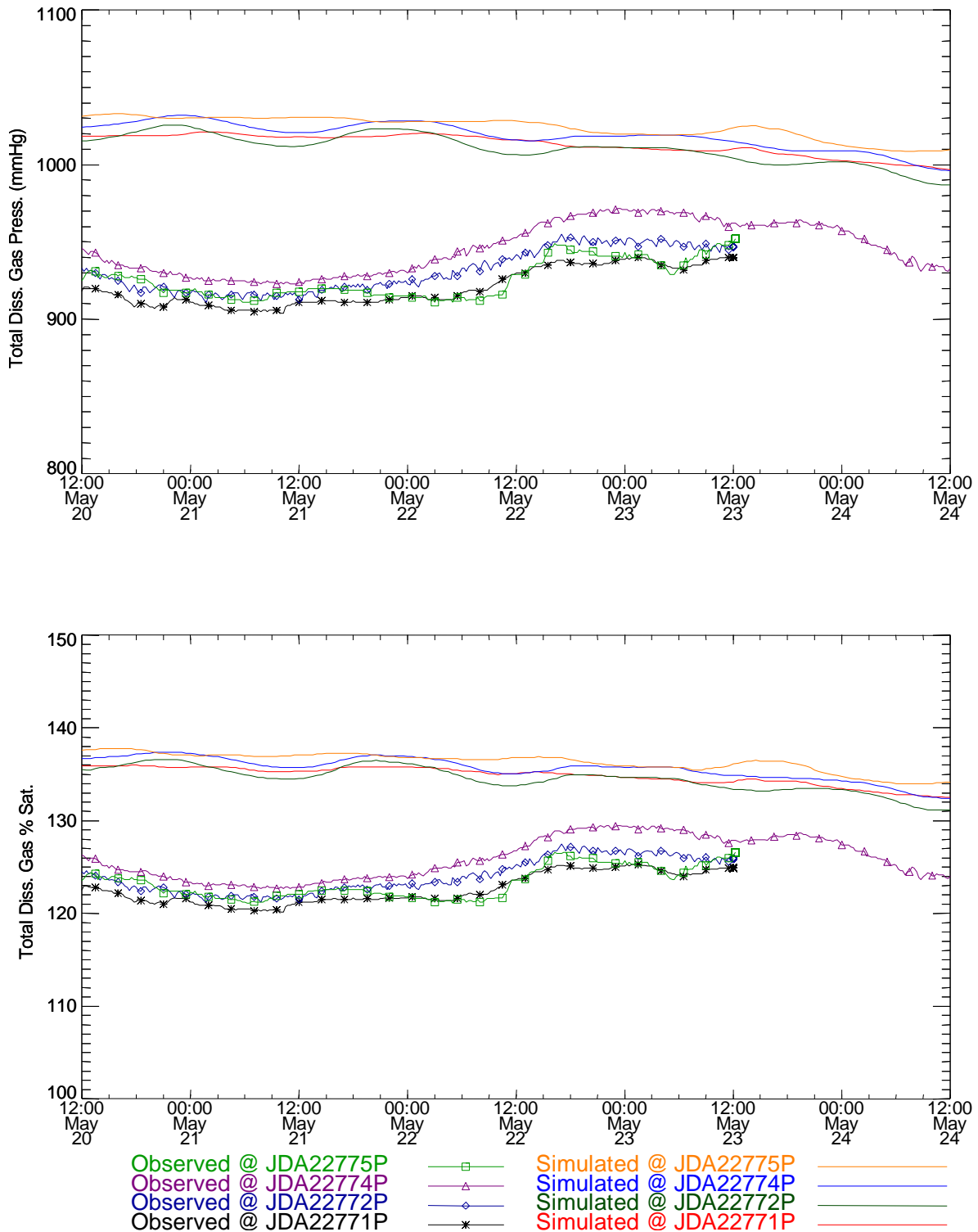


Figure 44. Total dissolved gas pressure and saturation time series comparisons near Columbia River Mile 227.7 for the JDA Spring 1997 study (TM-BC).

A statistical summary of the model performance is shown in Table 13. The table shows the average and standard deviation for the model and measurements over the comparison time period. The root mean square error (RMS) is also computed. This quantifies the

level of TDG over prediction when air/water gas exchange is not activated in the model. Table 12 shows the percentage of time the model is within the performance (plus or minus) criteria noted in the table. Again, the model fails to meet the performance criteria over the entire simulation period.

Table 13. Statistical summary of measurements and simulations at river mile 227.7 during JDA Spring 1997 pool study.

Station	Measured Ave.	Simulated Ave.	Measured Std.Dev	Simulated Std.Dev.	RMS Error
Temperature					
JDA22771P	12.57	12.55	0.21	0.24	0.11
JDA22772P	12.49	12.38	0.17	0.2	0.12
JDA22774P	12.48	12.44	0.17	0.21	0.11
JDA22775P	12.73	12.61	0.16	0.27	0.22
Concentration					
JDA22771P	35.58	38.93	0.65	0.15	3.42
JDA22772P	36.05	38.97	0.65	0.23	3.03
JDA22774P	36.45	39.24	0.71	0.2	2.9
JDA22775P	35.72	39.31	0.64	0.14	3.66
Gas Pressure					
JDA22771P	925.38	1013.13	13.41	6.83	89.9
JDA22772P	935.22	1010.65	13.56	9.49	78.41
JDA22774P	945.73	1018.88	16.54	8.64	76.27
JDA22775P	932.19	1024.19	15.41	7.17	94.49
% Saturation					
JDA22771P	123.16	134.87	1.74	0.97	11.98
JDA22772P	124.49	134.54	1.79	1.35	10.43
JDA22774P	125.93	135.63	2.25	1.22	10.12
JDA22775P	124.1	136.34	2.04	1.02	12.57

Table 14. Percentage of time during the simulation where the computed value is within the given variance compared to the measurements at river mile 227.7 for the Spring 1997 study (TM-BC).

Station	1.00 C	1.00 mg/l	38.00 mmHg	5.00% Sat
JDA22771P	100	0	0	0
JDA22772P	100	0	0	0
JDA22774P	100	0	0	0
JDA22775P	100	0	0	0

The following figures and tables show the effect of activating the air/water gas exchange option in the model. The model results are drastically improved in this simulation compared to the previous results where no surface gas transfer was allowed to occur. The simple empirical transfer coefficient yields substantial improvement the downstream part of the JDA pool.

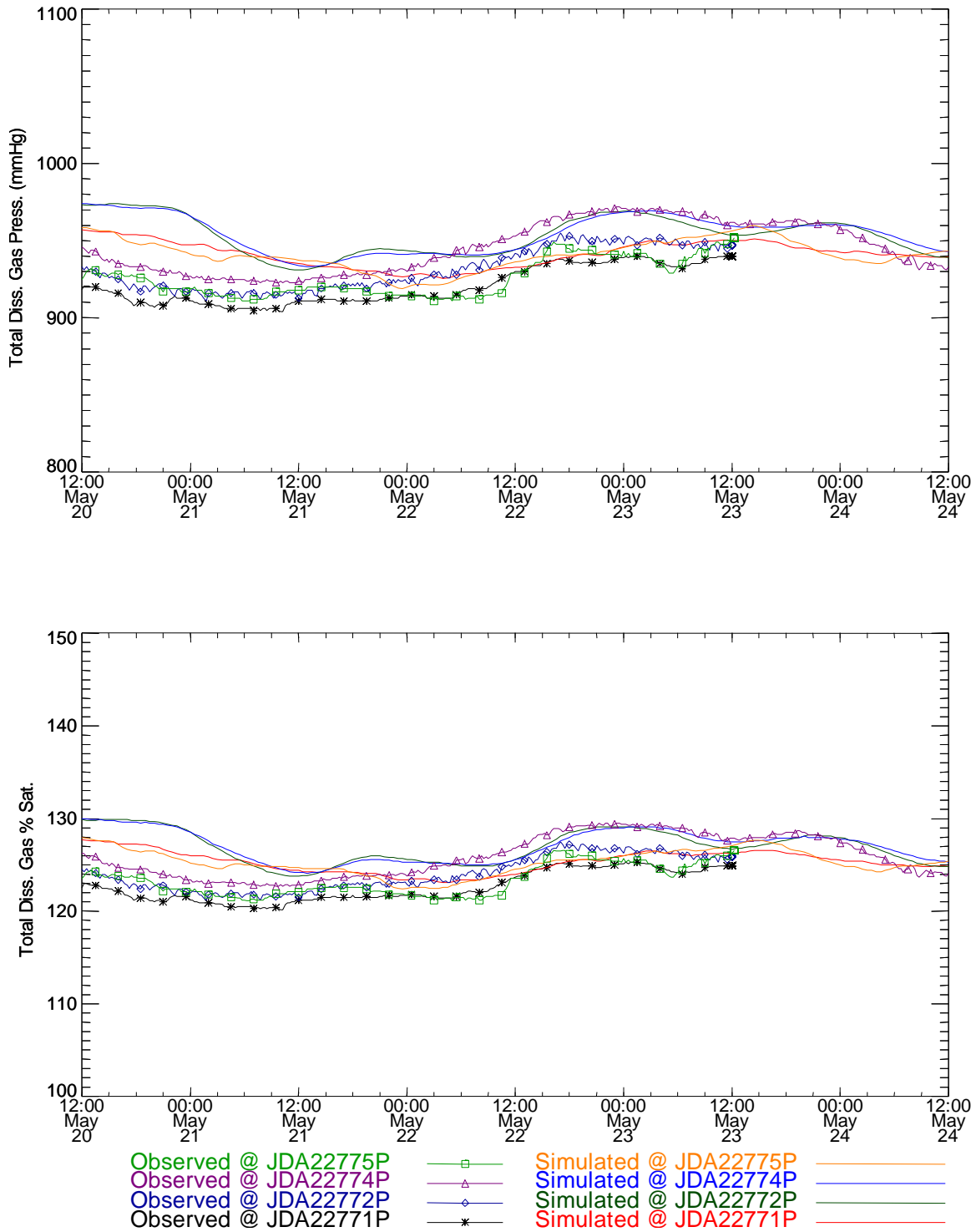


Figure 45. Total dissolved gas pressure and saturation time series comparisons near Columbia River Mile 227.7 for the Spring 1997 study (TM-BC). Air/water gas exchange option activated.

As illustrated in

Table 15, activating the empirical air/water gas exchange relationship in the model leads to substantial reduction in the RMS error for %saturation. The model still shows a consistent trend to overpredict TDG that indicates that the empirical exchange coefficient may be too low. This could be from caused by the failure of the simple formula to account for all the mechanisms at work or the fact that local wind speeds are extrapolated from distant weather stations.

Table 15. Statistical summary of measurements and simulations at river mile 227.7 during Spring 1997 pool study. Air/water gas exchange option activated.

Station	Measured Ave.	Simulated Ave.	Measured Std.Dev	Simulated Std.Dev.	RMS Error
Temperature C					
JDA22771P	12.57	12.55	0.21	0.24	0.11
JDA22772P	12.49	12.38	0.17	0.2	0.12
JDA22774P	12.48	12.44	0.17	0.21	0.11
JDA22775P	12.73	12.61	0.16	0.27	0.22
Concentration mg/l					
JDA22771P	35.58	36.14	0.65	0.36	0.76
JDA22772P	36.05	36.74	0.65	0.49	0.90
JDA22774P	36.45	36.74	0.71	0.49	0.62
JDA22775P	35.72	36.08	0.64	0.43	0.55
Gas Pressure mmHg					
JDA22771P	925.38	941.39	13.41	8.33	21.08
JDA22772P	935.22	953.40	13.56	12.46	23.67
JDA22774P	945.73	954.34	16.54	11.99	17.16
JDA22775P	932.19	941.08	15.41	9.83	15.77
% Saturation					
JDA22771P	123.16	125.32	1.74	1.17	2.80
JDA22772P	124.49	126.91	1.79	1.77	3.15
JDA22774P	125.93	127.04	2.25	1.69	2.27
JDA22775P	124.1	125.27	2.04	1.37	2.08

Table 16. Percentage of time during the simulation where the computed value is within the given variance compared to the measurements at river mile 227.7 for the JDA Spring 1997 study (TM-BC). Air/water gas exchange option activated.

Station	1.00 C	1.00 mg/l	38.00 mmHg	5.00% Sat
JDA22771P	100	76.68	90.67	90.67
JDA22772P	100	81.35	83.94	84.46
JDA22774P	100	85.49	93.26	92.23
JDA22775P	100	95.85	100.00	100.00

5.8.3 JDA Summary

The water quality simulations confirmed that air/water gas exchange is an important mechanism and must be included to obtain results that compare well with the field observations on an absolute basis.

Table 17 compares the performance of the model to the measured field data. The table shows the number of times the model was within or outside of the stated RMS error summed over the total number of field measurement stations for a given study period. For JDA, the table shows that the activating air/water gas exchange in the model yields a large improvement in the %saturation.

Table 17. Summary of model performance compared to field measurements for JDA pool. Table shows the number of occurrences within and outside of the RMS error noted.

John Day Report				
Fixed Monitor Locations		Spring 1997	Summer 1997	Total
Total # Stations		32	29	61
Temperature (RMS Error +/- 1.00 C)	# Within	32	29	61
	# Outside	0	0	0
Concentration (RMS Error +/- 1.00 mg/l)				
	# Within	14	19	33
	# Outside	18	10	28
Gas Pressure (RMS Error +/- 38.00 mmHg)				
	# Within	21	23	44
	# Outside	11	6	17
% Saturation (RMS Error +/- 5.00% Sat.)				
	# Within	21	23	44
	# Outside	11	6	17
Temporary Monitor Locations				
Total # Stations		33	28	61
Temperature (RMS Error +/- 1 C)	# Within	33	28	61
	# Outside	0	0	0
Concentration (RMS Error +/- 1.00 mg/l)				
	# Within	8	16	24
	# Outside	25	12	37
Gas Pressure (RMS Error +/- 38.00 mmHg)				
	# Within	10	20	30
	# Outside	23	8	31
% Saturation (RMS Error +/- 5.00% Sat.)				
	# Within	10	20	30
	# Outside	23	8	31
Temporary Monitor Locations With Air/Water Gas Exchange Option Activated				
Total # Stations		33		33
Temperature (RMS Error +/- 1 C)	# Within	33		33
	# Outside	0		0
Concentration (RMS Error +/- 1.00 mg/l)				
	# Within	26		26
	# Outside	7		7
Gas Pressure (RMS Error +/- 38.00 mmHg)				
	# Within	29		29
	# Outside	4		4

% Saturation (RMS Error +/- 5.00% Sat.)	# Within	29		29
	# Outside	4		4

5.9 The Dalles (TDA)

The Dalles pool extends from the forebay of The Dalles Dam (TDA) near Columbia River Mile 192 to the tailrace of John Day Dam at River Mile 217. The MASS2 model domain extended from over the entire pool between the two dams.

This section only shows examples from the complete set of simulations. Additional details in the form of plots and summary tables are presented in Part 8 of the report series (Richmond and Perkins, 1998g).

5.9.1 TDA Hydrodynamics

Hydrodynamic simulations and comparisons to ADCP data were performed for the Spring 1996 and Summer 1997 measurement periods. Figure 46 shows one of the poorest quality simulation results. A transient eddy (recirculation zone) appears upstream of The Dalles Dam in many cases. Investigation showed that this was related to the large bathymetric “hole” at river mile 192.8. This is a situation where the depth-averaged assumptions break down. To lessen the severity of the problem the hole was partially ‘filled-in’ to decrease the abrupt elevation change. This led to results that were more consistent with the field data. As noted , the eddy is transient and is not as large when at the time of the snapshot shown in Figure 47.

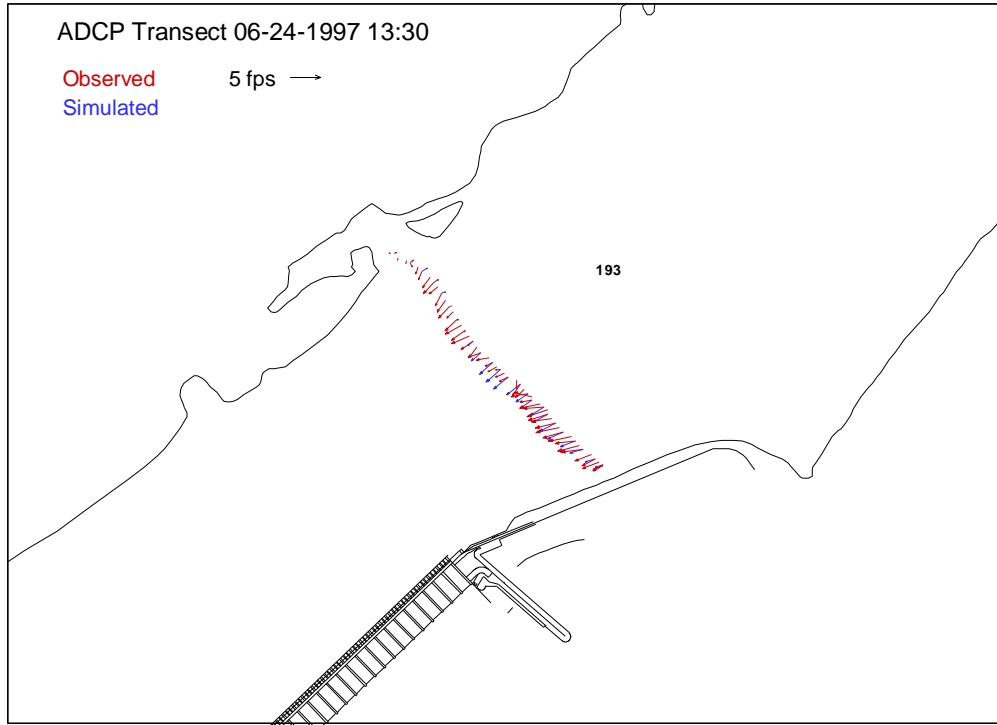


Figure 46. Simulated and observed depth-averaged velocities near The Dalles dam on June 24, 1997.

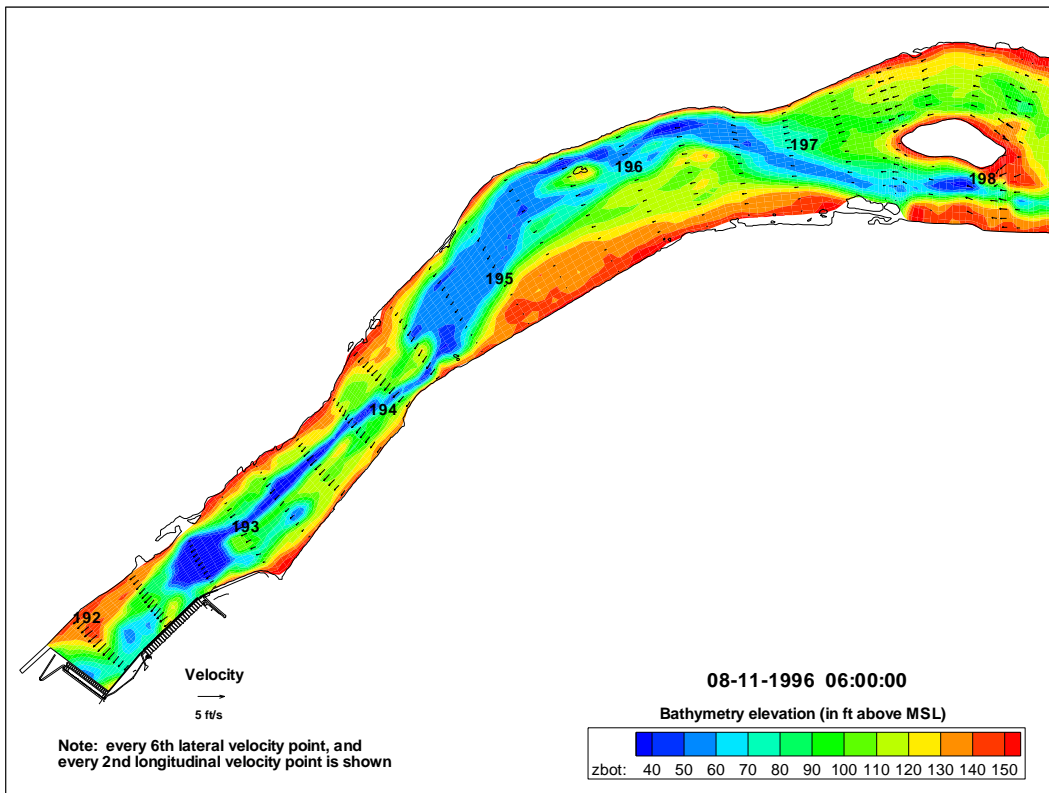


Figure 47. Simulated spatial velocity distribution in TDA pool upstream of The Dalles Dam.

5.9.2 TDA Water Quality

Water quality simulation cases were done for the Spring 1996, Summer 1996, and Summer 1997 field sampling periods. Time series example are shown in Figure 48 and Figure 49.

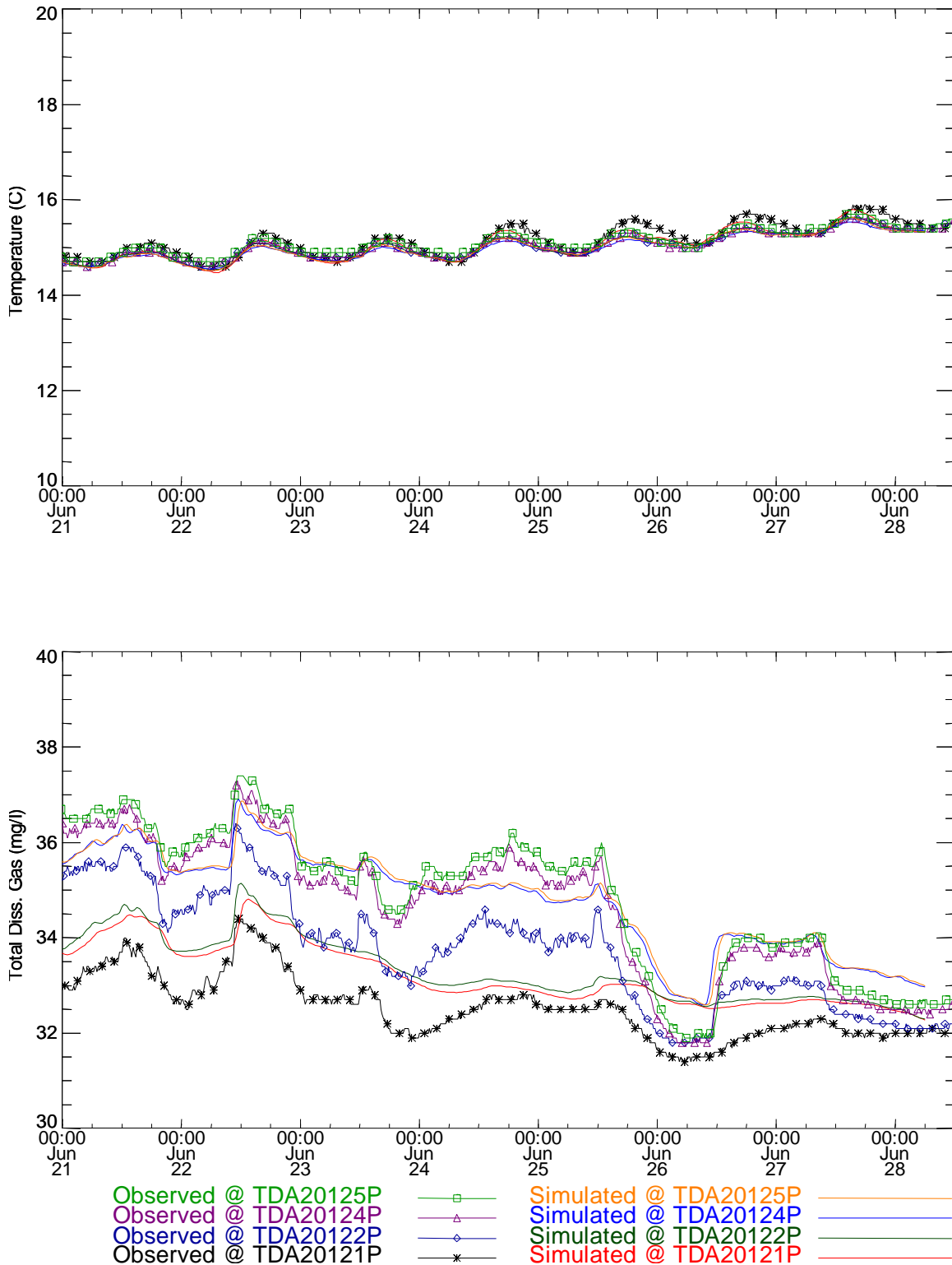


Figure 48. Temperature and total dissolved gas time series near Columbia River Mile 201.2 during the Summer 1997 pool study (TM-BC).

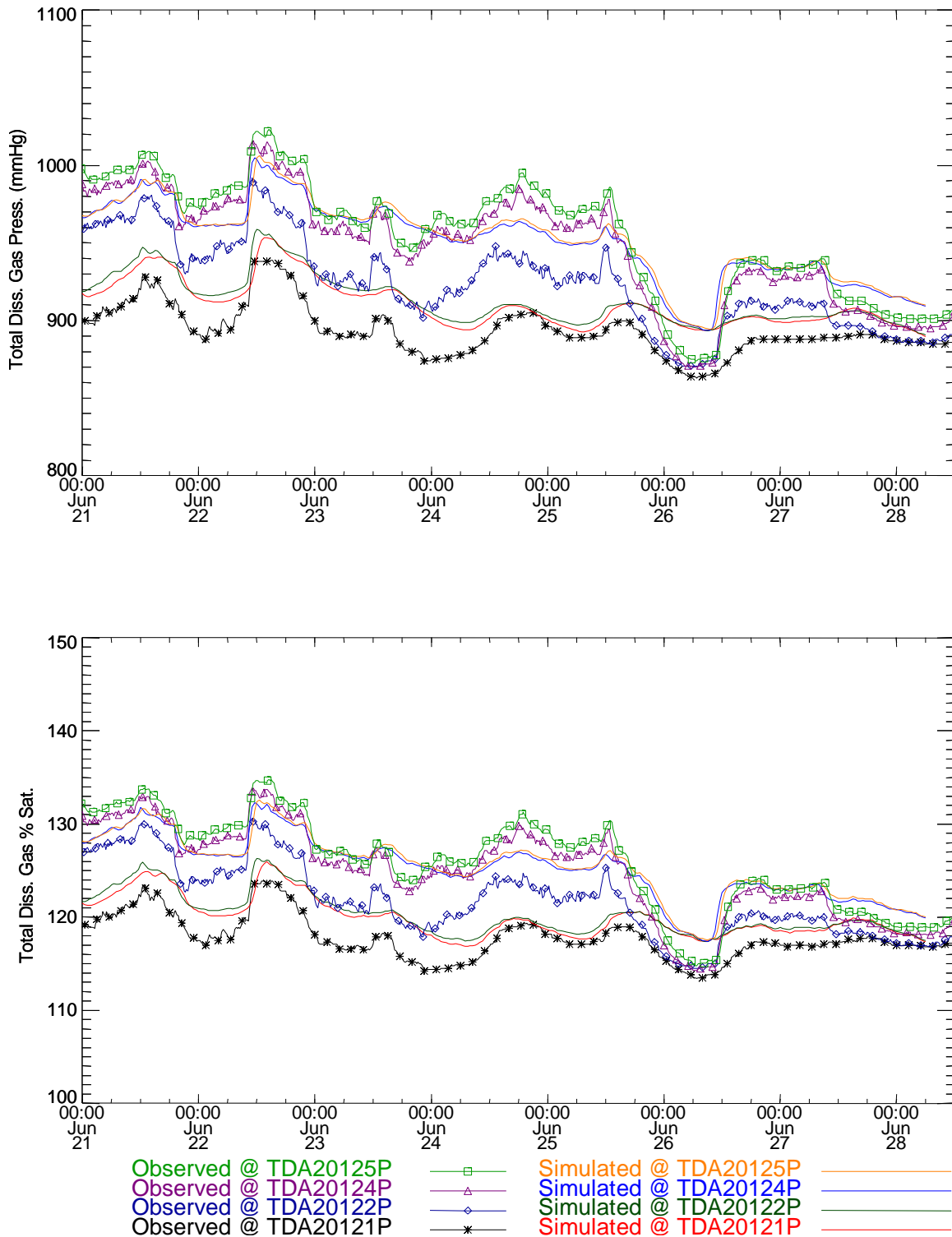


Figure 49. Total dissolved gas time series comparisons at the river mile 201.2 during the TDA Summer 1997 pool study (TM-BC).

A statistical summary of the model performance is shown in Table 18. The table shows the average and standard deviation for the model and measurements over the comparison time period. The root mean square error (RMS) is also computed. Table 19 shows the

percentage of time the model is within the performance (plus or minus) criteria noted in the table.

Table 18. Statistical summary of measurements and simulations at Columbia River mile 201.2 during the TDA Summer 1997 pool study (TM-BC).

Station	Measured Ave.	Simulated Ave.	Measured Std.Dev	Simulated Std.Dev.	RMS Error
Temperature					
TDA20121P	15.17	15.06	0.33	0.31	0.13
TDA20122P	15.06	15.03	0.26	0.27	0.06
TDA20124P	15.07	15	0.26	0.26	0.08
TDA20125P	15.12	15.02	0.26	0.27	0.12
Concentration					
TDA20121P	32.54	33.19	0.66	0.66	0.73
TDA20122P	33.72	33.3	1.19	0.7	0.78
TDA20124P	34.59	34.71	1.47	1.09	0.51
TDA20125P	34.84	34.75	1.51	1.09	0.54
Gas Pressure					
TDA20121P	893.62	910.02	15.7	15.14	18.54
TDA20122P	923.67	912.38	29.02	16	21.25
TDA20124P	947.14	949.77	36.46	25.9	13.77
TDA20125P	955.03	951.2	37.67	26.04	15.17
% Saturation					
TDA20121P	117.73	119.89	2.28	2.15	2.45
TDA20122P	121.69	120.2	3.94	2.25	2.81
TDA20124P	124.78	125.12	4.85	3.43	1.82
TDA20125P	125.82	125.31	5.01	3.46	2.01

Table 19. Percentage of time during the simulation where the computed value is within the given variance compared to the measurements at Columbia river mile 201.2 during the TDA Summer 1997 study (TM-BC).

Station	1.00 C	1.00 mg/l	38.00 mmHg	5.00% Sat.
TDA20121P	100	78.92	100	100
TDA20122P	100	75.31	96.39	96.39
TDA20124P	100	99.17	99.86	100
TDA20125P	100	98.34	100	100

5.9.3 TDA Summary

Table 20 compares the performance of the model to the measured field data. The table shows the number of times the model was within or outside of the stated RMS error summed over the total number of field measurement stations for a given study period. For

TDA, the table shows that the use of the temporary monitor data for the upstream boundary condition yields a significant improvement in the %saturation.

Table 20. Summary of model performance compared to field measurements for TDA pool. Table shows the number of occurrences within and outside of the RMS error noted.

The Dalles Pool					
Fixed Monitor Locations					
		Spring 1996	Summer 1996	Summer 1997	Total
Total # Stations		19	14	16	49
Temperature (RMS Error +/- 1.00 C)	# Within	19	14	16	49
	# Outside	0	0	0	0
Concentration (RMS Error +/- 1.00 mg/l)	# Within	13	7	7	27
	# Outside	6	7	9	22
Gas Pressure (RMS Error +/- 38.00 mmHg)	# Within	15	12	9	36
	# Outside	4	2	7	13
% Saturation (RMS Error +/- 5.00% Sat.)	# Within	15	12	9	36
	# Outside	4	2	7	13
Temporary Monitor Locations					
Total # Stations		19	14	16	49
Temperature (RMS Error +/- 1 C)	# Within	16	14	16	46
	# Outside	3	0	0	3
Concentration (RMS Error +/- 1.00 mg/l)	# Within	14	13	14	41
	# Outside	5	1	2	8
Gas Pressure (RMS Error +/- 38.00 mmHg)	# Within	15	14	16	45
	# Outside	4	0	0	4
% Saturation (RMS Error +/- 5.00% Sat.)	# Within	15	14	16	45
	# Outside	4	0	0	4

5.10 Bonneville (BON)

Bonneville pool extends from the forebay of Bonneville Dam (BON) near Columbia River Mile 145 to the tailrace of The Dalles Dam at River Mile 192. The MASS2 model domain extended from over the entire pool between the two dams.

This section only shows examples from the complete set of simulations. Additional details in the form of plots and summary tables are presented in Part 9 of the report series (Richmond and Perkins, 1998h).

5.10.1 BON Hydrodynamics

Hydrodynamic simulations and comparisons to ADCP data were performed for the Spring 1996 and Summer 1997 measurement periods. The model performance was good over the entire pool. A typical result is shown in Figure 50 in the reach just upstream of Bonneville Dam. The spatial distribution of simulated velocities is shown in Figure 51.

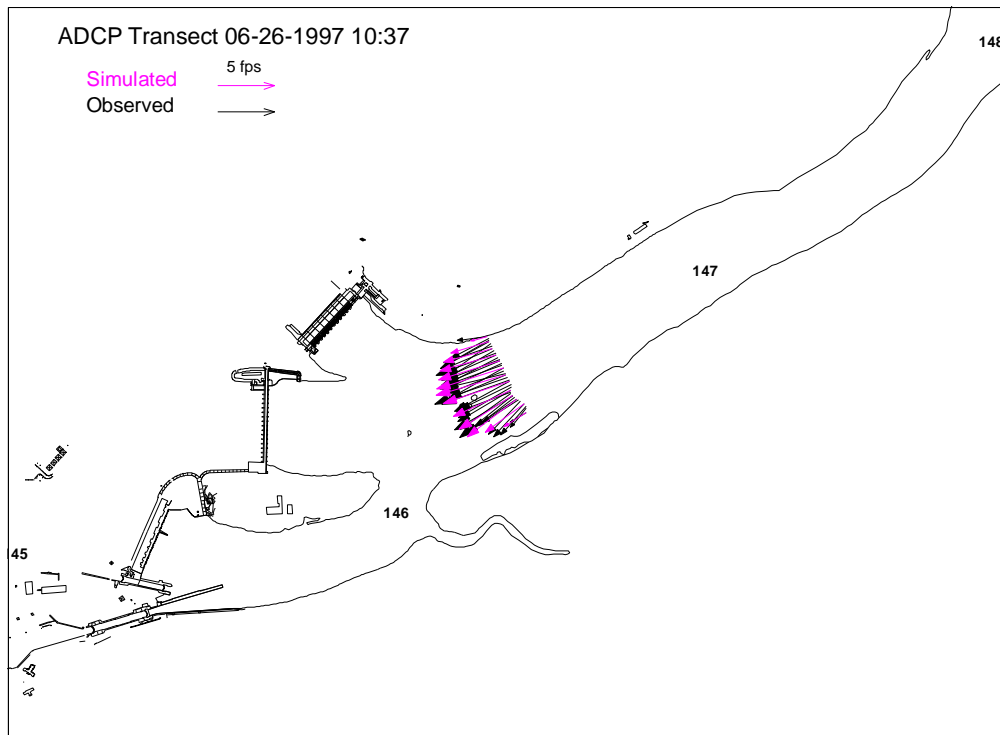


Figure 50. Simulated and observed depth-averaged velocities near Columbia River Mile 146.5 on 6-26-1997.

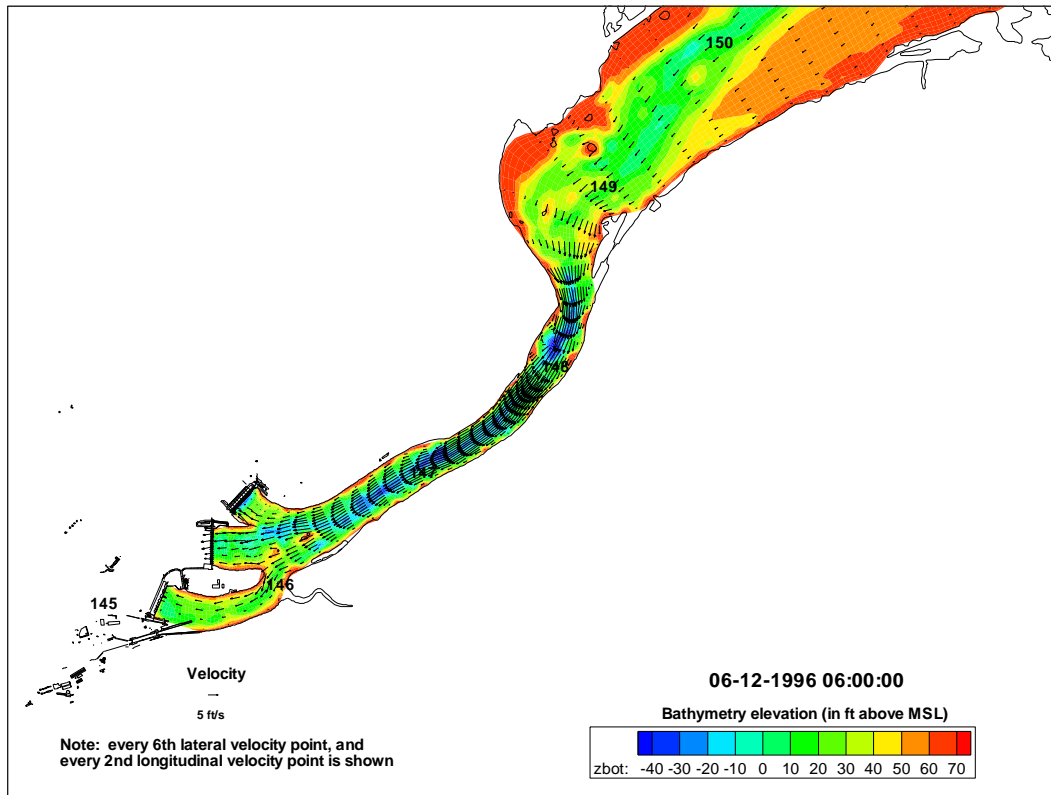


Figure 51. Simulated spatial velocity distribution upstream of Bonneville Dam.

5.10.2 BON Water Quality

Water quality simulation cases were done for the Spring 1996, Summer 1996, and Summer 1997 field sampling periods. A time series example are shown in Figure 52. In some cases, use of the air/water gas exchange option would have help improve the simulation results.

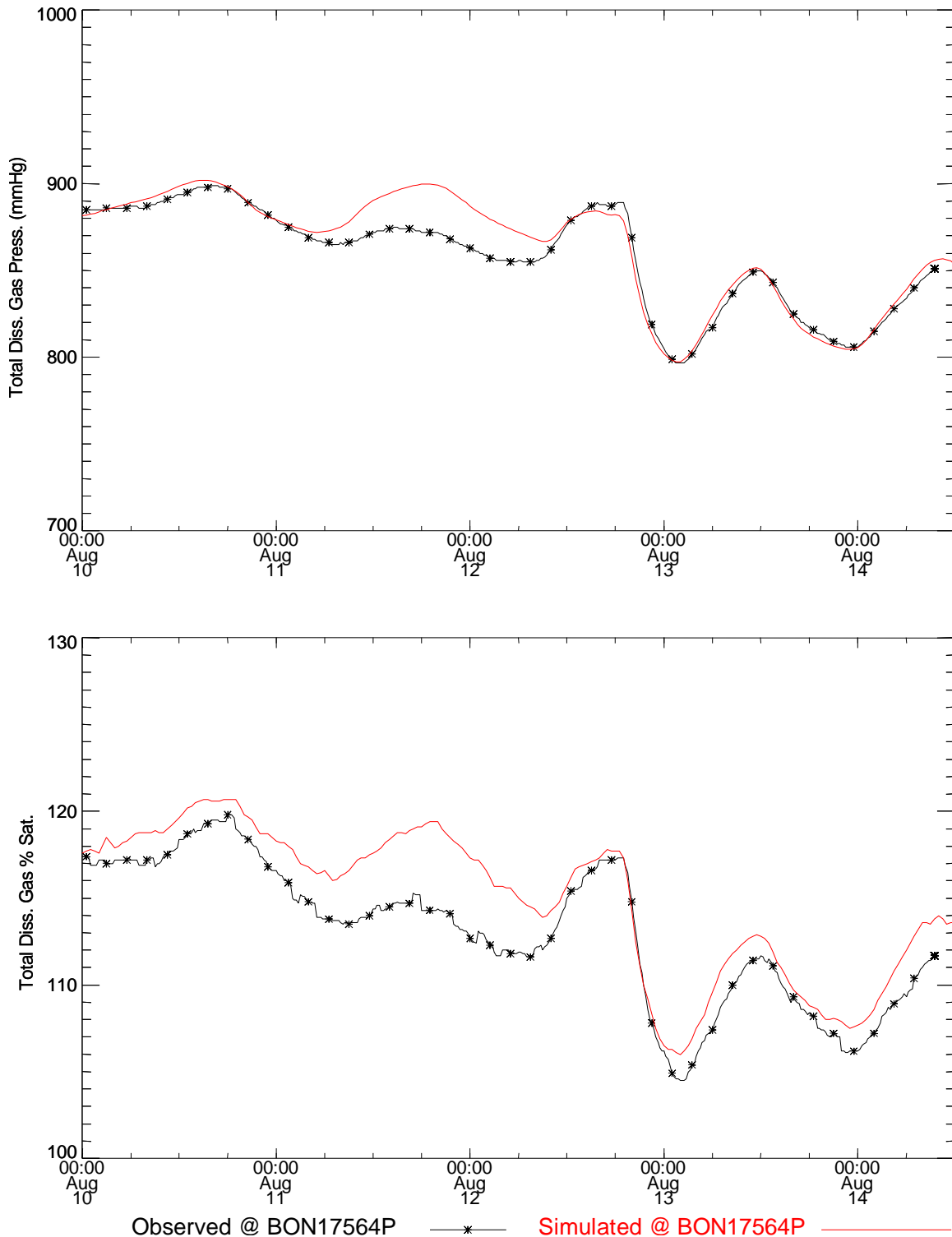


Figure 52. Total dissolved gas pressure and saturation time series comparisons near Columbia River Mile 175.6 for the BON Summer 1996 study period (TM-BC).

A statistical summary of the model performance is shown in Table 21. The table shows the average and standard deviation for the model and measurements over the comparison time period. The root mean square error (RMS) is also computed. Table 22 shows the

percentage of time the model is within the performance (plus or minus) criteria noted in the table.

Table 21. Statistical summary of measurements and simulations near Columbia River mile 175.6 during the BON Summer 1996 study period (TM-BC).

Station	Measured Ave.	Simulated Ave.	Measured Std.Dev	Simulated Std.Dev.	RMS Error
Temperature BON17564P	20.37	20.18	0.16	0.14	0.22
Concentration BON17564P	28.16	28.38	0.96	1.07	0.38
Gas Pressure BON17564P	858.04	863.57	28.77	31.82	10.93
% Saturation BON17564P	112.99	114.91	3.98	4.21	2.3

Table 22. Percentage of time during the simulation where the computed value is within the given variance compared to the measurements near Columbia River mile 175.6 for the BON Summer 1996 study period (TM-BC).

Station	1.00 C	1.00 mg/l	38.00 mmHg	5.00% Sat.
BON17564P	100	100	100	99.08

5.10.3 BON Summary

Table 23 compares the performance of the model to the measured field data. The table shows the number of times the model was within or outside of the stated RMS error summed over the total number of field measurement stations for a given study period. For BON, the table shows that the use of the temporary monitor data and fixed monitor system boundary condition performed about the same.

Table 23. Summary of model performance compared to field measurements for BON pool. Table shows the number of occurrences within and outside of the RMS error noted.

Bonneville Pool					
Fixed Monitor Locations					
		Spring 1996	Summer 1996	Summer 1997	Total
Total # Stations					
Temperature (RMS Error +/- 1 C)	# Within	14	10	16	40
	# Outside	0	0	0	0
Concentration (RMS Error +/- 1.00 mg/l)	# Within	7	9	12	28
	# Outside	7	1	4	12
Gas Pressure (RMS Error +/- 38.00 mmHg)	# Within	11	9	16	36
	# Outside	3	1	0	4
% Saturation (RMS Error +/- 5.00% Sat.)	# Within	11	9	16	36
	# Outside	3	1	0	4
Temporary Monitor Locations					
Total # Stations					
Temperature (RMS Error +/- 1 C)	# Within	13	5	11	29
	# Outside	0	2	5	7
Concentration (RMS Error +/- 1.00 mg/l)	# Within	8	5	11	24
	# Outside	5	2	5	12
Gas Pressure (RMS Error +/- 38.00 mmHg)	# Within	10	7	14	31
	# Outside	3	0	2	5
% Saturation (RMS Error +/- 5.00% Sat.)	# Within	10	6	13	29
	# Outside	3	1	3	7

5.11 Tidal Reach (TID)

The Tidal Reach (TID) extends from Columbia River Mile 110 near Portland, Oregon to the tailrace of Bonneville Dam near Columbia River Mile 145; the MASS2 model domain extends between these two boundaries.

Time-varying water surface elevations that accounted for tidal fluctuations and Bonneville project operations were assigned using output from the MASS1 model at the downstream boundary of the MASS2 model near River Mile 110. The MASS1 unsteady flow model has its downstream boundary in the Columbia River estuary and tidal conditions at Astoria, Oregon were used as the downstream boundary in that model.

This section only shows examples from the complete set of simulations. Additional details in the form of plots and summary tables are presented in Part 10 of the report series (Richmond and Perkins, 1998i).

5.11.1 TID Hydrodynamics

ADCP measurements were collected in the Tidal Reach during Spring 1996 and Summer 1997. Figure 53 shows the comparison of the simulated and measured depth-averaged velocities at the transect near Columbia River Mile 120.5. A snapshot of the computed velocity distribution in the reach below Bonneville Dam is shown in Figure 54. Note that upstream model boundaries are approximately 500 feet downstream of the spillway and powerhouse although that area is not shown in the figure below.

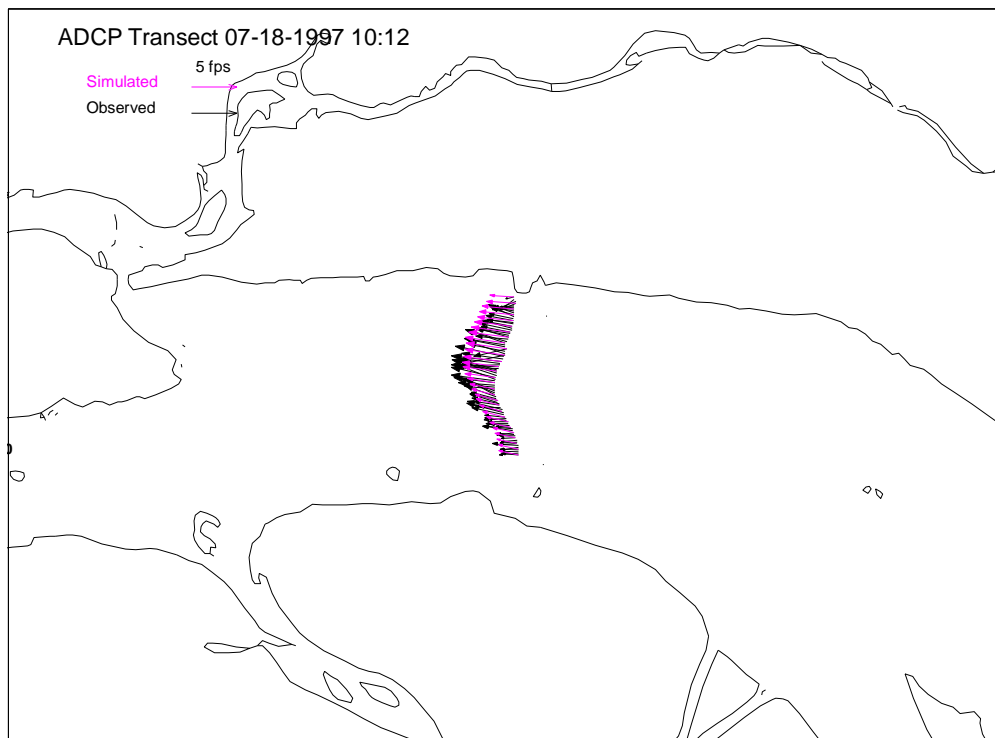


Figure 53. Simulated and observed depth-averaged velocities near Columbia River Mile 120.5 on 7-18-1997.

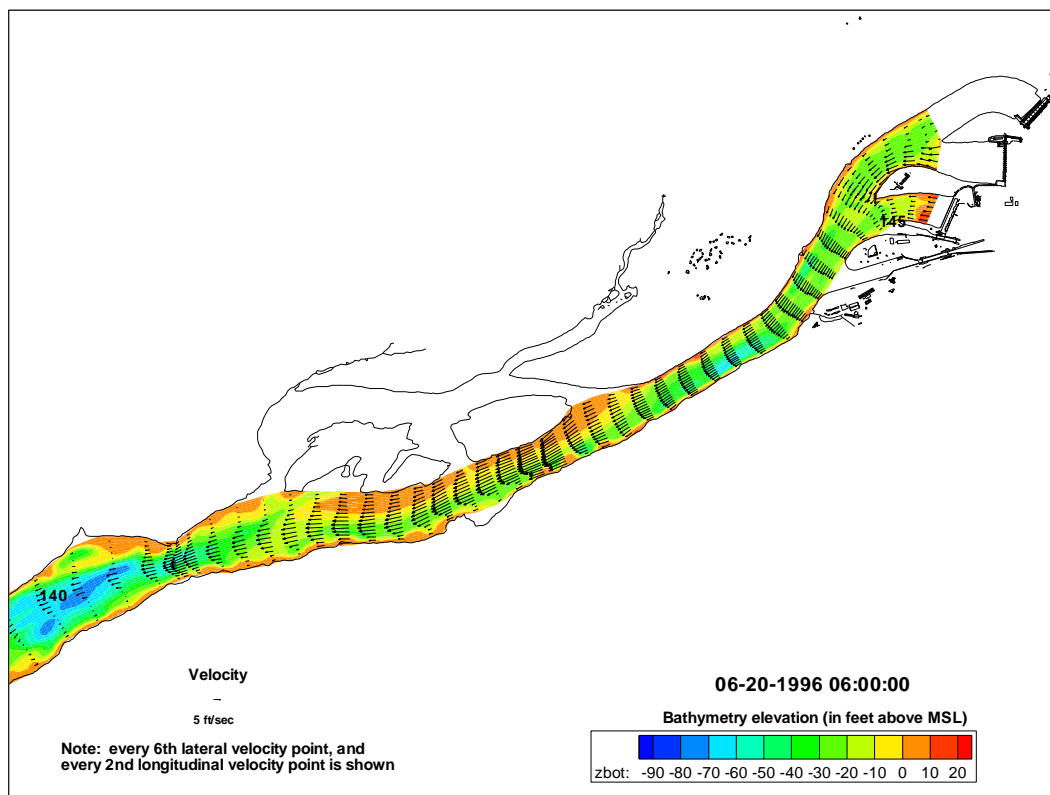


Figure 54. Simulated spatial velocity distribution downstream of Bonneville dam.

5.11.2 TID Water Quality

Water quality simulation cases were done for the Spring 1996, Summer 1996, and Summer 1997 field sampling periods. A time series example is shown in Figure 55.

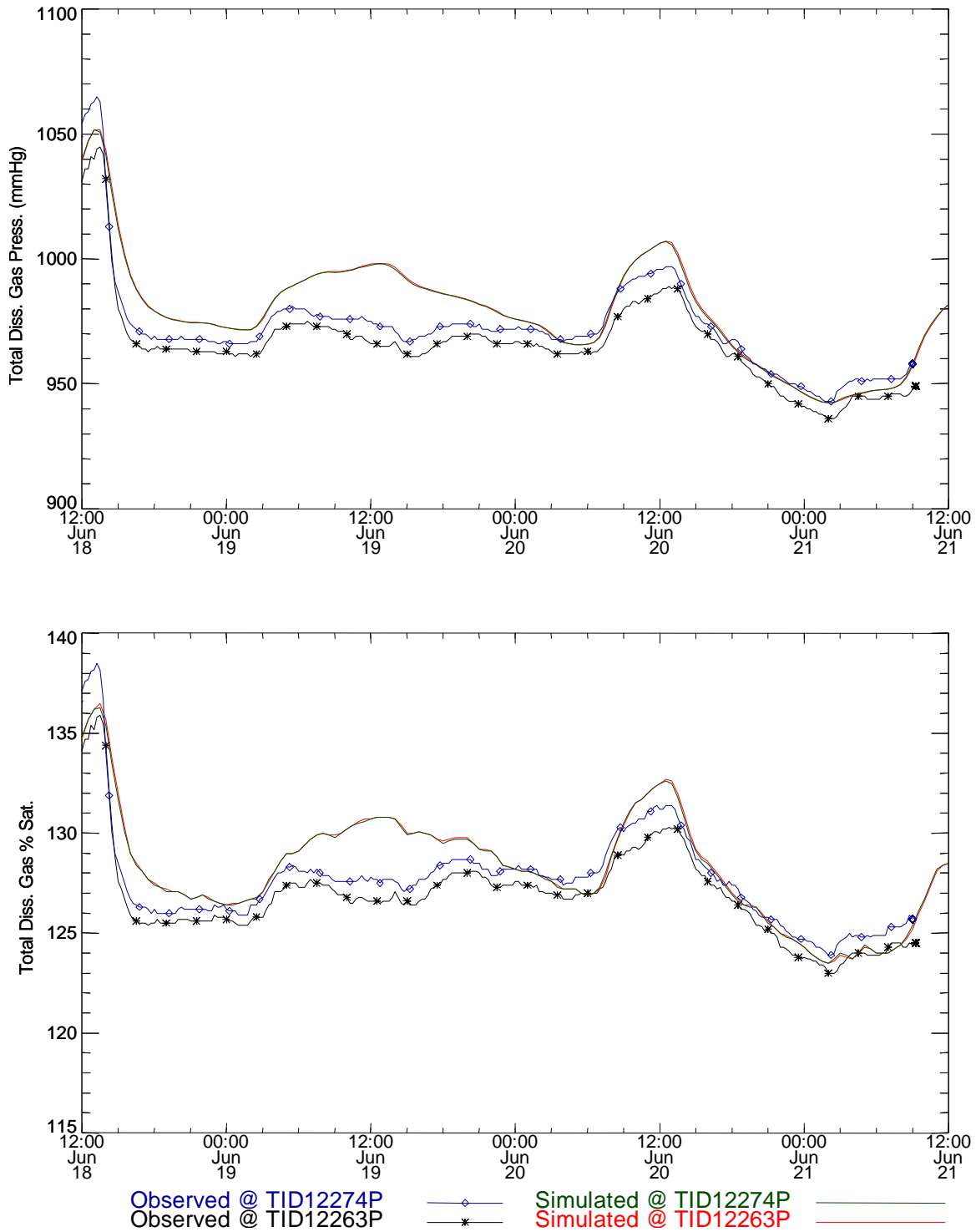


Figure 55. Total dissolved gas pressure and saturation time series comparisons near Columbia River mile 122.6 for the TID Spring 1996 study period (FMS-BC).

A statistical summary of the model performance is shown in Table 24. The table shows the average and standard deviation for the model and measurements over the comparison time period. The root mean square error (RMS) is also computed. Table 25 shows the

percentage of time the model is within the performance (plus or minus) criteria noted in the table.

Table 24. Statistical summary of measurements and simulations near Columbia River mile 122.6 during the TID Spring 1996 study (FMS-BC).

Station	Measured Ave.	Simulated Ave.	Measured Std.Dev	Simulated Std.Dev.	RMS Error
Temperature					
TID12263P	15.23	15.14	0.15	0.19	0.15
TID12274P	15.17	15.14	0.14	0.19	0.12
Concentration					
TID12263P	35.13	35.61	0.72	0.88	0.58
TID12274P	35.42	35.61	0.78	0.87	0.38
Gas Pressure					
TID12263P	965.56	979.02	18.14	21.83	16.02
TID12274P	972.08	978.87	19.63	21.67	11.31
% Saturation					
TID12263P	126.74	128.24	2.27	2.72	1.92
TID12274P	127.6	128.22	2.46	2.69	1.39

Table 25. Percentage of time during the simulation where the computed value is within the given variance compared to the measurements at river mile 122.6 for the TID Spring 1996 study (FMS-BC).

Station	1.00 C	1.00 mg/l	38.00 mmHg	5.00% Sat.
TID12263P	100	91.72	100	100
TID12274P	100	99.31	100	100

5.11.3 TID Summary

Table 26 compares the performance of the model to the measured field data. The table shows the number of times the model was within or outside of the stated RMS error summed over the total number of field measurement stations for a given study period. For TID, the table shows that the use of the temporary monitor data for the upstream boundary condition yields an improvement in the %saturation simulation.

Table 26. Summary of model performance compared to field measurements for TID. Table shows the number of occurrences within and outside of the RMS error noted.

Tidal Reach					
Fixed Monitor Locations					
		Spring 1996	Summer 1996	Summer 1997	Total
Total # Stations		18	15	18	51
Temperature (RMS Error +/- 1.00 C)	# Within	18	15	18	51
	# Outside	0	0	0	0
Concentration (RMS Error +/- 1.00 mg/l)	# Within	15	8	17	40
	# Outside	3	7	1	11
Gas Pressure (RMS Error +/- 38.00 mmHg)	# Within	17	12	17	46
	# Outside	1	3	1	5
% Saturation (RMS Error +/- 5.00% Sat.)	# Within	17	11	17	45
	# Outside	1	4	1	6
Temporary Monitor Locations					
Total # Stations		16	15	18	49
Temperature (RMS Error +/- 1 C)	# Within	16	15	18	49
	# Outside	0	0	0	0
Concentration (RMS Error +/- 1.00 mg/l)	# Within	16	14	17	47
	# Outside	0	1	1	2
Gas Pressure (RMS Error +/- 38.00 mmHg)	# Within	16	15	18	49
	# Outside	0	0	0	0
% Saturation (RMS Error +/- 5.00% Sat.)	# Within	16	14	18	48
	# Outside	0	1	0	1

6 Conclusions and Recommendations

Overall the MASS2 model hydrodynamic and water quality model performed well over the wide range of conditions that are represented in the Lower Columbia and Snake River system. The model can be used as a tool to evaluate the relative performance different gas abatement alternatives. The model can also be useful for simulating the potential absolute differences in dissolved gas levels provided that key uncertainties such as upstream influx of dissolved gas and air/water gas exchange are considered in the analysis.

Table 27 presents the overall performance of the MASS2 model for all the Lower Columbia and Snake River studies. When using TM-BC temperature simulation is within ± 1.0 degrees C for all but 5% of the cases. Without considering air/water gas exchange the TM-BC cases are within $\pm 5\%$ saturation for approximately 80% of the comparisons.

Table 27. Summary of model performance compared to field measurements for all simulated cases. Table shows the number of occurrences within and outside of the RMS error noted.

	Temperature (RMS Error +/- 1.00 C)		% Saturation (RMS Error +/- 5.00% Sat.)	
	# Within	# Outside	# Within	# Outside
Fixed Monitor Locations BC				
Lower Granite	14	0	14	0
Little Goose	35	4	19	20
Lower Monumental	31	3	14	20
Ice Harbor	16	18	32	2
McNary	47	1	43	5
John Day	61	0	44	17
The Dalles	49	0	36	13
Bonneville	40	0	36	4
Tidal Reach	51	0	45	6
Totals	344	26	283	87
Temporary Monitor Locations BC				
Lower Granite	0	0	0	0
Little Goose	38	1	37	2
Lower Monumental	28	1	26	3
Ice Harbor	31	1	28	4
McNary	66	4	62	8
John Day	61	0	30	31
The Dalles	46	3	45	4
Bonneville	29	7	29	7
Tidal Reach	49	0	48	1
Totals	282	13	243	52
Temporary Monitor Locations With Air/Water Gas Exchange Option Activated				
John Day	33	0	29	4

Inclusion of the empirical air/water gas exchange mechanism yields improved results using air/water gas exchange we see 12.5% (21% without air/water gas exchange) of the stations are outside the RMS saturation criteria using the TM-BCs as compared to 30% using the FMS-BCs.

The following are the general conclusions from the study:

- The model meets the objectives to develop a tool to perform relative comparisons between different DGAS alternatives.
- Achieved the criteria of $\pm 5\%$ RMS and ± 1 degree C RMS error over a substantial number of the monitor locations.
- Specifying the upstream influx of TDG using either regression equations or measured data has a large and direct effect on the quality of the simulations. Errors in the influx are simply propagated downstream.
- Powerhouse discharge entertainment into the spillway flow and potential increases in gas production must be considered. Estimates of this effect need to be incorporated into the specification of any gas abatement alternative; appropriate gas production algorithms will have to be developed for the model boundary conditions.
- Air/water exchange is an important mechanism especially for absolute predictions.
- Good bathymetric data contributed to hydrodynamic simulation success and aided in developing an automated model configuration procedure. Incorporating new bathymetric data can be easily done using the GIS database developed in this work.
- Hydrodynamics results are good over the entire region with the exception of zones of extreme bathymetric changes where a depth-averaged approach is not a reasonable assumption. Further investigation of the model performance within the first mile downstream of a project could be done using the results of the DGAS near-field studies and other field or physical modeling studies.
- Temperature results consistent given the upstream influx dependency. Some comparison locations that exhibited under/over prediction for near-shore monitors may be related to horizontal or vertical position uncertainties. Also, the model is depth-averaged and vertical temperature gradients could be significant in some areas.

The following are items recommended for inclusion in the system-alternatives evaluation phase of the DGAS modeling effort:

- Run additional simulations using the existing cases further test air/water gas exchange outside of John Day pool. Since all input data are prepared this task would require very little effort to complete and can be done “in the background” as other tasks.

progress. Investigate the potential of using an improved air/water gas exchange parameterization.

- Complete testing and parameterization of FINS for McNary Pool when the required radio tracking and hydroacoustic data become available.
- Investigate grid transitions and grid coarsening to reduce computer time while maintaining acceptable accuracy as compared to the present fine-grid simulations.
- Implement simulation methods to link all the pools and do system-wide simulations.
- Develop measures to quantify the performance of DGAS alternatives.

These items (among many) should be considered as additional options or improvements to the MASS2 model:

- Implement a higher-order advection scheme to minimize artificial diffusion effects in the hydrodynamics and transport solutions. A TVD scheme is presently being considered for inclusion in the model.
- Implement a depth-averaged two-equation turbulence model to better represent mixing in zones of large velocity gradients (i.e., eddy or recirculation zones).
- In principal, the model can be applied to supercritical or mixed sub-super critical flow regimes; proper boundary conditions should be implemented and model testing performed to realize this additional capability.
- Sediment and sediment-sorbed contaminant transport.

7 References

- Brown, L. C. and T. O. Barnwell, Jr. 1987. *The Enhanced Stream Water Quality Models QUAL2E and QUAL2E-UNCAS: Documentation and User Manual*. EPA/600/3-87/007, Environmental Research Laboratory, U.S. Environmental Protection Agency, Athens, Georgia, 189 pp.
- Colt, J., 1984. *Computation of Dissolved Gas Concentrations in Water as Functions of Temperature, Salinity and Pressure*. American Fisheries Society Special Publication 14, Bethesda, Maryland. ISBN 0-913235-02-4, 154 pp.
- Edinger, J.E., D.K. Brady, and J.C. Geyer. 1974. *Heat Exchange and Transport in the Environment*, Electric Power Research Institute (EPRI) Publication No. 74-049-00-3, Palo Alto, CA.
- Fischer, H.B., E.J. List, R.C.Y. Koh, J. Imerger, N.H. Brooks. 1979. Mixing in Inland and Coastal Waters. Academic Press, New York, New York.
- Fidler, L.E. 1998. *Configuration, Preliminary Calibration, and Operation of the Dynamic Gas Bubble Trauma Mortality Model*. Draft Final Report submitted to U.S. Army Corps of Engineers, Walla Walla District. Aspen Applied Sciences, Kalispell, Montana.
- O'Connor, D.J., 1982. *Wind Effects on Gas-Liquid Transfer Coefficients*. J. Environmental Engineering, v. 109, n. 3, pp. 731-752.
- Patankar, S.V., 1980. Numerical Heat Transfer and Fluid Flow. Hemisphere, New York, New York.
- Payne, J.A. Introduction to Simulation, New York: McGraw-Hill Inc., 1982
- Rastogi, A.K. and W. Rodi, 1978. *Predictions of Heat and Mass Transfer in Open Channels*. J. Hydraulic Engineering, v. 104, n. 3, pp. 397-420.
- Richmond, M.C., H.C. Chen, and V.C. Patel. 1986. *Equations of Laminar and Turbulent Flows in General Curvilinear Coordinates*. IIHR Report No. 300, Iowa Institute of Hydraulic Research, Univ. of Iowa, Iowa City, IA.
- Richmond, M.C. and W.A. Perkins. 1998a. *Two-Dimensional Hydrodynamic, Water Quality, and Fish Exposure Modeling of the Columbia and Snake Rivers. Part 2: Lower Granite Reservoir*. Draft Final Report submitted to U.S. Army Corps of Engineers, Walla Walla District. Battelle Pacific Northwest Division, Richland, Washington.
- Richmond, M.C. and W.A. Perkins. 1998b. *Two-Dimensional Hydrodynamic, Water Quality, and Fish Exposure Modeling of the Columbia and Snake Rivers. Part 3: Little Goose Reservoir*. Draft Final Report submitted to U.S. Army Corps of Engineers, Walla Walla District. Battelle Pacific Northwest Division, Richland, Washington.

- Richmond, M.C. and W.A. Perkins. 1998c. *Two-Dimensional Hydrodynamic, Water Quality, and Fish Exposure Modeling of the Columbia and Snake Rivers. Part 4: Lower Monumental Reservoir*. Draft Final Report submitted to U.S. Army Corps of Engineers, Walla Walla District. Battelle Pacific Northwest Division, Richland, Washington.
- Richmond, M.C. and W.A. Perkins. 1998d. *Two-Dimensional Hydrodynamic, Water Quality, and Fish Exposure Modeling of the Columbia and Snake Rivers. Part 5: Ice Harbor Reservoir*. Draft Final Report submitted to U.S. Army Corps of Engineers, Walla Walla District. Battelle Pacific Northwest Division, Richland, Washington.
- Richmond, M.C. and W.A. Perkins. 1998e. *Two-Dimensional Hydrodynamic, Water Quality, and Fish Exposure Modeling of the Columbia and Snake Rivers. Part 6: McNary Reservoir*. Draft Final Report submitted to U.S. Army Corps of Engineers, Walla Walla District. Battelle Pacific Northwest Division, Richland, Washington.
- Richmond, M.C. and W.A. Perkins. 1998f. *Two-Dimensional Hydrodynamic, Water Quality, and Fish Exposure Modeling of the Columbia and Snake Rivers. Part 7: John Day Reservoir*. Draft Final Report submitted to U.S. Army Corps of Engineers, Walla Walla District. Battelle Pacific Northwest Division, Richland, Washington.
- Richmond, M.C. and W.A. Perkins. 1998g. *Two-Dimensional Hydrodynamic, Water Quality, and Fish Exposure Modeling of the Columbia and Snake Rivers. Part 8: The Dalles Reservoir*. Draft Final Report submitted to U.S. Army Corps of Engineers, Walla Walla District. Battelle Pacific Northwest Division, Richland, Washington.
- Richmond, M.C. and W.A. Perkins, 1998h. *Two-Dimensional Hydrodynamic, Water Quality, and Fish Exposure Modeling of the Columbia and Snake Rivers. Part 9: Bonneville Reservoir*. Draft Final Report submitted to U.S. Army Corps of Engineers, Walla Walla District. Battelle Pacific Northwest Division, Richland, Washington.
- Richmond, M.C. and W.A. Perkins, 1998i. *Two-Dimensional Hydrodynamic, Water Quality, and Fish Exposure Modeling of the Columbia and Snake Rivers. Part 10: Tidal Reach*. Draft Final Report submitted to U.S. Army Corps of Engineers, Walla Walla District. Battelle Pacific Northwest Division, Richland, Washington.
- Richmond, M.C. and W.A. Perkins, 1998j (in preparation). *Modular Aquatic Simulation System 1D (MASS1): A One-Dimensional Hydrodynamic and Water Quality Model for River Systems*. Draft Final Report. Battelle Pacific Northwest Division, Richland, Washington.
- Schneider, M.L., and S.C. Wilhelms, 1997. *Total Dissolved Gas Production at Spillways on the Snake and Lower Columbia Rivers*. Memorandum for Record, CEWES-HS-L, U.S. Army Corps of Engineers, Available (limited access): limnos.wes.army.mil Directory: /data3/dgas/Documents/reports/ File: dgasprod.exe.
- Smith, L. S., 1982. *Decreased swimming performance as a necessary component of the smolt migration in salmon migration in the Columbia River*, *Aquaculture*, **28**:153-161.

Spasojevic, M. and F.M. Holly, Jr., 1990. *2-D Bed Evolution in Natural Watercourses – New Simulation Approach*. J. of Waterway, Port, Coastal, and Ocean Engineering, v. 116, n. 4, pp. 425-443.

Steinbrenner J.P., and J.R. Chawner, 1995. *The GRIDGEN Version 9 Multiple Block Grid Generation Software*. MDA Engineering, Inc., Arlington, Texas.

Wigmosta, M.S. and W. A. Perkins, 1997. *A GIS-based Modeling System for Watershed Analysis*. Report to the National Council of the Paper Industry for Air and Stream Improvement (NCASI), Weyerhaeuser Co., and MacMillan Bloedel Limited. Battelle Memorial Institute, Pacific Northwest Laboratories.

Ye, J. and J.A. McCorquodale. 1997. *Depth-Averaged Model in Curvilinear Collocated Grid*. J. Hydraulic Engineering, v. 123, n. 5, pp. 380-388.

Zabel, R. W. "Spatial and Temporal Models of Migrating Juvenile Salmon with Applications", Ph.D. dissertation, University of Washington, 1994.

Zhou, J.G., 1995. *Velocity-Depth Coupling in Shallow-Water Flows*. J. of Hydraulic Engineering, v. 121, n. 10, pp 717-724.